Chapter 1

Introduction to Supramolecular Materials via Block copolymer

1-1 Supramolecular Materials from Block Copolymers

Most of today's materials require additional processing or modification steps in order to obtain the properties that make them suitable for a particular application. As an alternative to these traditional fabrication pathways, routes that use the self-assembly of low molecular weight oligomeric or polymeric building blocks are attracting increasing attention.[1,2] By designing these building blocks in such a way that they contain all the necessary information to direct their self-assembly into functional materials, additional processing or modification steps could become superfluous.

Whereas it is difficult to organize low molecular weight organic molecules into periodic macroscopic assemblies, macromolecules can be assembled into a large variety of ordered morphologies covering several length-scales. Here, we focus on block copolymer type building blocks and discusses their potential for the development of self-assembled materials.

Block copolymers are macromolecules composed of two or more polymer blocks of chemically different monomers that are linked together by chemical bonds. The resulting chain topologies can be linear, branched, or cyclic. Systematic studies of these materials became possible through developments in polymerization techniques, which made possible the synthesis of well-defined block copolymers with a very small polydisperisty. Different microphase separated morphologies occur depending on the relative compositions of the different components and the total molecular weight as expressed by the degree of polymerization. In addition, the aggregation state of the blocks largely influences the morphology, too.

Among the binary linear block copolymers the diblock copolymers have been studied in great detail. They can be considered as model systems for more complicated block copolymers, such as block copolymers with more than two components, or block copolymers with other block distributions.

Two different classes of block copolymer type architectures will be distinguished: (a) coil-coil diblock copolymer and (b) rod-coil diblock copolymer. First, the self-assembly of the well-known coil-coil type diblock copolymers will be reviewed. The rod-coil diblock copolymer architecture is composed of a rigid rod-segment and a flexible coil-block. Furthermore, the rod-coil diblock copolymer is composed of low molecular weight and high molecular weight rod-coil block copolymers. Molecules with a total molecular weight less than 20 000 g/mol will be considered rod-coil diblock oligomers, while systems with a total molar mass exceeding 20 000 g/mol are regarded as rod-coil diblock copolymers. This division is not completelyarbitrary, since diblock oligmers with molar masses lower than 20 000 g/mol generally can be prepared using (multistep) organic chemistry synthetic procedures and purification methods (e.g., column chromatography). High molecular weight rod-coil diblock copolymers typically are only accessible via polymer chemistry methods (which inherently produce polydisperse materials) and are usually difficult to purify chromatographically.

1-2 Coil-Coil Diblock Copolymers

Coil-coil diblock copolymers, i.e., block copolymers comprised of two flexible, chemically incompatible and dissimilar blocks (e.g., polystyrene-*b*-polyisoprene) can microphase separate into a variety of morphologies. The phase behavior of such diblock copolymers has been the subject of numerous theoretical and experimental

studies over the past decades, and is relatively well understood.[3-5] This self-assembly process is driven by an unfavorable mixing enthalpy and a small mixing entropy, while the covalent bond connecting the blocks prevents macroscopic phase separation. The microphase separation of coil-coil diblock copolymers depends on the total degree of polymerization N (= N_A+N_B), the Flory-Huggins χ-parameter (which is a measure for the incompatibility between the two blocks) and the volume fractions of the constituent blocks (f_A and f_B, $f_A = 1-f_B$). The segregation product χN determines the degree of microphase separation. Depending on χN, three different regimes are distinguished; (a) the weak-segregation limit (WSL) for $\chi N \leqq 10$; (b) the intermediate segregation region (ISR) for $10 < \chi N \leqq 50$; (c) the strong segregation limit (SSL) for $\chi N \rightarrow \infty$.

Most of the experimental work on the phase behavior of coil-coil diblock copolymers has been performed in the SSL. In this regime, the phase boundaries are vertical lines and the microphase separated morphology can be varied from spheres via lamellae to inverse spheres by changing the volume fractions of the blocks (f). Well know are the results on the morphology of polystyrene-b-polyisoprene diblock copolymers by means of transmission electron microscopy (TEM) as a function of composition (Figure 1-1). (bcc = microspheres of the minority component ordered on a body-centered cubic lattice in a matrix of the second block; hex = hexagonally packed cylindrical microdomains of the minority component embedded in a matrix formed by the senond block; obdd = ordered bicontinuous double diamond microstructure formed by the minority component embedded in a matrix of the second block; lam = microstructure consisting of alternating lamellae of the constituent blocks; ODT = order-disorder transition). Early theoretical work by Leibler, however, suggested that close to the ODT the phase boundaries are no longer vertical lines but acquire more and more curvature as they approach the ODT.[3] This is shown in the

phase diagram depicted in Figure 1-2. As an implication of the curved phase boundaries, thermally induced order-order transitions should become possible near the ODT.

During the past decades, coil-coil diblock copolymers have found widespresd application as thermoplastic elastomers or as additives such as surfactants or viscosity modifiers.[6] Thomas et al. have investigated symmetrical coil-coil diblock copolymers that can self-assemble into periodic lamellar structures for applications in integrated optics.[7-9] Provided there is a difference in refractive index between the constituent blocks, such materials behave as photonic crystals, i.e., structures with a periodic variation of refractive index. Photonic crystals are of interest for a wide variety of optical applications including waveguides and mirrors.

It is interesting to control the morphology of microphase separated block copolymers by adding a homopolymer or another block copolymer. Stadler et al. reported the preparation of non-centrosymmetric superlattices using coil-coil block copolymer building blocks.[10,11] By blending equal amounts of a polystyrene-*b*-polybutadiene-*b*-poly(*tert*-butyl methacrylate) triblock copolymer and a polystyrene-*b*-poly(*tert*-butyl methacrylate) diblock copolymer, the authors were able to prepare non-centrosymmetric lamellar structures with a domain spacing of ~60 nm (Figure 1-3).

In comparison to binary block copolymers relatively little work on ternary block copolymers has so far been published. There are more independent variables in ternary block copolymers as compared to binary block copolymers. While in the latter only one independent composition variable and one interaction parameter exist, in ternary systems there are two independent composition variables and three interaction parameters. This leads to a richer phase diagram. In addition, the block sequence also can be changed, which introduces another tool to influence the morphology.[12] Mogi et

al.[13] and Gido et al.[14] studied triblock copolymers based on polystyrene (S), polyisoprene (I), and polyvinylpyridine (VP) with different block sequences. The difference in block sequence resulted in a different morphology for a similar overall composition of the systems. While polyisoprene-*b*-polystyrene-*b*-polyvinylpyridine (I-S-VP) with similar amounts of all three components forms lamellar stacks (Figure 1-4a),[13] I-S-VP forms hexagonally packed core shell cylinders (Figure 1-4b).[14]

This behavior can be understood as a consequence of the competition between the different interfacial tensions of adjacent blocks: while the interfacial tensions between S and I on one side and S and VP on the other side are of approximately similar magnitude, the interfacial tension between I and VP is much larger than that between I and S. As a consequence the system favors a smaller interface between I and VP as compared to I and S, which leads to a morphology with different interfacial areas on both ends of the middle block in the case of S-I-VP. In comparison, the system I-S-VP will from lamellae due to the fact that the interfacial areas on both ends of the middle block are of approximately the same size.

For the preparation of nanoporous membranes, block copolymers that self-assemble into cylindrical or bicontinuous (gyroid) mesophases are most attractive, since these morphologies consist of a continuous phase (e.g., cylinders, gyroids) of one block embedded in a matrix of the second one. Since coil-coil diblock copolymers typically form phase-separated morphologies with domain sizes between 10 - 100 nm, degradation of the block that constitutes the cylindrical or gyroid phase could give access to nanoporous materials.

Liu and co-workers have successfully demonstrated the feasibility of this approach using a series of poly(*tert*-butyl acrylate)-*b*-poly(2-cinnamoylethyl methacrylate) (P*t*BA-*b*-PCEMA) diblock copolymers.[15] At appropriate block length ratios, the P*t*BA block self-assembles into cylindrical domains, which are embedded

in a PCEMA matrix. Photocrosslinking of the PCEMA phase and hydrolysis of the *tert*-butyl groups results in nanoporous films, whose water permeability was found to be strongly dependent on the pH and the presence of cations. By adjusting the length of the P*t*BA block, the pore size of the films could be varied between 10-50 nm. Films with larger pores could be prepared by blending a poly(isoprene)-*b*-poly(2-cinnamoylethyl methacrylate)-*b*-poly(*tert*-butyl acrylate) (PI-*b*-PCEMA-*b*-P*t*BA) triblock copolymer with 10 wt.-% of a P*t*BA homopolymer.[16] The P*t*BA mixes with the P*t*BA block of the triblock copolymer, and swells the cylindrical P*t*BA domains. After extraction of the PtBA homopolymer and hydrolysis of the *tert*-butyl groups, films were obtained with pore sizes up to 100 nm. These membranes were impermeable to water, but showed high gas permeabilities.

1-3 Rod-Coil Block Copolymers

1-3.1 Rod-Coil Block Copolymer Theories

Coil-coil multiblock systems built of incompatible coil segments have been found to exist in a wide range of microphase separated supramolecular structures such as spheres, cylinders, double diamond (DD), double gyroid (DG), and lamellae. Their phase behavior mostly results from the packing constraints imposed by the connectivity of each block and by the mutual repulsion of the dissimilar blocks. Phase separation and therefore the resulting stable morphology in diblock systems is greatly influenced by the total degree of polymerization (N), the Flory-Huggins χ parameter, and the composition expressed by volume fractions f_A, f_B …

Here, we focus on block copolymers and comblike polymers in which at least one component is based on a conformationally rigid segment. A measurement of the stiffness of a polymer is afforded by the so-called persistence length which gives an

estimate of the length scale over which the tangent vectors along the contour of the chain's backbone are correlated. Typical values for persistence lengths in synthetic and biological systems can be several orders of magnitude larger than for flexible, coil-like polymers. Rod-like polymers have been found to exhibit lyotropic liquid-crystalline ordered phases such as nematic and /or layered smectic structures with the molecules arranged with their long axes nearly parallel to each other. Supramolecular assemblies of rod-like molecules are also capable of forming liquid-crystalline phases.

By combining these different classes of polymers a novel class of self-assembling materials can be produced since the molecules share certain general characteristics typical of diblock molecules and thermotropic calamitic molecules. The difference in chain rigidity of rod-like and coil-like blocks is expected to greatly affect the details of molecular packing in the condensed phases and thus the nature of thermodynamically stable morphologies in these materials. The thermodynamic stable morphology should be originated as the result of the interdependence of microsegregation and liquid crystallinity.

Including both rod and block characters, Semenov and Vasilenco (SV) have initiated a theoretical study on the phase behavior of rod-coil block copolymers.[17] In their study, SV only considered the nematic phase and smectic A lamellar phases where rods remain perpendicular to the lamellae. The smectic phase has either a monolayer or bilayer structure. In the following study, Semenov included the smectic C phases, where the rods are tilted by an angle theta to the lamellar normal.[18,19] The model also included a weak phase in which lamellar sheets containing the rigid rod were partly filled by flexible coil. For free energy calculations, SV introduced four main terms: ideal gas entropy of mixing, steric interaction among rods, coil stretching, and unfavorable rod-coil interactions. The ideal gas entropy of the mixing term is

7

associated with the spatial placement of the junction point of rod-coil molecules. To find the steric interaction energy term of the rods SV used the lattice packing model (Flory lattice approach). Coil stretching arises from the constraint of the density uniformity, and it restricts the number of possible conformations of flexible coil in the structured system. The Flory-Huggins interaction parameter measures unfavorable rod-coil interaction energy. The schematic phase diagram calculated shows various phases as a function of the volume fraction of the flexible component f, the product χN and the ratio ν of the characteristic coil to rod dimensions. In rod-coil block copolymers, the shape of the phase diagram is affected by the ratio ν. It was also shown that the nematic-smectic transition is a first-order transition, while the smectic A-smectic C transition is a continuous second-order transition.

Williams and Fredrickson proposed the hockey puck micelle (one of the nonlamellar structure) where the rods are packed axially to form finite-sized cylindrical disk covered by coils (Figure 1-5).[20] They predicted that the hockey puck structure should be stable at large coil fractions ($f > 0.9$). The main advantage of micelle formation relative to lamellae is the reduction of the stretching penalty of coils; because in a rod-coil block copolymer the coils are permanently attached to the rods, complete separation is never possible, and there is always some interface between the two. In general, the sharper the interface, the more the coils have to stretch and the greater the stretching free energy. At high χ values, the system can be modeled as a set of chains grafted to a wall. In the lamellae structure, the highly grafted chains pay a large stretching penalty. This penalty is governed by how rapidly the volume away from the interface increases. In a micellar puck, the rods are assumed to be well aligned to get rid of the strong steric problems, and the chains are assumed to form a hemispherical shell at a radius of R from the disk with a constant surface density on this shell. The coils are strongly stretched inside the hemisphere. The model assumed

that coils travel in straight line trajectories, consistent with constant density constraints. After the chains have passed this hemisphere, they are assumed to have radial trajectories as if they emanated from the center of the puck. This model has only one free parameter R to minimize free energy. The main disadvantage of forming the hockey puck relative to lamellae is the creation of an extra surface, for which they pay a surface energy penalty. WF, following the SV approach, included the hockey puck micelle phase in the phase diagram by comparing the free energy of micelle to that of the lamellar structures (Figure 1-6).

Müller and Schick (MS) studied the phase behavior of rod-coil molecules by applying the numerical selfconsistent field theory within the weak segregation limit.[21] In the strong segregation limit at high incompatibilities, MS used a brush-like approximation to determine the phase boundaries. Their most interesting finding was that in stable morphologies the coils are on the convex side of the rod-coil interface. This result emphasizes the importance of the conformational entropy of the flexible component, which is increased when the coil occupies the larger space on the convex side of the interface. They also found that the extreme structural asymmetry in rod-coil blocks has a pronounced influence on the phase diagram. The wide region encompassing cylinder phase was also predicted in the phase diagram of a rod-coil block copolymer in the weak segregation limit. Matsen and Barrett also applied the selfconsistent field techniques to the SV model for lamellar structures.[22] Their theory predicts a nematic phase composed by the mixing of rods and coils when $\chi N < 5$. By increasing χN, the various lamellar phases appear as a stable phase.

Scaling approaches have been used to theoretically predict the structures of rod-coil block molecules in a selective solvent.[23-25] Halperin investigated the transition between smectic A and smectic C by comparing interfacial and coil deformation free energy. Since the tilt increases the surface area per coil, tilting is

favored when the stretching penalty of the coil is dominant. At high *f*, the suggested shape of the stable micelle was similar to hockey puck structure presented by WF. In addition, Raphael and de Gennes suggested "needles" and "fence" morphologies of coil-rod-coil triblock copolymers in a selective solvent.

1-3.2 Rod-Coil Copolymers Based on Helical Rods

Polymers with a stiff helical rod-like structure have many advantages over other synthetic polymers because they possess stable secondary structures due to cooperative intermolecular interactions. An example of polymers with helical conformation is polypeptides in which the two major structures include α-helices and *β*-sheets. The α-helical secondary structure enforces a rod-like structure, in which the polypeptide main chain is coiled and forms the inner part of the rod.[26] This rod-like feature is responsible for the formation of the thermotropic and lyotropic liquid crystalline phases. Polypeptide molecules with α-helical conformation in the solution are arranged with their long axes parallel to each other to give rise to a nematic liquid crystalline phase. However, even long chain polypeptides can exhibit a layered supramolecular structure, when they have a well-defined chain length. For example, the monodisperse poly(α,L-glutamic acid) prepared by the bacterial synthetic method assembles into smectic ordering on length scales of tens of nanometers.[27,28]

Incorporation of an elongated coil-like block to this helical rod system in a single molecular architecture may be an attractive way of creating new supramolecular structures due to its ability to segregate incompatible segment of individual molecules. The resulting rod-coil copolymers based on a polypeptide segment may also serve as models providing insight into the ordering of complicated biological systems.

Low molecular weight block copolymers consisting of poly(γ-benzyl-L-glutamate) with degrees of polymerization of 10 or 20 and polystyrene with degree of polymerization of 10 were synthesized by Klok, Lecommandoux, and a co-worker.[29] The rod-coil polymer was observed to exhibit thermotropic liquid-crystalline phases with assembled structures that differ from the lamellar structures. Incorporation of a polypeptide segment into a polystyrene segment was observed to induce a significant stabilization of the α-helical secondary structure as confirmed by FT-IR spectra. However, small-angle X-ray diffraction patterns indicated that α-helical polypeptides do not seem to assemble into hexagonal packing for the rod-coil copolymer with 10 γ-benzyl-L-glutamate repeating units. The amorphous character of the polystyrene coil is thought to frustrate a regular packing of the α-helical fraction of the short polypeptide segments. Increasing the length of the polypeptide segment to a DP of 20 gives rise to a strong increase in the fraction of diblock copolymers with α-helical polypeptide segment. By studying this block copolymer with small-angle X-ray analysis, a 2-D hexagonal columnar supramolecular structure was observed with a hexagonal packing of the polypeptide segments adopting an 18/5 α-helical conformation with a lattice constant of 16 Å. The authors proposed a packing model for the formation of the "double-hexagonal" organization (Figure 1-7). In this model, the rod-coil copolymers are assembled in a hexagonal fashion into infinitely long columns, with the polypeptide segments oriented perpendicularly to the director of the columns. The subsequent supramolecular columns are packed in a superlattice with hexagonal periodicity parallel to the α-helical polypeptide segments with a lattice constant of 43 Å.

1-3.3 Rod-Coil Copolymers Based on Mesogenic Rods

It is well-known that classical rod-like mesogenic molecules arrange themselves with their long axes parallel to each other to give rise to nematic and/or layered smectic types of supramolecular structures.[31,32] Because of the preferred parallel arrangement of the rigid, rod-like units, the formation of curved interfaces is strongly hindered in the mesogenic rods. On the contrary, rod-coil block systems based on mesogenic rods can provide a variety of supramolecular structures due to the effect of microphase separation and the molecular anisometry of rod block. Even though the molecular weight is very small, microphase separated structures can form due to large chemical differences between each block.

Stupp et al. synthesized triblock rod-coil copolymers containing oligostyrene-*block*-oligoisoprene as the coil block and three biphenyl units connected by ester linkages as the rod block (Scheme 1-1).[32,33] Carboxylic acid functionalized coil block was prepared by anionic sequential living polymerization of styrene and then isoprene, followed by end capping with CO_2. The resulting coil block was then connected to a rigid block made up of two biphenyl units through a ester bond, followed by deprotection at the phenolic terminus. The final rod-coil copolymers were synthesized by following the same sequence of reactions, i.e., esterification and then subsequent deprotection of a protecting silyl group. The rod-coil copolymer containing a (styrene)$_9$- (isoprene)$_9$ block oligomer as coil segment was observed to self-assemble into uniform narrow-sized aggregates and to subsequently organize into a superlattice with periodicities of 70 and 66 Å as evidenced by transmission electron microscopy (Figure 1-8a) and small-angle electron diffraction.[32] The wide-angle electron diffraction pattern revealed an a*b* reciprocal lattice plane, suggesting that the rod segments are aligned axially with their preferred direction with respect to the plane normal of the layer with long-range order. Transmission electron microscopy of the microtomed sections revealed a layered structure with characteristic periods of the

70 Å layers consisting of one dark and one light band with thicknesses of 30 and 40 Å, respectively. On the basis of these experimental data together with molecular modeling calculations, the authors proposed that these rod-coil copolymers self-assemble into fascinating mushroom-shaped supramolecular structures containing 100 rod-coil molecules with a molar mass about 200 kD, which assemble in a "cap to stem" arrangement (Figure 1-8b). Spontaneous polar organization in this system was reported and was presumably due to the nature of the supramolecular units of molecule preformed in solution. Both microphase separations between the two coil blocks and the crystallization of the rod segments are likely to play important roles in the formation of the unusual mushroom-shaped aggregate. This leads to the asymmetrical packing of the nanostructures that form micrometer-sized platelike objects exhibiting tapelike characteristics with nonadhesive-hydrophobic and hydrophilic-sticky oppsite surfaces.

1-3.4 Rod-Coil Copolymers Based on Conjugated Rods

As a result of great interest in the optically and electronically active properties of highly conjugated and stiff rod-like molecules, a variety of oligomers and polymers have been synthesized to establish the molecular structure and property relationship.[35,35] In addition to molecular structure, supramolecular structure was reported to have a dramatic effect on the physical properties of conjugated rodlike molecules.[36,37] Thus, manipulation of supramolecular structure in conjugated rods is of paramount importance to achieving efficient optophysical properties in solid-state molecular materials. One way to manipulate the supramolecular structure might be incorporation of the conjugated rod into a rod-coil molecular architecture which would allow formation of well-defined one-, two-, or three-dimensional conjugated

domains in nanoscale dimensions. Here, we will introduce the studies of rod-coil systems based on well-defined conjugated rods.

Müllen et al. prepared perfectly endfuctionalized oligo(2,5-diheptyl-*p*-phenylenes) (Scheme 1-2).[38] Further reaction of the end functionalized rod with either polystyrene or poly(ethylene oxide) yielded corresponding luminescent rod-coil block copolymers (**6** and **7**, respectively). Rod-coil copolymers consisting of poly(*p*-phenyleneethynylene) as the rod block and poly(ethylene oxide) as the coil block (**8**) were also synthesized by coupling reaction of monofunctionalized rod to poly(ethylene oxide) (Scheme 1-2).[39] More recently, the synthesis of triblock poly(isoprene*block*- *p*-phenyleneethynylene-*block*-isoprene) (**9**) was reported by Godt et al. by using hydroxy functionalized polyisoprene (Scheme 1-2).[40] Lazzaroni et al. showed that rod-coil copolymers containing poly(*p*-phenylene) or poly(*p*-phenyleneethynylene) as the rod segments have a strong tendency to spontaneously assemble into stable ribbonlike fibrillar morphology when coated on mica substrate as evidenced by AFM images.[41] The ribbonlike supramolecular structure was proposed that in the first observed layer, the conjugated segments are packed according to a head-to-tail arrangement with their conjugated system parallel to each other surrounded by coil segments (Figure 1-9). A similar ribbonlike morphology was also observed from rodcoil copolymers consisting of poly(*p*-phenylene) as the rod block and poly(methyl methacrylate) as the coil block.[42]

Jenekhe et al. reported on the self-assembling behavior of rod-coil diblock copolymers consisting of poly(phenylquinoline) as the rod block and polystyrene as the coil block (Scheme 1-3).[43,44] The rod-coil copolymers were prepared by condensation reaction of ketone methylene-terminated polystyrene and 5-acetyl-2-aminobenzophenone in the presence of diphenyl phosphate. The degree of polymerization of the conjugated rod block in the rod-coil copolymers was controlled

by the stoichiometric method. These block copolymers were found to self-assemble into fascinating supramolecular structures, although the rod block might not be monodisperse. For example, a rod-coil copolymer consisting of poly(phenylquinoline) with a degree of polymerization of 50 of polystyrene with degree of polymerization of 300 was observed to aggregate in the form of hollow spheres, lamellar, hollow cylinders, and vesicles in a selective solvent for the rod segment (Figure 1-10). The observed shape of supramolecular structures was dependent on the type of solvent mixture and drying rate. Photoluminescence emission and excitation studies showed that the photophysical properties strongly depend on the supramolecular structure of π-conjugated rod segments. Interestingly, their rod-coil systems proved to be possible for encapsulating fullerenes into the spherical cavities. As compared to conventional solvent for C_{60}, such as dichloromethane or toluene, the solubility is enhanced by up to 300 times when the molecules are encapsulated into micelles. In a further study, the authors observed that these rod-coil copolymers in a selective solvent for the coil segment self-assemble into hollow spherical micelles with diameters of a few micrometers, which subsequently self-organize into a 2-dimensional hexagonal superlattice (Figure 1-11).[45] Solution-cast micellar films were found to consist of multilayers of hexagonally ordered arrays of spherical holes whose diameter, periodicity, and wall thickness depend on copolymer molecular weight and block composition.

1-4 Introduction to the Honeycomb Morphology and the "breath figures" Method

A variety of templating methods that use self-assembly can create structures with submicrometer dimensions. Recent developments using colloidal crystal

templating allow the preparation of ordered macroporous materials that have three-dimensional (3D) ordering of pores with dimensions of tens to thousands of nanometers.[46-48] With macroporous materials formed by colloidal crystal templating, colloidal crystals of polystyrene or silica spheres are infiltrated with a fluid that fills and solidifies in the vacant space between the spheres. In a subsequent step, the templating spheres are removed by either thermal decomposition or solvent extraction, thus creating a solid skeleton that contains a 3D array of pores whose dimensions match those of the templating spheres. It is obvious that the dominant length scale of the porous solid formed by such methods is "built in" by the template used, thus making dynamic control of the length scale virtually impossible.

Here, we introduce a simple and robust method that uses evaporative cooling to form ordered structures with dimensions that can be controlled from about 0.20 to 2 μm. The ordered structures are formed by evaporating solutions of a simple coil-like polymer in a volatile solvent, in the presence of moisture with forced airflow across the solution surface. A hexagonally packed array of holes then forms on the surface of the polymer. When a solvent less dense than water is used, such as benzene or toluene, the hexagonal array propagates through the film. In contrast, in samples generated from a solvent more dense than water, such as carbon disulfide (CS_2), only a single layer of pores is formed and a 3D array is not produced.

When moist air is in contact with a cold surface (solid or liquid), moisture condenses, forming water droplets that grow with time and form ordered patterns on the surface. Such a pattern formation has been termed "breath figures". The phenomenon of breath figures has been studied for over a century starting with the early works of Lord Rayleigh,[49] Baker,[50] and Aitken,[51] and more recently by knobler, Beysens, and co-works.[52]

The proposed model for the formation of ordered macroporous structures in

polystyrene films is illustrated in Figure 1-12. The high vapor pressure of the solvent and the velocity of air across the surface drive solvent evaporation, rapidly cooling the surface. This cooling leads to the nucleation and growth of water droplets that grow as a function of time. Airflow across the surface, coupled with convection currents on the solution surface due to evaporation, drive the ordering or packing of the water droplets into hexagonally packed arrays. Further, these structures are analogous to the "bubble rafts" that Bragg and Nye created using surfactant bubbles to model the motion of defects or dislocations in a crystal. When the surface is completely covered by water droplets, the temperature difference between the surface and the droplets eventually dissipates, and the droplets, being denser than the solvent, sink into the solution. Once the solution surface is free, the whole process of evaporative cooling, water droplet condensation and subsequent ordering repeats itself. Furthermore, the first layer of droplets can act as a template for successive layers, leading to the 3D architecture observed upon complete evaporation of the solvent. Once the film returns to ambient temperature, the condensed water and residual solvent evaporate, leaving behind the 3D polymer scaffold.

References

(1) Lehn, J. M. *Supramolecular Chemistry*; VCH: Weiheim, Germany, 1995.

(2) Loos, L.; Munoz-Guerra, S. *Supramolecular Polymers*; Marcel Dekker: New York, 2000.

(3) Leibler, L. *Macromolecules* **1980**, *13*, 1602.

(4) Bates, F. S. *Science* **1991**, *251*, 898.

(5) Fredrickson, G. H.; Bates, F. S. *Annu. Rev. Mater. Sci.* **1996**, *26*, 501.

(6) Riess, G.; Hurtez, C.; Badahur, P. "Block Copolymers", in *Encyclopedia of Polymer Science and Engineering*, 2nd ed,. Vol. 2; Kroschwitz, J. L.: Wiley, New York 1985.

(7) Chen, J. T.; Thomas, E. L.; Zinba, C. G.; Rabolt, J. F. *Macromolecules* **1995**, *28*, 5811.

(8) Urbas, A.; Fink, Y.; Thomas, E. L. *Macromolecules* **1999**, *32*, 4748.

(9) Urbas, A.; Sharp, R.; Fink. Y.; Thomas, E. L.; Xenidou, M.; Fetters, L. J. *Adv. Mater.* **2000**, *12*, 812.

(10) Goldacker, T.; Abetz, V.; Stadler, R.; Erukhimovich, I.; Leibler, L. *Nature* **1999**, *398*, 137.

(11) Abetz, V.; Goldacker, T. *Macromol. Rapid Commum.* **2000**, *21*, 16.

(12) Abetz, V.; Stadler, R. *Macromol. Symp.* **1997**, *113*, 19.

(13) Mogi, Y.; Nomura, M.; Kotsuji, H.; Ohnishi, K.; Matsushita, Y.; Noda, I. *Macromolecules* **1994**, *27*, 6755.

(14) Gido, S. P.; Schwark, D. W.; Thomas, E. L.; Goncalves, M. C. *Macromolecules* **1993**, *26*, 2636.

(15) Liu, G.; Ding, J.; Guo, A.; Herfort, M.; Bazett-Jones, D. *Macromolecules* **1997**, *30*, 1851.

(16) Liu, G.; Ding, J.; Stewart, S. *Angew. Chem. Int. Ed.* **1999**, *38*, 835.

(17) Semenov, A. N.; Vasilenko, S. V. *Sov. Phys. JETP S. V.* **1986**, *63* (1), 70.

(18) Semenov, A. N. *Mol. Cryst. Liq. Cryst.* **1991**, *209*, 191.

(19) Semenov, A. N.; Subbotin, A. V. *Sov. Phys. JETP S. V.* **1992**, *74* (4), 690.

(20) Williams, D. R. M.; Fredrickson, G. H. *Macromolecules* **1992**, *25*, 3561.

(21) Müller, M.; Schick, M. *Macromolecules* **1996**, *29*, 8900.

(22) Matsen, M. W.; Barrett. C. J. *Chem. Phys.* **1998**, *109*, 4108.

(23) Halperin, A. *Europhys. Lett.* **1989**, *10*, 549.

(24) Halperin, A. *Macromolecules* **1990**, *23*, 2724.

(25) Raphael, E.; de Gennes, P. G. *Makromol. Symp.* **1992**, *62*, 1.

(26) Gallot, B. *Prog. Polym. Sci.* **1996**, *21*, 1035.

(27) Zhang, G.; Fournier, M. J.; Mason, T. L.; Tirrell, D. A. *Macromolecules* **1992**, *25*, 3601.

(28) Yu, S. M.; Conticello, V. P.; Zhang, G.; kayser, C.; Fournier, M. J.; Mason, T. L.; Tirrell, D. A. *Nature* **1997**, *389*, 167.

(29) Klok, H.-A.; Langenwalter, J. F.; Lecommandoux, S. *Macromolecules* **2000**, *33*, 7819.

(30) Collings, P. J.; Hird, M. *Introduction to Liquid Crystals*: Taylor & Francis: London, 1997.

(31) Stegemeyer, H. *Liquid Crystals*; Springer: New York, 1994.

(32) Stupp, S. I.; Lebonheur, V.; Walker, K.; Li, L. S.; Huggins, K. E.; Keser, M.; Amstutz, A. *Science* **1997**, *276*, 384.

(33) Pralle, M. U.; Whitaker, C. M.; Braun, P. V.; Stupp, S. I. *Macromolecules* **2000**, *33*, 3550.

(34) Kraft, A.; Grimsdale, A. C.; Holmes, A. B. *Angew. Chem., Int. Ed.* **1998**, *37*, 402.

(35) Segura, J. L.; martin, N. *J. Mater. Chem.* **2000**, *10*, 2403.

(36) Osaheni, J. A.; Jenekhe, S. A. *J. Am. Chem. Soc.* **1995**, *117*, 7389.

(37) Berresheim, A. J.; Müller, M.; Müller, K. *Chem. Rev.* **1999**, *99*, 1747.

(38) Marsitzky, D.; Brand, T.; Geerts, Y.; Klapper, M.; Müllen, K. *Macromol. Rapid Commun.* **1998**, *19*, 385.

(39) Francke, V.; Räder, H. J.; Müllen, K. *Macromol. Rapid Commun.* **1998**, *19*, 275.

(40) KuKula, H.; Ziener, U.; Shöps, M.; Godt, A. *Macromolecules* **1998**, *31*, 5160.

(41) Leclere, P.; Calderone, A.; Marsitzky, D.; Francke, V.; Geerts, Y.; Müllen, K.; Bredas, J. L.; Lazzaroni, R. *Adv. Mater.* **2000**, 12, 1042.

(42) Leclere, P.; Parente, V.; Bredas, J. L.; Francois, B.; Lazzaroni, R. *Chem. Mater.* **1998**, *10*, 4010.

(43) Jenekhe, S. A.; Chen, X. L. *Science* **1998**, *279*, 1903.

(44) Chen, X. L.; Jenekhe, S. A. *Langmuir* **1999**, *15*, 8007.

(45) Jenekhe, S. A.; Chen, X. L. *Science* **1999**, *283*, 372.

(46) Holland, B. T.; Blanford, C. F.; Stein, A. *Science* **1998**, *281*, 538.

(47) Kulinowski, K. M.; Jiang, P.; Vaswani, H.; Colvin, V. L. *Adv. Mater.* **2000**, *12*, 833.

(48) Velev, O. D.; Jede, T. A.; Lobo, R. F.; Lenhoff, A. M. *Nature* **1997**, *389*, 447.

(49) (a) Lord Rayleigh *Nature* **1911**, *86*, 416. (b) Lord Rayleigh *Nature* **1912**, *90*, 436.

(50) Baker, J. T. *Philos. Mag.* **1922**, *56*, 752.

(51) Aitken, J. *Nature* **1911**, *86*, 516.

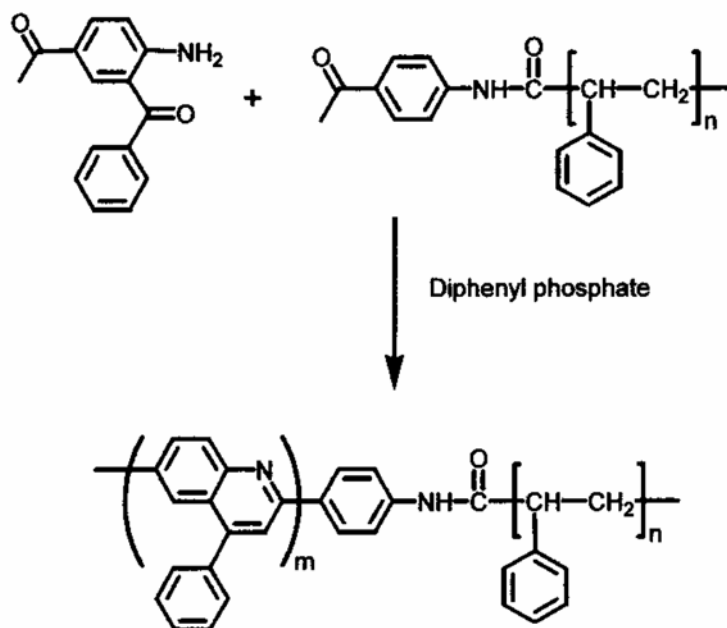(52) Beysens, D.; Steyer, A.; Guenoun, P.; Fritter, D.; Knobler, C. M. *Phase Transitions* **1911**, *31*, 219.

Scheme 1-1.

Scheme 1-2.

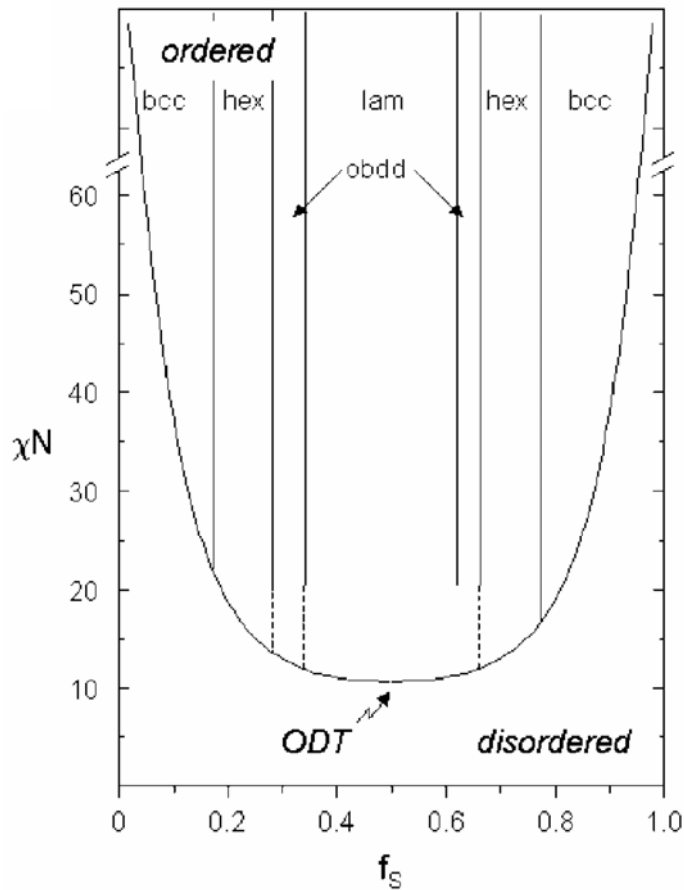R = C₇H₁₅, R' = H, C₆H₅

Scheme 1-3.

Diphenyl phosphate
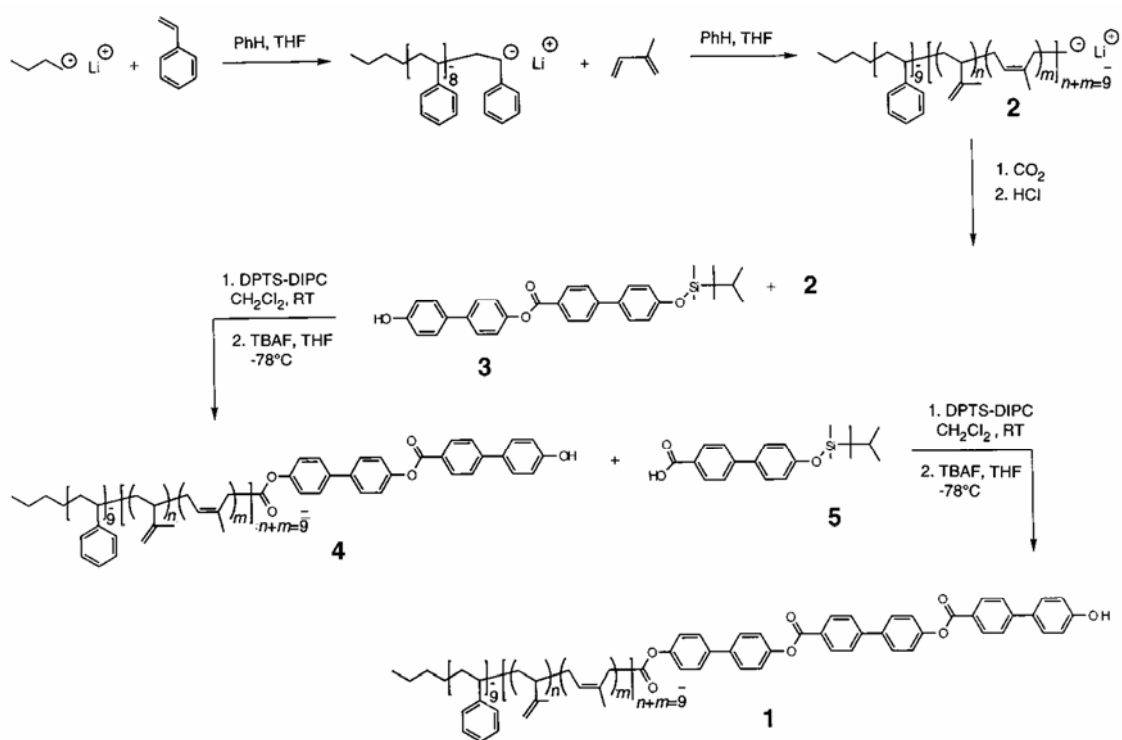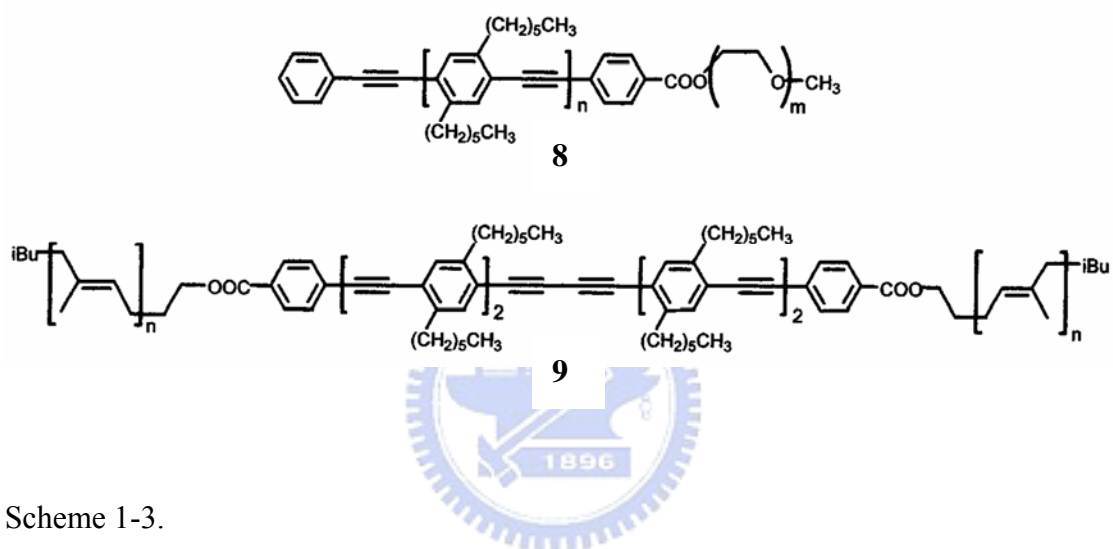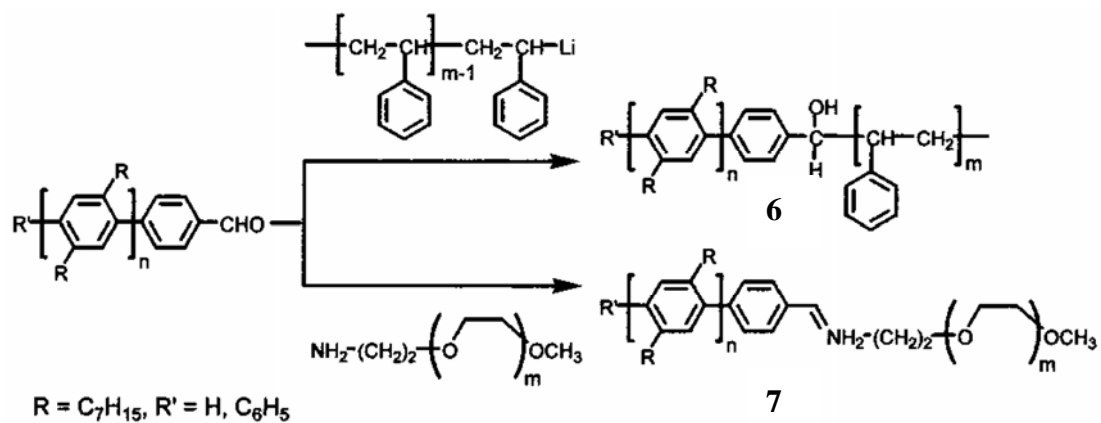
Figure 1-1: Experimental phase diagram for polystyrene-*b*-polyisoprene diblock copolymers.
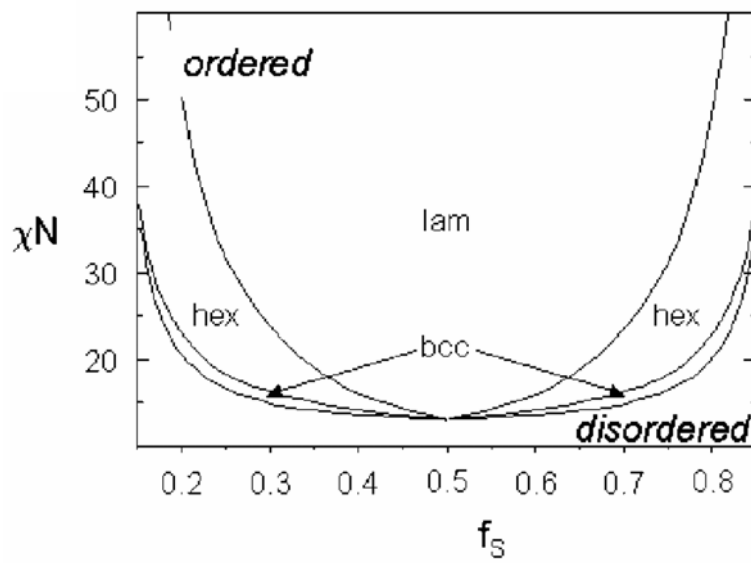

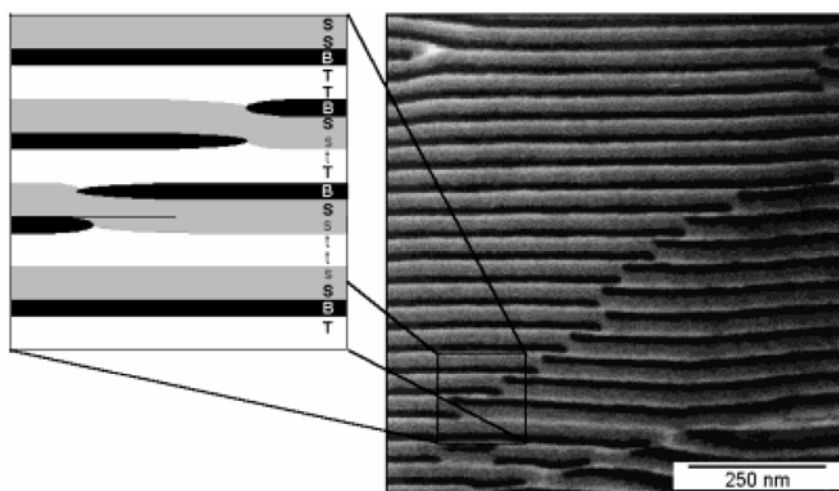Figure 1-2: Theoretical phase diagram for a diblock copolymer near the ODT.

Figure 1-3: Transmission electron micrograph of a blend containing 75 wt.-% of a polystyrene-*b*-polybutadiene-*b*-poly(*tert*-butyl methacrylate) (SBT) triblock copolymer and 25 wt.-% of a polystyrene-*b*-poly(*tert*-butyl methacrylate) (st) diblock copolymer. The non-centrosymmetric supramolecular structure of this blend is schematically illustrated in the diagram that assigns the different phases observed in the marked part of the micrograph.
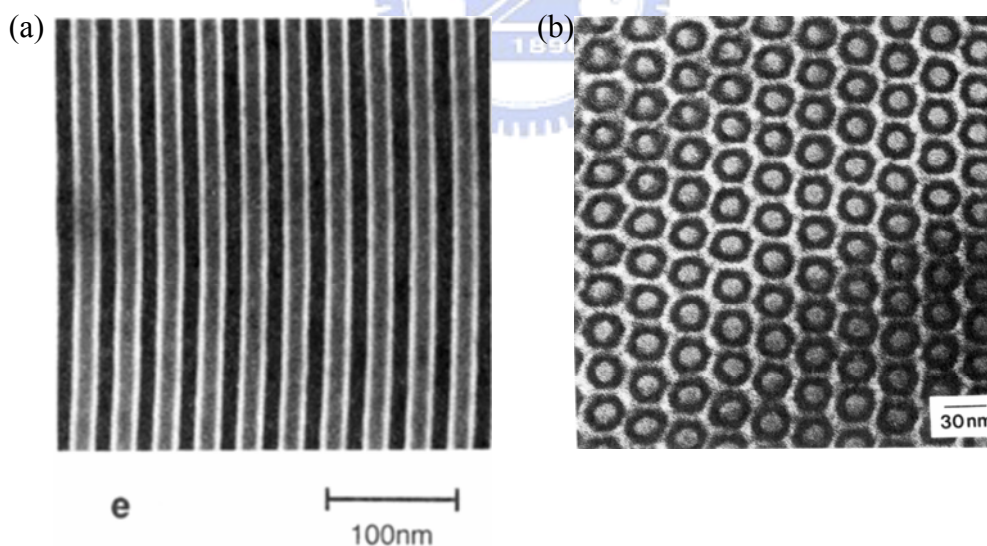
(a)   (b)

Figure 1-4: Transmission electron micrographs of (a) polyisoprene-*b*-polystyrene-*b*-polyvinylpyridine. (From Ref. 13) (b) Axial TEM projection of hexagonally packed structural units. The darkest regions correspond to the OsO_4,-stained PI domains, while the gray regions are CH_3I-stained P2VP domains. (From Ref. 14)
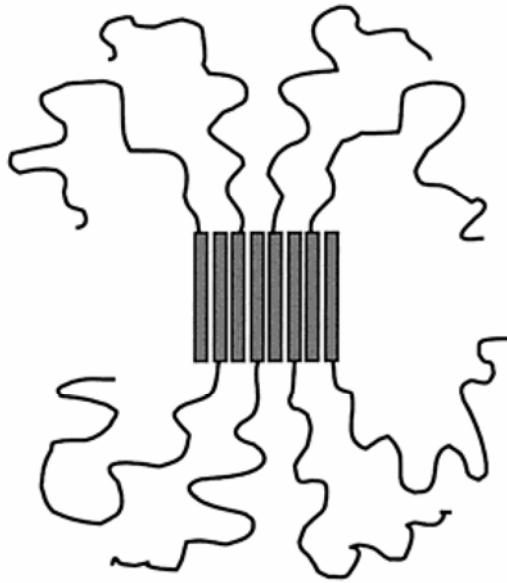
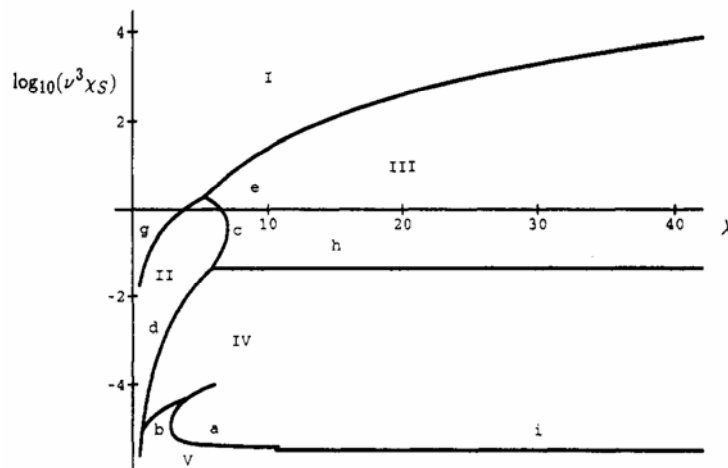Figure 1-5: Schematic representation of a monolayer puck.

Figure 1-6: Phase diagram including the hockey puck and lamellae phases. The phases are (I) bilayer lamellae, (II) monolayer lamellae, (III) bilayer hockey pucks, (IV) monolayer hockey pucks, and (V) incomplete monolayer lamellae. $\text{Log}(v^3\chi_s)$ is plotted against λ. $\lambda = \phi/(1-\phi)$ where ϕ is the volume fraction of the coil. $v = \kappa/\lambda$ and $\kappa = Na^2/L^2$ where the coil part is assumed to consist of N segments with a mean-square separation between adjacent segments of $6a^2$, and L is the rod length. χ is the Flory-Huggins interaction parameter.
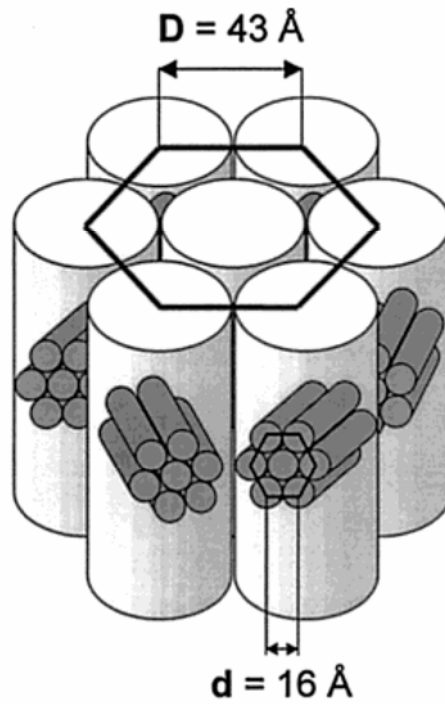
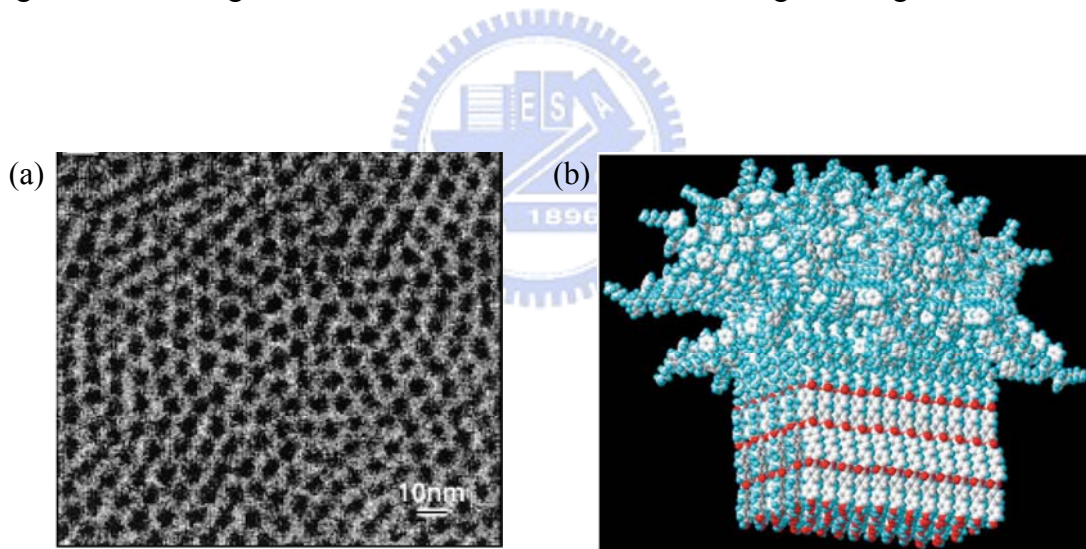Figure 1-7: Packing model for the formation of "double-hexagonal" organization.

Figure 1-8: (a) TEM image. (b) Schematic packing structure of rod-coil copoloymer.
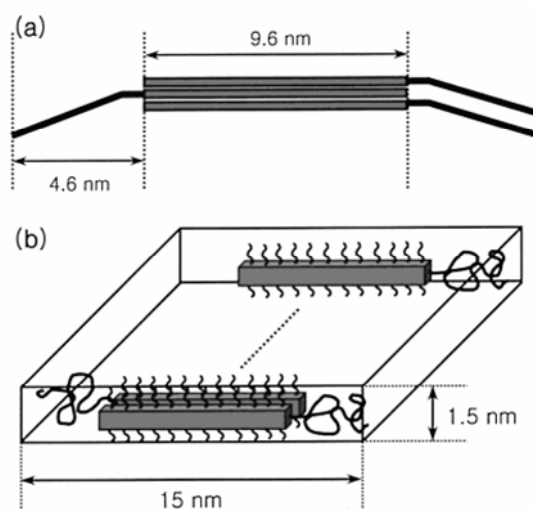
Figure 1-9: (a) Schematic molecular arrangement of three head-to-tail PPE-*block*-PDMS. (b) Schematic representation of the ribbonlike supramolecular structure formed by PPE-*block*-PDMS.
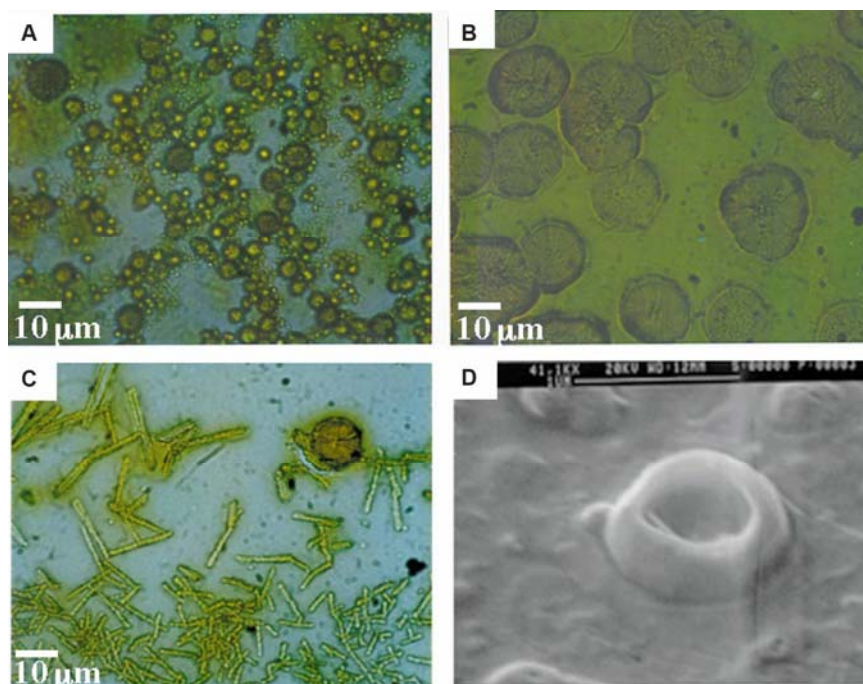
Figure 1-10: Optical (**A** to **C**) and scanning electron (**D**) micrographs of the typical morphologies of PPQ_{50}-PS_{300}. Drops of dilute solutions (0.5 to 1.0 mg/ml) of the diblock copolymers were spread and dried on glass slides and aluminum substrates, respectively. (A) Spherical aggregates (1:1 TFA:DCM, v/v, 95 °C); (B) lamellae (1:1 TFA:DCM, 25 °C); (C) cylinders (9 :1 TFA:DCM, 25 °C); and (D) vesicles (1:1–1:4 TFA:DCM, 25 °C).

(a)

PPQ_mPS_n

Rod   Coil

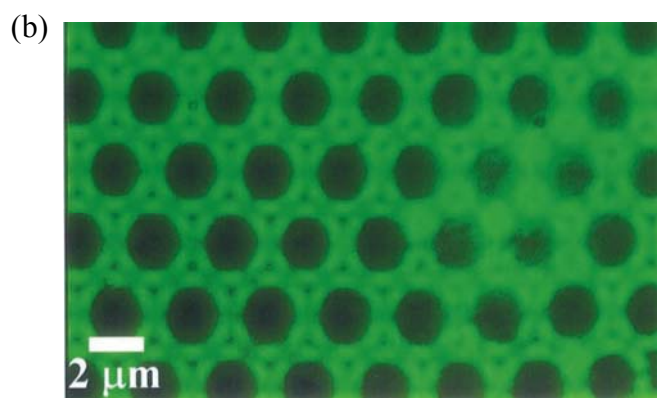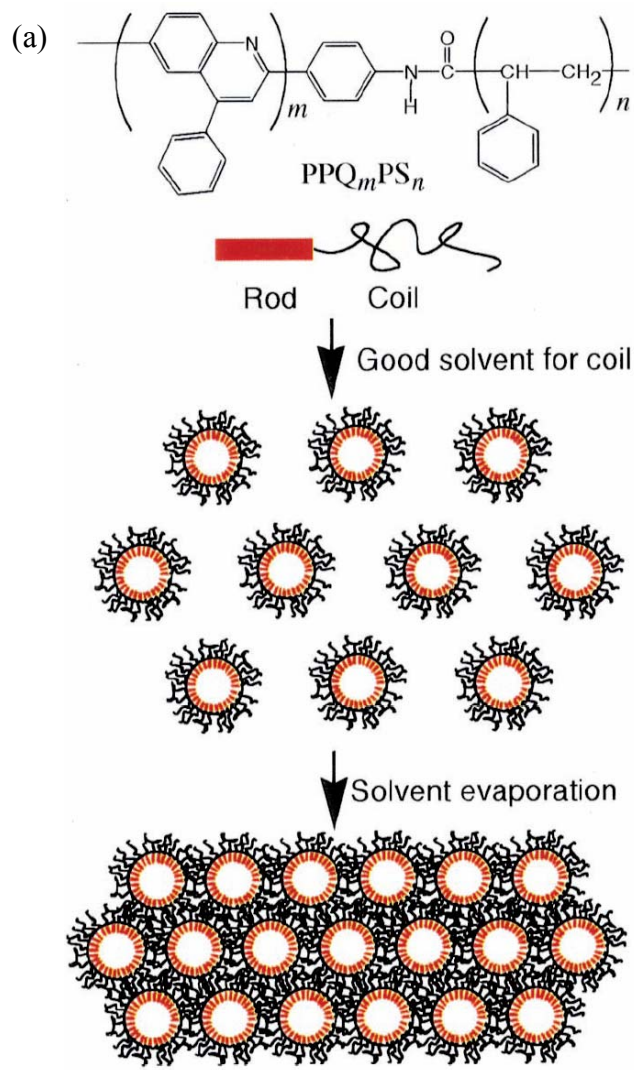Good solvent for coil

Solvent evaporation

(b)

2 μm

Figure 1-11: (a) Schematic representation of hierarchical self-organization of PPQ-*b*-PS into ordered microporous structure. (b) Fluorescence photomicrograph of solution-cast micellar film of PPQ_m-*b*-PS_n with *m* =10 and *n* = 300.
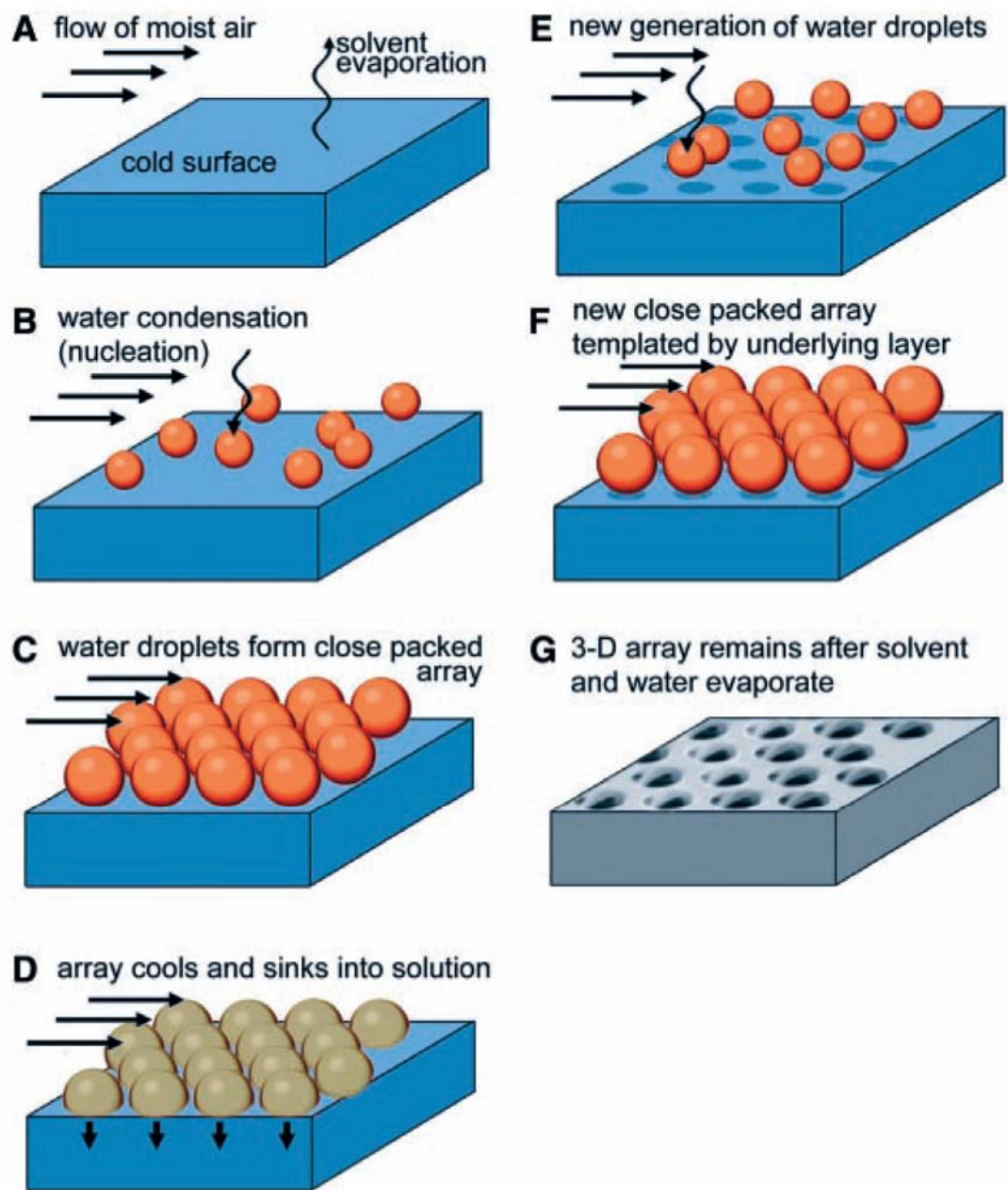
Figure 1-12: A model for the formation of the structure in polymer films.

Chapter 2

Introduction to Hydrogen Bonds in Polymer Blends

2-1 Polymer Blend

The production of polymer materials has grown rapidly in the past 50 years. The versatility of plastics, not exceeded by any other class of materials, guarantees that polymers will continue to be very important in the future. However, at present a distinct change is taking place in polymer research and development. In the pioneering days of plastics, new polymer properties were determined by the choice of suitable new monomers. Today the commercialization of polymers from new monomers is restricted to a few specialities. On the other hand, the number of new polymer blends and alloys based on known polymers is increasing very rapidly. The market for polymer blend based materials has increased continuously during the past two decades.

Polymer blending is a convenient route for the development of new polymeric materials, able to yield materials with property profiles superior to those of the individual components. This method is usually cheaper and less time-consuming for the creation of polymeric materials with new properties than the development of new monomers and/or new polymerization routes. An additional advantage of polymer blends is that the properties of the materials can be tailored by combining component polymers and changing the blend composition.

Polymer blends are either homogeneous or heterogeneous. In homogeneous blends, the final properties are often an arithmetic average of the properties of the blend components. In heterogeneous blends, the properties of all blend components are present. A deficiency in the properties of one component can be camouflaged to a certain extent by strengths of the others.

The role of polymer interaction in determining the phase behavior of polymer blends is fascinating from a number of concentrations. Polymer interactions are usually meaning "strong," specific, and orientation dependent. In polymer blends, most it has been widely concerned with the following intermolecular or inter-segment forces:

(a) Strong dipoles

(b) Hydroghen bonds

(c) Charge transfer complexes

(d) Ionic interactions in ionomers

Although a few studies of miscibility in blends where polymer segments interact through charge transfer complexes and ionic forces have appeared, by far the most common and important systems involving strong interactions are those involving hydrogen bonds and /or strong dipole interactions.

In 1995, Coleman and Painter published an excellent review on hydrogen-bonded polymer blends. This review mainly dealt with the association models and the related theories. Since then, there has been significant progress in the field of hydrogen bonded polymer blends through the work of many research groups, with several hundred papers published since 1995.

2-2 Introduction to Painter-Coleman Association Model

Homogeneous miscibility in polymer blends requires a negative free energy of mixing, that is $\Delta G_{mix} < 0$. According to Flory–Huggins equation:

$$\frac{\Delta G_{mix}}{RT} = \frac{\Phi_1}{N_1} \ln \Phi_1 + \frac{\Phi_2}{N_2} \ln \Phi_2 + \chi_{12} \Phi_1 \Phi_2 \tag{1}$$

where ΔG_{mix} is the change of free energy on mixing two polymers, R is the gas constant, T is the temperature, Φ_1 and Φ_2 are the volume fractions and N_1 and N_2 are

the segment numbers of the two blend components, respectively, and χ_{12} is the Flory

interaction parameter. When two high molecular weight polymers are blended, the

gain in entropy, $\Phi_1\ln(\Phi_1)/N_1+\Phi_2\ln(\Phi_2)/N_2$, is quite small, and the free energy of

mixing, ΔG_{mix}, can be negative only if the heat of mixing is near zero or negative. The

third term of Eq. 1 contains the ubiquitous Flory interaction parameter χ, and

expresses a generally unfavorable contribution (except in rare cases when $\chi = 0$) to

the free energy of mixing emanating from so-called "physical" forces. Values of χ for

polymer mixtures appear to be estimated fairly accurately from Eq. 2,

$$\chi = \frac{V_B}{RT}(\delta_A - \delta_B)^2 \tag{2}$$

using solubility patameters (denoted δ_A, δ_B for (co)polymer A and B, respectively)

calculated from group molar attraction and molar volume constants that were derived

from a set of model compounds that do not self-associate to any measurable extent (i.e.

molecules in which the interaction forces are dispersive or only weakly polar in

nature).

Painter and Coleman used association model to describe hydrogen bonding

interactions and simply added this contribution to the Flory-Huggins equation for the

free energy of mixing:

$$\frac{\Delta G_m}{RT} = N_B \ln \Phi_B + N_A \ln \Phi_A + n_B \Phi_A \chi + \frac{\Delta G_H}{RT} \tag{3}$$

where N_B, N_A are the number of polymer molecules present and n_B is the total number

of B segments. In essence, this is the classic Flory/Huggins equation plus an

additional term, $\Delta G_H/RT$, that accounts for the (generally favorable) free energy

contribution that arises from "chemical" forces. The free energy contribution from

$\Delta G_H/RT$ was originally derived using a simple association model. For the

uncomplicated equilibrium scheme depicted below:

$$B_h + B_1 \xleftrightarrow{\quad K_B \quad} B_{h+1}$$

$$B_h + A \xleftrightarrow{\quad K_A \quad} B_h A$$
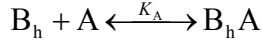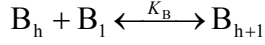
where the distribution of hydrogen bonded species in the polymer blend may by adequately described by two equilibrium constants, one that describes "chain-like" self-association, K_B, and the other that describes interassociation, K_A, $\Delta G_H/RT$ was expressed as:

$$\frac{\Delta G_H}{RT} = \sum n_{B_h} \ln\left(\frac{\Phi_{B_h}}{h}\right) + \sum n_{B_h A} \ln\left(\frac{\Phi_{B_h A}}{h+r}\right) + n_{A_1} \ln\left(\frac{\Phi_{A_1}}{r}\right) + n_{BB}^h + n_{AB}^h +$$

$$\text{(terms in z and } \sigma) - \left[n_B \ln \Phi_B + n_A \ln \Phi_A\right] - n_{BB}^h \ln K_B - n_{AB}^h \ln K_A \qquad (4)$$

The association model (from Flory) were used to describes the mixing of small molecules, or in effect, describes the mixing of disconnected polymer segments and therefore contains an excess combinatorial entropy of mixing (ΔS_{excess}), which must be subtracted. The excess entropy term is contained in the square bracket of Eq. 4.

With the "physical" force deduced from solubility parameters, ΔG_H may be determined from the equilibrium constants and enthalpies of hydrogen bond formation. As the combinatorial entropy is very small, the free energy of mixing, and thus the miscibility, are dominated by the balance of the "physical" force and enthalpy of hydrogen bond formation.

2-3 Intramolecular Screening and Functional Group Accessibility Effects in

Polymer Blends

Sets of equilibrium constants that describe the distribution of hydrogen bonded species for a particular miscible polymer blend system as a function of composition and temperature, [e.g., blends of poly(4-vinyl phenol) (PVPh) with poly(vinyl acetate)

33

(PVAc)], may be experimentally determined from measurements of the fraction of intermolecular hydrogen bonded acceptor groups (carbonyls in the case of PVPh/PVAc blends) using infrared spectroscopy.[1,2] It was very quickly established, however, that if these experimentally determined equilibrium constant values were used to calculate the contribution to the free energy of mixing from the $\Delta G_H/RT$ term (Eq. 4), its magnitude was seriously underestimated. Accordingly, the predicted phase diagrams (and their close relatives, miscibility windows and miscibility maps) calculated from the derivatives of the total free energy of mixing (Eq. 3) were inconsistent with experimental observations of phase behavior. An example is shown at the top of Figure 2-1. PVPh forms single phase mixtures over the entire composition range and at temperatures from at least ambient to 200 ^{o}C (before the onset of serious degradation) with an ethylene-*stat*-vinyl acetate copolymer that contains 70 wt.-% vinyl acetate (EVA[70]). However, using the equilibrium constant values experimentally determined from an infrared analysis of the fraction of hydrogen bonded carbonyl groups in PVPh/EVA[70]-films,[2] the spinodal phase diagram seen at the top of Figure 2-1 (calculated from the derivatives of Eqs. 3 and 4) predicts an immiscible system from −100 to 300 ^{o}C (i.e., not a single phase over the entire composition range at a particular temperature).

After much debate, Coleman et al. concluded that the magnitude of the excess entropy term (that contained in the square bracket of Eq. 4) was the source of the problem, i.e.,

$$\Delta S_{excess} = -\left[n_A \ln \Phi_A + n_B \ln \Phi_B \right] \tag{5}$$

which results in a negative contribution from the $\Delta G_H/RT$ term that is too small. They convinced ourselves that the above excess entropy term was not applicable to hydrogen bonded polymer blends because one component (B) also form dynamic

networks of hydrogen bonded "chains" in the pure state, and that a modified excess entropy term,

$$\Delta S_{\text{excess}} = -\left[n_A \ln \Phi_A + \frac{n_B}{\bar{h}_0} \ln \Phi_B \right] \qquad (6)$$

where $\bar{h}_0$ is the number average length of the hydrogen bonded "chains" formed in pure B, was more appropriate (see ref. 2 for a rationalization of this concept). With this modification to the excess entropy term in Eq. 4 everything appeared to fall into place. Now the predicted phase diagram of the PVPh/EVA[70] blend system, shown at the bottom of Figure 2-1, reflected experimental reality. Furthermore, using experimental equilibrium constant values that were obtained from this single miscible PVPh/EVA[70] blend system, Painter and Coleman were able to predict (details are again given in ref. 2) with remarkable accuracy, phase diagrams, miscibility windows and maps for (co)polymer blend systems having similar intermolecular hydrogen bonding interactions (i.e., phenolic hydroxyl/acetoxy carbonyl interactions). For exegetic purposes we show at the top of Figure 2-2 the predicted miscibility map for styrene-*stat*-4-vinyl phenol (STVPh) copolymer blends with ethylene-*stat*-vinyl acetate (EVA) copolymers calculated using the regular solution excess entropy term (Eq. 5), while at the bottom of Figure 2-2 is that calculated using the modified excess entropy term (Eq. 6). The latter is almost a perfect match to experimental observations (the large white and black filled circles represent experimentally verified miscible and immiscible blend systems, respectively), but the former, while predicting overall trends reasonably well, does a poor job in the predicting the miscibility maps.

So it is the rub that how to introduce the $\bar{h}_0$ parameter into the denominator of the term of Eq. 6. In effect, Coleman et al. essentially removed its contribution (i.e., reduced its magnitude to close to zero) which, in turn, increased the negative free

energy contribution from the $\Delta G_H / RT$ term in Eq. 3 by an amount that fortuitously brought the theoretical predictions and experimental observations into close agreement. In other words, the $\bar{h}_0$ parameter was a "fudge" factor that was compensating for something that they evidently had not taken into consideration.

At about the same time Coleman et al. had occasion to experimentally measure the fraction of hydrogen bonded carbonyl groups present in miscible (single phase) blends of PVPh with poly(ethyl methacrylate) (PEMA) as a function of composition and temperature. These results were compared to analogous ethyl methacrylate-*stat*-4-vinyl phenol (EMAVPh) copolymers, polymer solutions of PVPh and ethyl isobutyrate (EIB) and low molecular weight model mixtures of 4-ethylphenol (EPh) and EIB.[6] There were significant differences in the equilibrium fraction of intermolecular hydrogen bonded carbonyl groups that were formed for equivalent concentrations at the same temperature, which can be conveniently expressed in terms of a standard interassociation equilibrium constant, K_A^{Std} (at 25 $^{\circ}$C based upon a standard molar volume of $V_B = 100$ cm^3/mol). K_A^{Std} values of 38.4, 67.4, 168 and 170 dimensionless units were obtained for PVPh/PEMA blends, EMAVPh copolymers, PVPh/EIB solutions and EPh/EIB mixtures, respectively. These are large differences and factors such as chain connectivity, functional group accessibility, chain flexibility etc., obviously play a role to varying extents.[7-9]

In a recent publication[10] Coleman et al. suggested that equilibrium constants determined from appropriate low molar mass mixtures could be used to calculate the hydrogen bonding contribution to the free energy of mixing of analogous polymer blends, after due account is taken of factors attributed to chain connectivity. Two of the more important chain connectivity effects, intramolecular screening and functional group accessibility, have been previously proposed.

We commence to discuss these effects with a well-established miscible polymer blend system composed of two amorphous homopolymers, poly(4-vinylphenol) (PVPh) and poly(vinyl acetate) (PVAc). Dimensionless standard equilibrium constant values (based on a common reference molar volume $V_B = 100$ cm^3/mol) have previously been determined from appropriate low molecular mass analogues [4-ethylphenol (EPh) and ethyl isobutyrate (EIB)].[6] These standard equilibrium constants [$K_2^{Std} = 21.0$; $K_B^{Std} = 66.8$ (self-association) and $K_A^{Std} = 170$ (interassociation)] describe the fraction of the various hydrogen bonded species present in a solution of EPh/EIB as a function of composition at 25 ^{o}C. This represents the case where there are no effects due to chain connectivity and all the values remain constant regardless of blend composition (depicted at the top of Figure 2-3; $\gamma = 0$).

Chain connectivity effects modify equilibrium constant values. Intramolecular screening is accounted for through the parameter γ, which is defined as the fraction of same chain contacts that originate from the polymer chain bending back upon itself, primarily through local, but also through long range effects.[9] It is probably sufficient to simply state that new self-association equilibrium constants $\tilde{K}_B$ (and $\tilde{K}_2$) are calculated that are now a function of blend composition (Φ_B). For example:

$$\tilde{K}_B = K_B \left[\frac{\gamma + (1-\gamma)\Phi_B}{\Phi_B} \right] \tag{7}$$

Typical results are depicted at the bottom of Figure 2-3 using an appropriate γ value for high molecular weight polymer blends of 0.30.[9] On the other hand, the new interassociation equilibrium constant, $\tilde{K}_A$, is not a function of blend composition and is given by:

$$\tilde{K}_A = K_A \left[\frac{1 - (\gamma + (1-\gamma)\Phi_B)}{\Phi_A} \right] = K_A \ (1\text{-}\gamma) \tag{8}$$

This invariance is also depicted at the bottom of Figure 2-1, labeled $\tilde{K}_A$, and has a value of $170 \times 0.70 = 119$ (dimensionless units).

Functional group accessibility (FGA) is a generic term that Coleman et al. have introduced to describe the reduction in the number of intermolecular hydrogen bonds formed between complementary functional groups (e. g., phenolic hydroxyls and acetoxy carbonyls) in (co)polymer blends that arises from the close proximity of either or both functional groups in their respective (co)polymer chains.[7,8] Naturally, this effect is most acute in a blend of two homopolymers like PVPh and PVAc, but becomes less important as they consider blends of copolymers where the functional groups are spaced well apart. Elsewhere Painter and Coleman have described an empirical equation determined from experimental infrared studies that describes this effect for independent copolymers containing phenolic hydroxyls and acetoxy carbonyls. This equation has the form:

$$\tilde{K}_A = 112.4 - \left[\frac{1630}{70 + R_A} + \frac{4100}{100 + R_B} \right] \tag{9}$$

where R_A and R_B are the average molar volumes between VAc and VPh groups, respectively, in the specific repeat of the respective copolymers. For PVPh-PVAc blends the value of $\tilde{K}_A$ is calculated to be 55 dimensionless units. This is also depicted in Figure 2-3.

It is now a relatively straightforward task to employ the relevant stoichiometric equations using the different sets of equilibrium constant values discussed above and calculate the theoretical equilibrium fraction of hydrogen bonded acetoxy groups present in a single phase mixture of PVPh and PVAc as a function of blend composition at 25 °C.[1,2] The results are displayed in Figure 2-4. The top curve denotes the fraction of hydrogen bonded carbonyl groups for the $\gamma = 0$ case (calculated using compositionally invariant values of $K_2^{Std} = 21.0$; $K_B^{Std} = 66.8$ and $K_A^{Std} = 170$

dimensionless units). If we now "switch on" intramolecular screening by introducing a c value of 0.30 (now the self-association equilibrium constants, $\tilde{K}_2$ and $\tilde{K}_B$, are compositionally dependent, but the interassociation equilibrium constant is not and has a constant value of $\tilde{K}_A = 119$ dimensionless units), we obtain the middle curve.

Note that the fraction of hydrogen bonded carbonyl groups has decreased significantly over that calculated in the absence of intramolecular screening, especially for blends that are compositionally rich in PVPh. There are further substantial decreases when FGA effects are taken into account through Eq. 9, and this is depicted in the lower curve (here $\tilde{K}_2$ and $\tilde{K}_B$ are still compositionally dependent and $\tilde{K}_A$ now has a constant value of 55 dimensionless units). If we compare, for example, the theoretical fraction of hydrogen bonded carbonyl groups present in a single phase 60:40 wt.-% PVPh-PVAc blend for the three different cases, we obtain values of approximately 0.67 ($\gamma = 0$), 0.58 ($\gamma = 0.30$) and 0.45 ($\gamma = 0.30 + $ FGA). These are large differences that have profound repercussions on the amount of favorable free energy that is available from the changing pattern of the hydrogen bonds formed in the mixture relative to the pure components. Clearly, intramolecular screening and functional group accessibility (spacing) effects cannot be ignored if we are to successfully predict phase behavior of polymer blends.

In brief, the free energy of mixing may be expressed as:

$$\frac{\Delta G_m}{RT} = \left[\frac{\Phi_A}{M_A} \ln \Phi_A + \frac{\Phi_B}{M_B} \ln \Phi_B \right] + \Phi_A \Phi_B \left(1 - \gamma\right)\chi + \frac{\Delta G_H}{RT} \tag{10}$$

where Φ_A, Φ_B and M_A, M_B are the volume fractions and degrees of polymerization of (co)polymers A and B, respectively, χ is the Flory interaction parameter, γ the intermolecular screening parameter, and $\Delta G_H/RT$ the free energy contribution from hydrogen bonding. Again, this equation can be conveniently split into three major contributions to the total free energy of mixing:

(1) Combinatorial entropy; a relatively small, but favorable to mixing contribution contained in the square brackets of Eq. 10.

(2) The χ (or "physical forces") term; an unfavorable contribution (except in rare cases when $\chi = 0$) that is essentially determined by the difference in the non-hydrogen bonding solubility parameters of the two (co)polymers and modified by the value of the intramolecular screening parameter, γ (i. e. there are more same chain contacts than would be found on the basis of a Flory approximation of a random mixing of segments).

3) The hydrogen bonding (or "chemical forces") term; a generally favorable to mixing contribution that is determined by the respective equilibrium constants that describe self- and interassociation.

2-4 Ternary Polymer Blends

Extension of the association model to a description of the phase behavior of ternary polymer blends is reasonably straightforward, but problems of accuracy and the unambiguous interpretation of experimental results increases dramatically for ternary blends compared to binary polymer blends. Nevertheless, there are good reasons to study the phase behavior of ternary polymer blend systems. Common questions that are asked include:

(1)   Is it possible to increase the range over which ternary blends are miscible by introducing specific interactions?

(2)   Can we add a polymer (PolyB) to an immiscible binary blend (PolyA/PolyC) and render the whole system homogeneous?

(3)   Will PolyB act as a compatibilizer and reduce the overall size of the domains in the heterogeneous ternary blend?

Consider three polymers denoted PolyA, PolyB, PolyC. PolyB is capable of self-association and represented by one equilibrium constant, K_B.

$$B_h + B_1 \xleftrightarrow{\quad K_B \quad} B_{h+1}$$
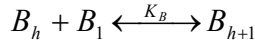
PolyA and PolyC do not self-associate, and there are also no strong intermolecular interactions (hydrogen bond) formed between them, but thery do have acceptor groups that are able to form hydrogen bonds with PolyB. These hydrogen bonds can be described by the equilibrium constants, K_A and K_C, respectively.

$$B_h + A \xleftrightarrow{\quad K_A \quad} B_h A$$

$$B_h + C \xleftrightarrow{\quad K_C \quad} B_h C$$
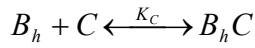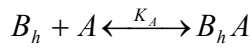
The equation describing the free energy of mixing of ternary hydrogen bonded blends, $\Delta G_H/RT$, has a form that is very similar to that obtained for binary blends, except that there are extra terms to account for the additional component of the blend:

$$\frac{\Delta G_m}{RT} = \frac{\Phi_A}{r_A N_A} \ln \Phi_A + \frac{\Phi_B}{r_B NB} \ln \Phi_B + \frac{\Phi_C}{r_C N_C} \ln \Phi_C +$$

$$\Phi_A \Phi_B \chi_{AB} + \Phi_A \Phi_C \chi_{AC} + \Phi_B \Phi_C \chi_{BC} + \frac{\Delta G_H}{RT}$$

(11)

where Φ_B, Φ_A, and Φ_C are the volume fractions of PolyB, PolyA, and PolyC in the blend, respectively, which have degrees of polymerization, N_i. The parameters $r_A = V_A/V_B$ and $r_C = V_C/V_B$ are the ratios of the segment molar volumes of PolyA to PolyB and PolyC to PolyB, respectively. As before the polymer/polymer interaction parameters, χ_{ij}, which have permissible values of ≥ 0, are determined from solubility parameters that are calculated from group molar attraction and molar volume constants designed to *specifically exclude contributions from hydrogen bonding.*[2] Finally, the $\Delta G_H/RT$ term which represents a favorable contribution to the free energy of mixing emanating from the changing pattern of hydrogen bonds in the mixtures, is a function of the magnitudes of the various equilibrium constants.

Spinodal phase diagrams reveal the general trends in the phase behavior of ternary polymer blends and are easily calculated. The criterion for thermodynamic stability of a ternary polymer mixture at a constant temperature and pressure is expressed by the following relationships:

$$\frac{\Delta G_m}{RT} < 0 \tag{12}$$

$$\begin{vmatrix} \Delta G''_{AA} & \Delta G''_{AB} & \Delta G''_{AC} \\ \Delta G''_{BA} & \Delta G''_{BB} & \Delta G''_{BC} \\ \Delta G''_{CA} & \Delta G''_{CB} & \Delta G''_{CC} \end{vmatrix} > 0 \tag{13}$$

where:

$$\Delta G''_{ij} = \frac{\partial^2 (\Delta G_m / RT)}{\partial \Phi_i \partial \Phi_j}$$

Eq. 13 is equivalent to the following inequalities:

$$\frac{\partial^2 (\Delta G_m / RT)}{\partial^2 \Phi_A} > 0 \tag{14}$$

and:

$$\left[\frac{\partial^2 (\Delta G_m)}{\partial^2 \Phi_A} \right]\left[\frac{\partial^2 (\Delta G_m)}{\partial^2 \Phi_B} \right] - \left[\frac{\partial^2 (\Delta G_m)}{\partial \Phi_A \partial \Phi_B} \right]^2 > 0 \tag{15}$$

where the derivatives in Eq. 14 and Eq. 15 are calculated with Φ_C as a dependent variable and Φ_A and Φ_B as independent variables.

If there are no specific interactions present (i.e. $K_B = K_A = K_C = 0$), Eq. 11 would reduces to the Flory-Huggins equation as $\Delta G_H/RT = 0$. The complete miscibility is predicted when $\chi_{AB} = \chi_{BC} = \chi_{AC} < \chi_{Crit}$. The requirements for miscibility are even more stringent if we now permit $\chi_{AB} \neq \chi_{BC}$, even though both values may be less than χ_{Crit}. This is the so-called "$\Delta\chi$ effect",[11,12] which is essentially a polymer induced phase separation caused by the different "physical" interactions between the segment of PolyB with PolyA and PolyC. The effect of specific interactions (hydrogen bonding)

was simulated by changing the relative values of the equilibrium constants while holding the χ_{ij} values constant. Again, we should not be surprised to learn that when $K_A = K_C > K_B$, i.e. when the unfavorable contribution of self-association to the free energy of mixing is offset by the favorable contributions derived from inter-association, we are more likely to obtain a single phase system. In other words, balanced inter-association (i.e. $K_A = K_C$) is favorable to mixing in ternary hydrogen bonded blends. In contrast, however, if $K_A \neq K_C$, we have the situation where the chemical interactions between the segments of PolyB with PolyA and PolyC are different and this again tends to induce phase separation (because PolyB favors one of the other components over the third). Analogous to the $\Delta\chi$ effect, but chemical in nature as it reflects the hydrogen bonding contribution to free energy of mixing, Coleman et al. have chosen to call this the ΔK effect. It generally has a deleterious effect on ternary miscibility.

In summary, the position, shape and size of the heterogeneous region in ternary phase diagrams of polymer blends that involve strong specific interactions is a sensitive function of (1) the magnitudes of the individual χ_{ij}, (2) the presence of $\Delta\chi$ effects, (3) the magnitudes of the individual equilibrium constants, K_i, describing self- and inter-association, (4) the presence of ΔK effects caused by differences in the inter-association equilibrium constants, the relative values of the molar volumes of the chemical repeat units, $r_i = V_i/V_B$ (which affects K_A and K_C), and /or the enthalpies of the hydrogen bond formation, h_i and (5) the molecular weight of the individual blend components.

Painter and Coleman generally conclude from the simulations that:

(1)   It will be difficult to find ternary polymer blends that exist in a single phase over a wide composition range. Only in very rare cases, where the physical ($\Delta\chi$) and chemical (ΔK) interaction differences are

negligible or finely balanced, can we expect to find miscible ternary polymer blend.

(2)   In most cases, an immiscible binary blend con not be made homogeneous by introducing a small amount of a third polymer (compatibilizer).

(3)   While the presence of specific intermolecular interactions enhances the probability of forming a homogeneous ternary polymer blend, they can concurrently exacerbate the situation through the ΔK effect, which promotes phase separation.

References

(1) Coleman, M. M.; Painter, P. C. *Prog. Polym. Sci.* **1995**, *20*, 1.

(2) Coleman, M. M.; Graf, J. F.; Painter, P. C. *Specific Interactions and the Miscibility of Polymer Blends*; Technomic Publishing, Inc.; Lancaster, PA, 1991.

(3) Painter, P. C.; Park, Y.; Coleman, M. M. *Macromolecules* **1988**, *21*, 66.

(4) Painter, P. C.; Park, Y.; Coleman, M. M. *Macromolecule*s **1989**, *22*, 570.

(5) Painter, P. C.; Park, Y.; Coleman, M. M. *Macromolecules* **1989**, *22*, 580.

(6) Coleman, M. M.; Xu, Y.; Painter, P. C. *Macromolecules* **1994**, *27*, 127.

(7) Coleman, M. M.; Pehlert, G. J.; Painter, P. C. *Macromolecules* **1996**, *29*, 6820.

(8) Pehlert, G. J.; Painter, P. C.; Veytsman, B.; Coleman, M. M. *Macromolecules* **1997**, *30*, 3671.

(9) Painter, P. C.; Veytsman, B.; Kumar, S.; Shenoy, S.; Graf, J. F.; Xu, Y.; Coleman, M. M. *Macromolecules* **1997**, *30*, 932.

(10) Coleman, M. M.; Painter, P. C. *Macromol. Chem. Phys.* **1998**, *199*, 1307.

(11) Zeman, L.; Patterson, D. *Macromolecules* **1972**, *5*, 513.

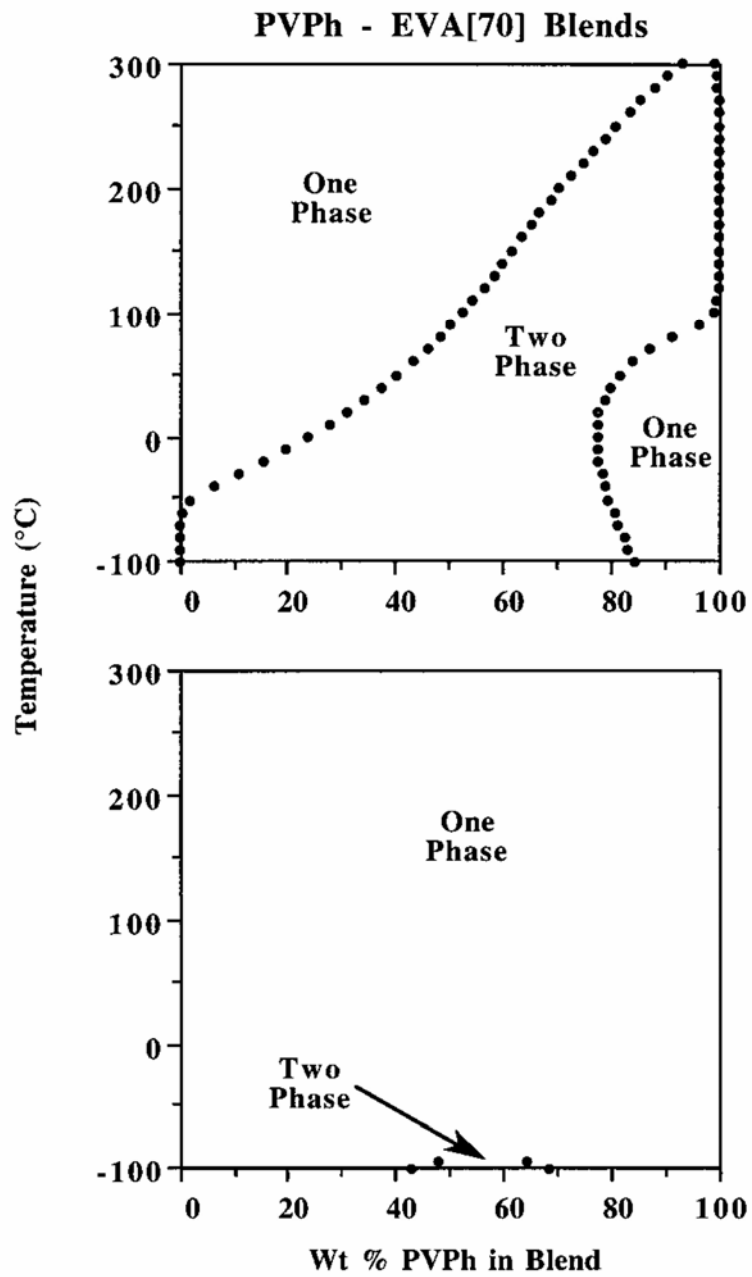(12) Patterson, D. *Polym. Eng. Sci.* **1982**, *22*, 64.

Figure 2-1: Theoretical spinodal phase diagrams for PVPh/EVA[70] blends. Top: Calculated from the derivatives of Eq. 3 containing the "correct" excess free entropy term Eq. 5. Bottom: The same calculation, but with the modified excess free entropy term Eq. 6.

Figure 2-2: Theoretical miscibility maps calculated at 25 $^{\circ}$C for STVPh/EVA blends. Top: Calculated from the derivatives of Eq. 3 containing the "correct" excess free entropy term Eq. 5. Bottom: The same calculation, but w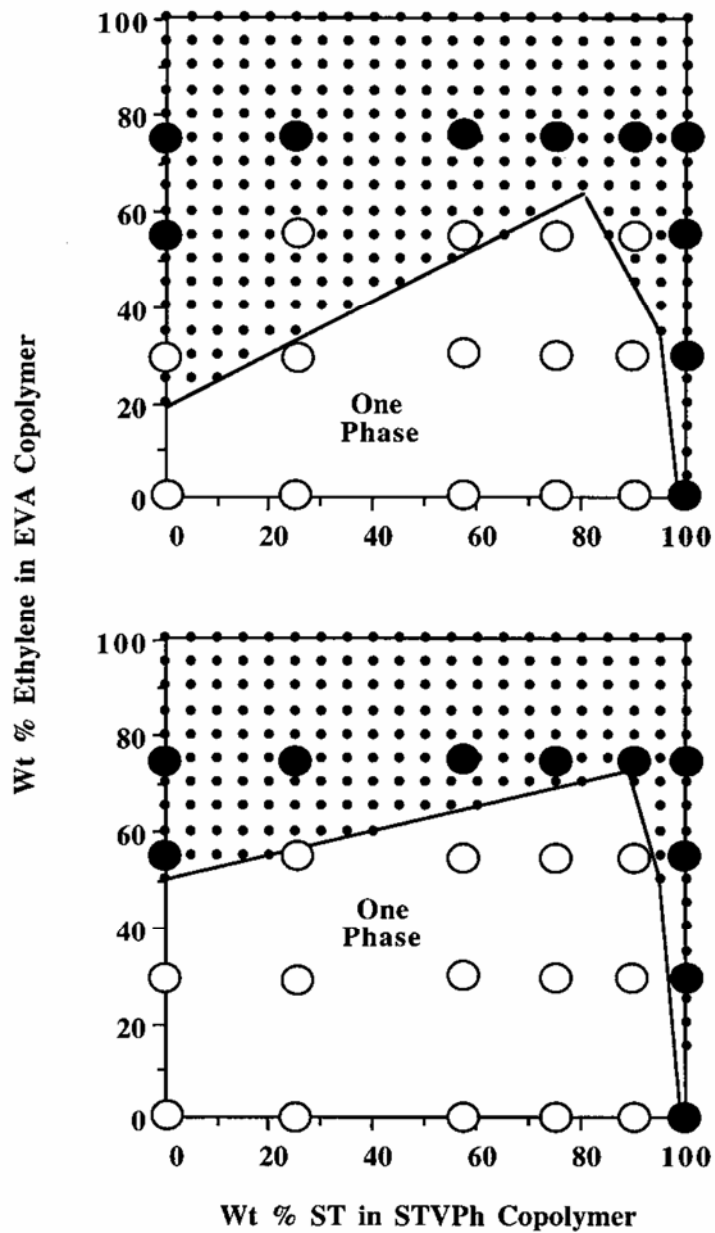ith the modified excess free entropy term Eq. 6. The areas encompassed by the small black dots denote predicted two phase regions. Experimentally determined single and two phase blends are denoted by the unshaded and black filled large circles, respectively.
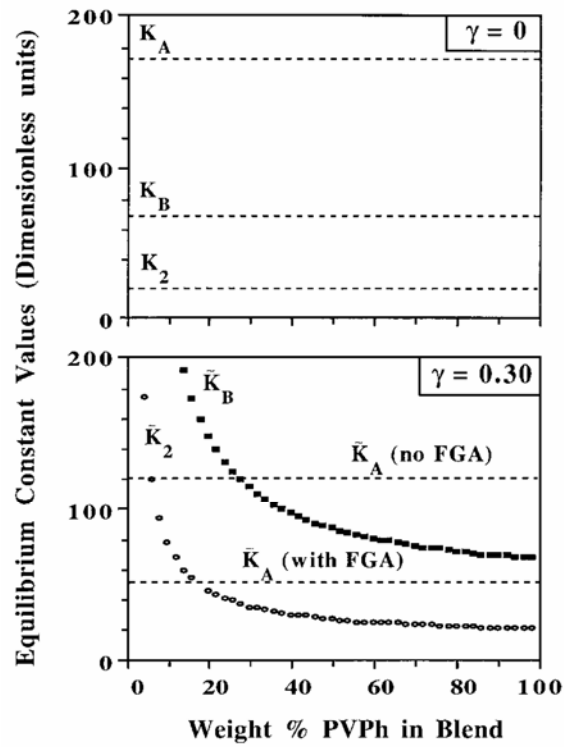
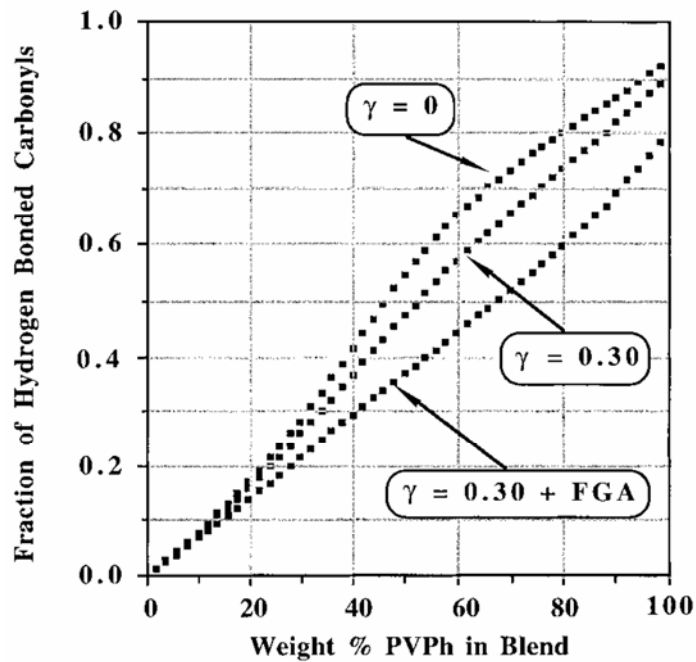Figure 2-3: Equilibrium constant values for the PVPh-PVAc blend system (FGA: functional group accessibility).

Figure 2-4: Calculated fraction of hydrogen bonded acetoxy carbonyl groups for the PVPh-PVAc blend system at 25 $^{\circ}$C.

48

Chapter 3

Synthesis of Rod-Coil Diblock Copolymers by ATRP and their Honeycomb Morphologies formed by the "Breath Figures" Method

Abstract

We have synthesized rod–coil diblock PPQ-*b*-PMMA copolymers by using the versatile atom-transfer radical polymerization method and have characterized them by differential scanning calorimetry (DSC), Fourier transform infrared spectroscopy (FTIR), and thermogravimetric analysis (TGA). The methyl ketone-terminated rod–coil diblock PMMA copolymer has a higher value of T_g, because of its syndiotactic-like structure, and a higher decomposition temperature than does the PMMA homopolymer. The presence of the PPQ block tends to retard the early decomposition of the PMMA chain. A regularly porous, honeycomb-structured film was prepared from the dichloromethane solution of the diblock copolymers under a flow of moist air. The diameters of the spherical pores can be controlled in the range from 0.8 to 3 μm by modifying both the rod–coil copolymers' relative molecular weights and the casting conditions. The wall thickness of the film is varied linearly with the relative molecular mass (M_r).

3-1 Introduction

During the last few decades, block copolymers have attracted an increasing amount of interest both from scientific and commercial points of view[1,2] because of their highly symmetrical morphological behavior on length scales ranging between a few nanometers and several hundreds of nanometers. In recent years, the rod-coil diblock copolymers have been developed that exhibit unique morphologies and phase separation behavior.[3-7] The difference in the chain rigidity of the rod-like and coil-like blocks greatly affects aspects of the molecular packing and the thermodynamically stable morphologies of these materials. Apart from the wide range of different self-assembling structures that form, another unique characteristic of these materials is that the rod segments can endow various functionalities, such as photophysical and electrochemical properties, to the materials. Incorporation of π-conjugated polymer chains into heterogeneous diblock copolymers can create new materials that present promising nonlinear optical, photoconductive, and electroluminescence properties.[8-10]

Porous materials with a perfect arrangement of pores provide interesting properties for various technological applications such as photonic bandgap materials, heterojunction devices, and picoliter beakers. Picoliter beakers[11-14] are of importance in analytical and bioanalytical chemistry because they allow isolating very small volumes of liquid or single cells and interrogating them by either electrochemical or enzymatic methods. However, the fabrication of ordered mesoporous/microporous solids is not trivial and often involves tedious photolithographic methods or templating using emulsions[15] that are expensive and complicated. On the contrary, microporous structures can be fabricated by a simple self-organization technique using star polymers,[16] amphiphilic copolymers,[17] or rod-coil block copolymers[18] in a moist atmosphere. As mentioned above, the rod-coil block copolymer has more

advantage to form porous materials because the rod segment can be cross-linking to render them insoluble[19] or endow conductive property.[20]

The preparation of rod-coil block copolymers consisting of conjugated rods is a great challenge in polymer synthesis because it is difficult to connect these two physically and chemically different blocks. Traditionally, polymer chains possessing terminal functional groups are prepared by controlled termination of living ionic polymerizations but because of the extreme sensitivity that living ionic polymerization displays to impurities and functional groups, strict experiments are necessary. Atom-transfer radical polymerization (ATRP) is an efficient technique for polymerizing various monomers in a controlled manner to yield polymers that have predetermined molecular weights and narrow polydispersity.[21] Since various ATRP initiators can be modified to fulfill the requirements of the linking bridge molecules of rod－coil copolymers, we chose to synthesize a flexible methyl ketone-terminated polymer chain and then to connect it to poly(phenylquinoline) (PPQ).

In this study, we first synthesized a methyl ketone-terminated poly(methyl methacrylate) (PMMA) and then used its ketone groups as linkage units with which to connect PPQ chains through a condensation reaction. The polymers were characterized by gel permeation chromatography (GPC), Fourier transform infrared spectroscopy (FTIR), thermogravimetric analysis (TGA), and differential scanning calorimetry (DSC) measurements. When the polymer was then cast into thin film using appropriate solvents on solid substrates, highly ordered, micro-porous honeycomb structures formed spontaneously; the empty spherical cells had diameters ranging from 0.8 to 2.5 μm.

3-2 Experimental Section

3-2.1 Materials.

MMA (SHOWA, 99 %) was passed through a basic activated alumina column and distilled from CaH_2 before use. Copper (I) bromide was purified according to a literature procedure.[22] *N, N, N', N'', N''*-pentamethyldiethylenetriamine (PMDETA, TCI, 98%), xylene (MEDIA, 99%), 1-(4-aminophenyl)ethanone (ACROS, 99%), and 2-bromo-2-methylpropanoyl bromide (TCI, 99%) were all commercial products and were used without further purification. 5-Acetyl-2-aminobenzophenone (**2**) was synthesized according to a literature procedure.[23]

3-2.2 Synthesis of *N*-(4-acetylphenyl)-2-bromo-2-methylpropanamide (1).

A dry 100 mL round-bottom flask equipped with a stirrer bar was charged with dry THF (40 mL), 1-(4-aminophenyl)ethanone (6.76 g, 50 mmol), and dry triethylamine (6.75 mL, 50 mmol). The solution was cooled to 0 $^{\circ}$C in an ice bath and then 2-bromo-2-methylpropanoyl bromide (13.8 mL, 60 mmol) in dry THF (30 mL) was added dropwisely using a dropping funnel (Scheme 3-1) to form a white precipitate. The slurry was stirred at room temperature for 3 h before being filtered. The solvent were evaporated under reduced pressure to yield a brown precipitate, which was then dissolved in EtOAc and washed three times with water. After one recrystallization from EtOAc/hexane, pure (**1**) was obtained (12.2 g, 86%): mp 129.4–132.3 °C; FTIR (KBr, pellet) 3322 (N-H), 1676 (C=O) cm^{-1}; ^{1}H NMR (500 MHz, CDCl$_3$) δ 8.6 (br, 1H, N*H*), 7.9 (d, 2H, aryl), 7.6 (d, 2H, aryl), 2.6 (s, 3H, COC*H$_3$*), 2.0 [s, 6H, CBr(C*H$_3$*)$_2$].

3-2.3 Polymerization of methyl ketone-terminated poly(methyl methacrylate) (3).

We prepared a polymerization system having [M]$_0$:[I]$_0$ of 800:1 by charging

MMA (10.75 mL, 100 mmol), CuBr (17.7 mg, 0.125 mmol), N-(4-acetylphenyl)-2-bromo-2-methylpropanamide (**1**; 35.5 mg, 0.125 mmol), and xylene (2.5 mL) into a reaction flask equipped with a magnetic stirrer bar (Scheme 3-2). The flask was sealed with a rubber septum and degassed by three freeze-pump-thaw cycles. The reaction flask was immersed in an oil bath at 80 °C and then PMDETA (52 μL, 0.25 mmol) was added by syringe. As the viscosity increased, the stirrer bar eventually stopped rotating, but the reaction continued and we collected the last sample after 12 h. After cooling to room temperature, THF was added to the reaction mixture to dissolve the polymer. The product was precipitated by pouring the solution into a large excess of methanol.

3-2.4 Synthesis of poly(phenylquinoline)-*block*-poly(methyl methacrylate) diblock copolymer.

PPQ-*b*-PMMA diblock copolymers were synthesized by copolymerization of 5-acetyl-2-aminobenzophenone (**2**) with (**3**) as presented in Scheme 3-3. A round-bottom flask was charged with (**2**) (0.12 g, 0.5 mmol), (**3**) (3.25 g, 0.025 mmol), diphenyl phosphate (DPP, 0.3 g), and freshly distilled *m*-cresol (4 mL). The temperature of the mixture was raised slowly to 140 °C over 3 h. Additional DPP was added as the viscosity of the mixture increased with time; a total of 1.25 g of DPP was added. The reaction mixture's temperature was maintained at 140 °C for 72 h under argon atmosphere. In general, the condensation reaction yield of copolymerization is 100 %.[18] The product was precipitated by pouring the mixture into 10 % triethylamine/ethanol (100 mL) and then purified by the Soxhlet extraction with 10 % triethylamine/ethanol for 48 h and THF for additional 72 h. The final diblock copolymer was collected from the THF-soluble product.

3-2.5 Measurements.

Molecular weights and molecular weight distributions were determined by GPC using a Waters 510 HPLC equipped with a 410 Differential Refractometer, a UV detector, and three Ultrastyragel columns (100, 500, and 10^3 Å) connected in series and using THF as the eluent at a flow rate of 0.4 mL/min. The molecular weight calibration curve was obtained using polystyrene standards. ^{1}H NMR spectroscopy was performed using an INOVA 500 instrument; $CDCl_3$ was the solvent. Infrared spectra were obtained using a Nicolet Avatar 320 FT-IR Spectrometer. A differential scanning calorimeter (Du-Pont TA 2010 instrument) was used to determine the thermal transitions at a heating rate of 20 °C/min^{-1}. The TGA thermograms were obtained on a Du-Pont TA Q-50 instrument at a heating rate of °C/min^{-1} under nitrogen. Polarized optical transmission microscopy was performed on an Olympus BX50 microscope equipped with digital camera (Olympus PD12). Prior to imaging by SEM , the samples were coated with Pt (10 nm). SEM images were recorded using a TOSHIBA S4700I field emission microscope working at a voltage of 5 kV and a beam current of 1×10^{-10} A.

3-3 Results and Discussion

3-3.1 Synthesis of methyl ketone-terminated PMMA and rod－coil diblock polymers.

A functional PMMA derivative was polymerized by ATRP, which has been demonstrated to be an efficient method for performing living polymerizations of a large number of monomers. The polymerization, which is depicted in Scheme 3-2, was carried out by using CuBr, complexed by PMDETA, as the catalyst in xylene solution at 80 °C and was initiated by the action of N-(4-acetylphenyl)-2-bromo-2-methylpropanamide (**1**). The molecular weights and polydispersities of the functionalized PMMAs were characterized by GPC. We performed additional molecular weight measurements by ^{1}H NMR spectroscopy by analyzing the relative intensities of the signals of the protons of both the initiator and PMMA; in particular, we performed these calculations by comparing the signals between 7.4 and 8 ppm, due to the aromatic protons of the initiator, with those at 3.5 ppm for the methyl ester groups of the PMMA segments. The calculated values, which are presented in Table 3-1, provide results that agree well with those obtained by GPC. In this Table, the subscript n of the descriptor "PMMA$_n$" reflects the degree of polymerization.

From Figure 3-1, the T_g obtained by DSC for the functionalized PMMA is higher than that of commercial PMMA by ca. 20 ^{o}C. In general, the glass transition temperature of PMMA is proportional to the degree of syndiotacticity and inversely proportional to the degree of isotacticity. The higher ratio of syndiotacticity results in a relatively regular structure and leads to an increase in the glass transition temperature. The FTIR analysis were performed to interpret the reasons for the observed higher T_g. Absorptions in the range 1300-1100 cm^{-1} of the FTIR spectrum

are sensitive to the tacticity of PMMA;[24] e.g., syndiotactic and isotactic PMMA present different absorption peaks, at 1270 cm^{-1} and 1260 cm^{-1}, respectively. Because of its highly restricted backbone conformation, syndiotactic PMMA has a higher absorption frequency at 1270 cm^{-1} and larger value of T_g than does isotactic PMMA. Figure 3-2 presents the FTIR spectra of PMMA with various tacticities; it reveals that the functional PMMA we synthesized has a characteristic peak at 1270 cm^{-1} and, hence, our functional PMMA is favoring a syndiotactic structure. ^{1}H NMR was also used to characterize the tacticities of PMMA. The methylene and α-methyl proton spectra of the functional PMMA$_{1300}$ were shown in Figure 3-3. It displays three distinct peaks appearing at the highest field, which represent methacrylate methyl groups of different tacticity.[25] The bands at about 0.8, 0.98, and 1.17 ppm arise from syndiotactic (rr), atactic (mr), and isotactic (mm) methyl groups, respectively. From Figure 3-3, the tacticity of the PMMA$_{1300}$ was calculated from the integrated ratios of rr, mr, and mm. The ratios of the triad tacticty for syndiotactic, atactic, and isotactic are 60.9, 35.5, and 3.6, respectively. According to these results, the functional PMMA has a syndiotactic-favoring configuration and possesses the higher value of T_g.

Scheme 3-3 outlines our synthetic approach to PPQ-*b*-PMMA. Although the polymerization of the PPQ block is a condensation-type reaction, the composition of the resultant diblock copolymer could be controlled by the stoichiometry. The reaction product was purified by Soxhlet extraction using a TEA/EtOAc solution; with this technique, we washed out PPQ-*b*-PMMA copolymers that had low degrees of polymerized PPQ blocks and any unreacted functionalized PMMAs. Furthermore, we separated the product into THF–soluble and –insoluble parts by the Soxhlet extraction procedure. The final diblock copolymer was collected from the THF–soluble part. These procedures ensure that the copolymer obtained is a rod–coil diblock copolymer and not just a physical blend. As a result, the product yield was

slightly below 80% (72–79%) after extraction.

We employed TGA to obtain the correct composition of the diblock copolymers.[5] Figure 3-4 displays TGA thermograms of these diblock copolymers; the corresponding thermograms of both the PPQ and PMMA homopolymers were also obtained for the sake of comparison. The 5%-weight-loss decomposition temperatures of PPQ and PMMA are 600 and 300 °C, respectively. The diblock copolymers undergo two-step decompositions under nitrogen. The first thermal decomposition temperature (300-450 ^{o}C) comes from the flexible PMMA block of the copolymer. After decomposition of this flexible block, the rigid PPQ block remains stable up to 600 ^{o}C, which is identical to the decomposition temperature of the PPQ homopolymer. Because the PMMA block is decomposed completely at 450 °C, the residual weight in the range from 450　to 550 °C is contributed by the PPQ block and, thus, the residual weight in this range can be used to calculate the composition of the diblock copolymer. Table 3-2 summarizes the calculated compositions (the subscripts n of "PPQ$_n$" reflect the number of repeat units of the PPQ blocks). The improved thermal stability of the PMMA block in the diblock copolymers, relative to that of the parent PMMA homopolymer, can be understood as being a consequence of the tethering of the PMMA chain onto the rod chain. Hence, the PPQ, which possesses a higher decomposition temperature, can prevent the PMMA chain from degrading sooner. From the DSC measurement, we found that all of the diblock copolymers exhibit one glass transition, at 130 °C. We detected no crystalline melting or glass transition for the PPQ block before the decomposition temperature of the PMMA block was reached.

Figure 3-5 indicates that the FTIR spectrum of the diblock copolymer is essentially a superposition of the spectra of the parent PMMA and PPQ homopolymers, but there are significant differences between the vibrational spectra of

the methyl ketone-terminated PMMA and the PPQ homopolymer and, therefore, their contributions to the FTIR spectra of the diblock copolymers can be determined. The stretching bands at 1730 cm^{-1}, which we assign to the carbonyl group of the functionalized PMMA, appear in the FTIR spectrum of the diblock copolymer. The vibrational bands at 1585/1550 and 1345/1028 cm^{-1} are characteristic peaks of the phenyl and the quinoline rings of the PPQ block. Thus, the results obtained by FTIR, TGA, and DSC all confirm the structure of the rod–coil diblock copolymer.

3-3.2 Micro-porous honeycomb morphology

Usually when preparing micro-porous materials, colloidal crystals of polystyrene or silica spheres are used as templates that must be removed either by thermal decomposition or by solvent extraction.[26-28] Such an approach, however, is probably not useful for dynamically controlling virtual length scales. In this study, we used a simple and facile method, the so-called "Breath Figure," to form ordered structures.[29-37] There are several factors may influence the formation of the honeycomb structure and different morphologies, including the concentration of the PPQ-PMMA solution, the relative humidity in the atmosphere, the rate of air flow, and the film formation temperature. In this study, effect of the PPQ-b-PMMA concentration and its relative molecular mass (M_r, the PPQ block relative to the PMMA block) were used to control the pore size of the resulted film.

Upon drop-casting a dichloromethane solution of the rod–coil diblock copolymer onto a glass slide in an air-flow hood, condensation of water on the cold surface of the liquid film was observed at relative humidities > 60%. After a few seconds, the whole surface of the solution began to scatter light, which turned the sample opaque. After complete evaporation of the solvent, the sample was characterized by polarized optical microscopy, as shown in Figure 3-6, showing highly ordered, hexagonal, close-packed pores in the polymer film. The polarized optical microscopy probe the film with conjugated rod-like PPQ block, thus the bright structure in the figure corresponds to the rod-coil block copolymer.

Figure 3-7 shows SEM images of the as-prepared honeycomb structures of PPQ-PMMA films from different concentrations of PPQ-b-PMMA solutions at a relative humidity of 75 % and air flow rate of 2 m/s at room temperature. As can be seen in Figure 3-7 (a)-(c), larger pore sizes are obtained when using lower concentrations of the polymer solution: as the concentration of the polymer solution

increased from 0.1 to 1 wt%, the pore size decreased from 2.3 to 1.2 μm.

We proposed that the relative molecular mass (M_r, PPQ block relative to PMMA block) is also an important factor in dictating the pore size, higher M_r resulting in higher pore size. At the same polymer concentration of these polymer solutions (1 wt%), the pore size of $PPQ_{48}PMMA_{1300}$ (ca. 1.1 μm) is about the same as that of $PPQ_{52}PMMA_{2500}$ (ca. 1 μm), as shown in Figures 3-8 (a) and (b), in which both diblock copolymers have different Mr values (0.07 vs. 0.04, Table 3-2). Nevertheless, the $PPQ_{52}PMMA_{800}$ (Figure 3-8 (c)) possessing a higher value of M_r (0.13) has a significantly larger pore size at 2.6 μm. The correlation of pore size and relative molecular mass is plotted in Figure 3-9, where the higher Mr value is tend to form the larger pore size. From Figure 3-8, the wall thickness between the pores is also strongly dependent on the value of Mr. As can be seen, the average wall thickness of the film formed by $PPQ_{52}PMMA_{2500}$ (Mr = 0.04) is ca. 220 nm. The wall thicknesses of the structures formed by $PPQ_{48}PMMA_{1300}$ (Mr = 0.07) and $PPQ_{50}PMMA_{800}$ (Mr = 0.13) are ca. 380 nm and 650 nm, respectively. Other PPQ-PMMA copolymers possessing different values of Mr have the same tendency. The wall thickness for the PPQ-PMMA copolymer increases linearly with the increase of it relative molecular mass M_r, as shown in Figure 3-9. Review Figure 3-7 again, although the film was formed by different concentrations of $PPQ_{52}PMMA_{2500}$, the wall thicknesses of these films are the same (220 nm). Hence, the value of wall thickness can not be altered by other factors; it only depends on the value of Mr.

The mechanism of the "Breath Figure" method has been proposed previously.[30,34,38-40] The high vapor pressure of the organic solvent drives solvent evaporation and rapidly cools the surface. This cooling leads to nucleation, and tiny water droplets cover the entire surface. Due to the incompatibility of the organic solvent and water, the polymer precipitates under this hydrophilic/hydrophobic

balance and the polymer layer is formed.[41,42] Only this "fast nucleation and slow growth" mechanism[43] provides the uniform size of the water droplets. These droplets are transported to the three-phase line and are hexagonally packed by the convectional flow or the capillary force generated at the solution front. After the solvent is evaporated, the membrane temperature rises up the ambient temperature and water contained inside the droplets evaporates by bursting the polymer film, leading to the formation of the circular holes network observed on the cross section of the membrane (see Figure 3-8 (a)).

According the mechanism mentioned above, controlling the pore size by varying the concentration of polymer solution should have its limit. The polymer possesses a "precipitate-like" behavior at the interface between the solution and water, and thus creates a solid polymer envelope around the isolated water droplet. This polymer layer is able to prevent the coalescence of the water droplets to form the highly regular honeycomb structure.[42] Hence, at a very low concentration, the polymer is unable to support the stable polymer envelope and the water droplets tend to coalesce with impulsive force to enlarge the pore size distribution and form the polygon structure as shown in Figure 3-7 (d).

3-4 Conclusions

Rod–coil diblock copolymers have been synthesized using the versatile ATRP method. This method is based on polymerizing MMA in the presence of a bifunctional initiator to obtain a methyl ketone-terminated PMMA. This functionalized PMMA was then copolymerized with 5-acetyl-2-aminobenzophenone to form the PPQ-b-PMMA diblock copolymer. The methyl ketone-terminated PMMA has a higher value of T_g than does the virgin PMMA because of its syndiotactic-like structure. The decomposition temperature (T_d) of the rod‑coil diblock copolymer is higher than that of the PMMA homopolymer because the presence of the PPQ block retards the early decomposition of PMMA chains. Regular, porous honeycomb-structured films were prepared from the dichloromethane solution of the diblock copolymer in an air-flow hood. A higher polymer concentration results in larger pores, because the aggregation of polymer is fast. If the concentration of the polymer solution is too low, water droplet coalescence tends to enlarge the pore size and size distribution, and forms polygon structures. Higher relative molecular masse (M_r) tends to create larger pores. The wall thickness between the pores increases linearly with the increase of the relative molecular mass (M_r).

References

(1)   Bates, F. S.; Fredrickson, G. H. *Annu. Rev. Phys. Chem.* **1990**, *41*, 525.

(2)   Matsen, M. W.; Schick, M. *Curr. Opin. Colloid Interface Sci.* **1996**, *1*,329.

(3)   Radzilowski, L. H.; Wu, J. H.; Stupp, S. I. *Macromolecules* **1993**, *26*, 879.

(4)   Li, W.; Maddux, T.; Yu, L. *Macromolecules* **1996**, *29*, 7329.

(5)   Jenekhe, S. A.; Chen, X. L. *Science* **1998**, *279*, 1903.

(6)   Chen, X. L.; Jenekhe, S. A. *Macromolecules* **2000**, *33* 4610.

(7)   Jenekhe, S. A.; Chen, X. L. *J Phys. Chem. B* **2000**, *104*, 6332.

(8)   Agrawal, A. K.; Jenekhe, S. A. *Macromolecules* **1993**, *26*, 895.

(9)   Zhang, X.; Shetty, A. S.; Jenekhe, S. A. *Macromolecules* **1999**, *32*, 7422.

(10) Agrawal, A. K.; Jenekhe, S. A. *Chem. Mater.* **1993**, *5*, 633.

(11) (a) Lapos, J. A.; Wwing, A. G. *Anal. Chem.* **2000**, *72*, 4598. (b) Clark, R. A.;
      Hietpas, P. B.; Ewing, A. G. *Anal. Chem*. **1997**, *69*, 259.

(12) Pris, A. D.; Porter, M. D. *Nano Lett.* **2002**, *2*, 1087.

(13) Cooper, J. M. *Trends Biotechnol.* **1999**, *17*, 226.

(14) Troyer, K. P.; Wightman, R. M. *Anal. Chem.* **2002**, *74*, 5370.

(15) Imhof, A.; Pine, D. J. *Nature* **1997**, *389*, 948.

(16) Stenzel-Rosenbaum, M. H.; Davis, T. P.; Fane, A. G.; Chen, V. *Angew. Chem., Int.
      Ed.* **2001**, *40*, 3428.

(17) Maruyama, N.; Koito, T.; Nishida, J.; Sawadaishi, T.; Cieren, X.; Ijiro, K.;
      Karthaus, O.; Shimomura, M. *Thin solid Films* **1998**, *327-329*, 854.

(18) Jenekhe, S. A.; Chen, X. L. *Science* **1999**, *283*, 372.

(19) Erdogan, B.; Song, L.; Wilson, J. N.; Park, J. O.; Srinivasarao, M.; Bunz, U. H. F.
      J. Am. Chem. Soc. **2004**, *126*, 3678.

(20) Yu, C.; Zhai, J.; Gao, X.; Wan, M.; Jiang, L.; Li, T.; Li, Z. *J. Phys. Chem. B* **2004**,

108, 4586.

(21) Matyjaszewski, K.; Xia, J. *Chem. Rev.* **2001**, *101*, 2921.

(22) Keller, R. N.; Wycoff, H. D. *Inorg. Synth.* **1946**, *2*, 1.

(23) Sybert, P. D.; Beever, W. H.; Stille, J. K. *Macromolecules* **1981**, *14*, 493.

(24) Grohens, Y.; Prud'homme, R. E.; Schultz, J. *Macromolecules* **1998**, *31*, 2545.

(25) Bovey, F. A. *Chain Structure and Conformation of Macromolecules*. Academic Press: New Yord; 1982.

(26) Holland, B. T.; Blanford, C. F.; Stein, A. *Science* **1998**, *281*, 538.

(27) Kulinowski, K. M.; Jiang, P.; Vaswani, H.; Colvin, V. L. *Adv. Mater.* **2000**, *12*, 833.

(28) Velev, O. D.; Jede, T. A.; Lobo, R. F.; Lenhoff, A. M. *Nature* **1997**, *389*, 447.

(29) Baker, J. T. *Philos. Mag.* **1922**, *56*, 752.

(30) Beysens, D.; Konbler, C. M. *Phys. Rev. Lett.* **1986**, *57*, 1433.

(31) Family, F.; Meakin, P. *Phys. Rev. Lett.* **1988**, *61*, 428.

(32) Widawski, G.; Rawiso, M.; François, B. *Nature* **1994**, *369*, 387.

(33) François, B.; Pitois, O.; François, J. *Adv. Mater.* **1995**, *7*, 1041.

(34) Srinivasarao, M.; Collings, D.; Philips, A.; Patel, S. *Science* **2001**, *292*, 79.

(35) Boer, B. D.; Stalmach, U.; Nijland, H.; Hadziioannou, G. *Adv. Mater.* **2000**, *12*, 1581.

(36) Karthaus, O.; Maruyama, N.; Cieren, X.; Shimomura, M.; Hasegawa, H.; Hashimoto, T. *Langmuir* **2000**, *16*, 6071.

(37) Song, L.; Bly, R. K.; Wilson, J. N.; Bakbak, S.; Park, J. O.; Srinivasarao, M.; Bunz, U. H. F. *Adv. Mater.* **2004**, *16*, 115.

(38) Stenzel, M. H.; Davis, T. P.; Fane, A. G. *J. Mater. Chem.* **2003**, *13*, 2090.

(39) Stenzel, M. H. *Aust. J. Chem.* **2002**, *55*, 239.

(40) Briscoe, B. J.; Galvin, K. P. *J. Phys. D* **1990**, *23*, 422.

(41) Pitois, O.; François, J. *Colloid Poym. Sci.* **1999**, *277*, 574.

(42) Pitois, O.; François, J. *Eur. Phys. J. B* **1999**, *8*, 225.

(43) Maruyama, N.; Karthaus, O.; Ijiro, K.; Shimomura, M.; Koito, T.; Nishimura, S.; Sawadaishi, T, Nishi, N.; Tokura, S. *Supramol. Sci.* **1998**, *5*, 331.

Table 3-1. Molecular weights and thermal properties of the methyl ketone-terminated

PMMA

	Time (h)	Conv. (%)	$M_{n,GPC}$	$M_{n,NMR}$	M_w/M_n	T_g
$PMMA_{800}$	12	85	78 600	80 100	1.28	129
$PMMA_{1300}$	12	74	127 000	128 000	1.34	127
$PMMA_{2500}$	16	60	230 800	246 500	1.35	128

Table 3-2. Yields of diblock copolymers calculated after solvent extraction. The values of T_g and T_d and the residual weights were measured and calculated from DSC and TGA measurements.

	Yield (%)	T_g (°C)	T_d (5% weight loss under N_2) (°C)	Residual weight at 500 °C (%)		M_r (PPQ/ PMMA)
				Calculated	Measured	
$PPQ_{50}PMMA_{800}$	77	127	362.2	4.9	11.5	0.13
$PPQ_{120}PMMA_{800}$	79	130	367.9	13.3	23.8	0.31
$PPQ_{48}PMMA_{1300}$	72	130	364.6	3.1	6.8	0.07
$PPQ_{117}PMMA_{1300}$	74	128	360.7	8.6	14.9	0.18
$PPQ_{52}PMMA_{2500}$	76	129	351.6	2.1	4.1	0.04
$PPQ_{125}PMMA_{2500}$	77	128	352.1	6.9	9.5	0.1

M_r: Molecular ratio of PPQ blocks/PMMA blocks

Scheme 3-1.

(1)
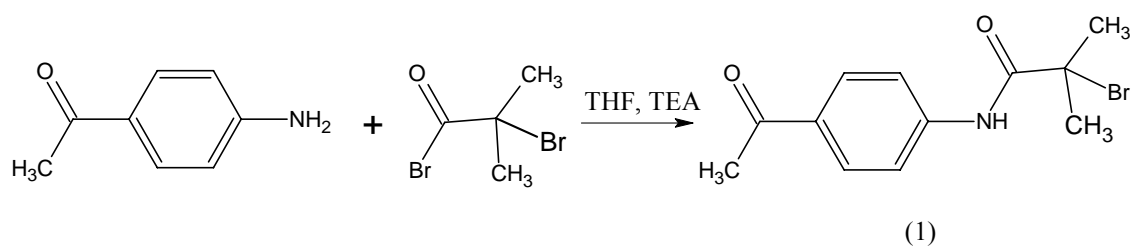
Scheme 3-2.

Scheme 3-3.

(2)   (3)

m-cresol, DPP
→

PPQ-*b*-PMMA
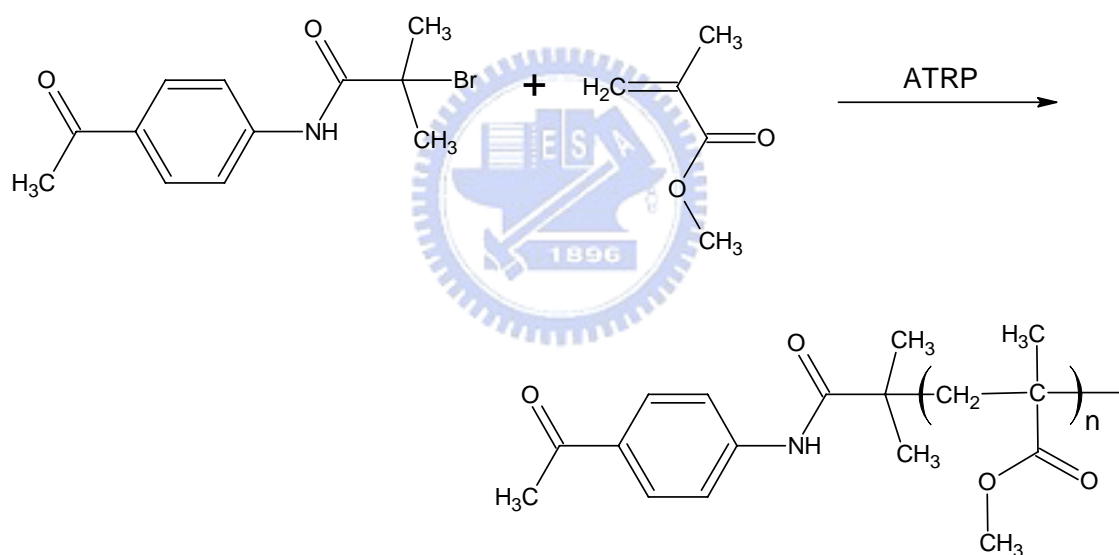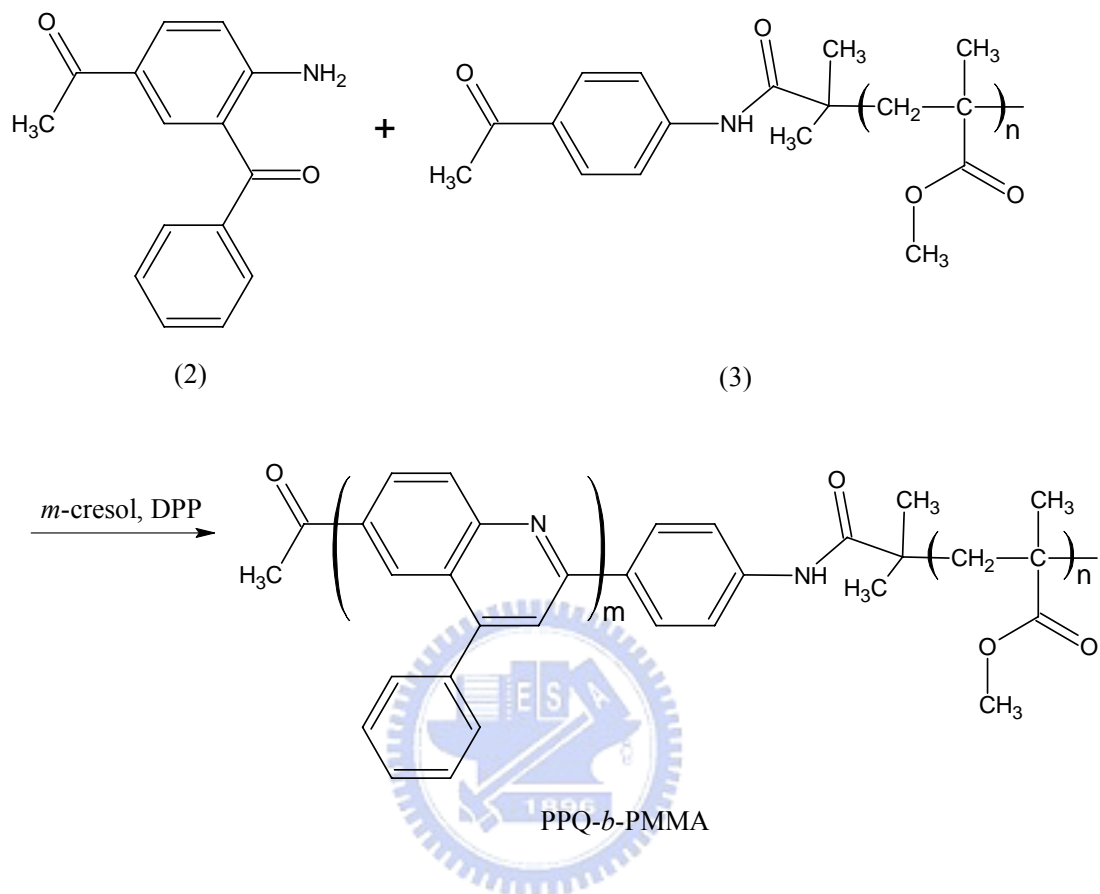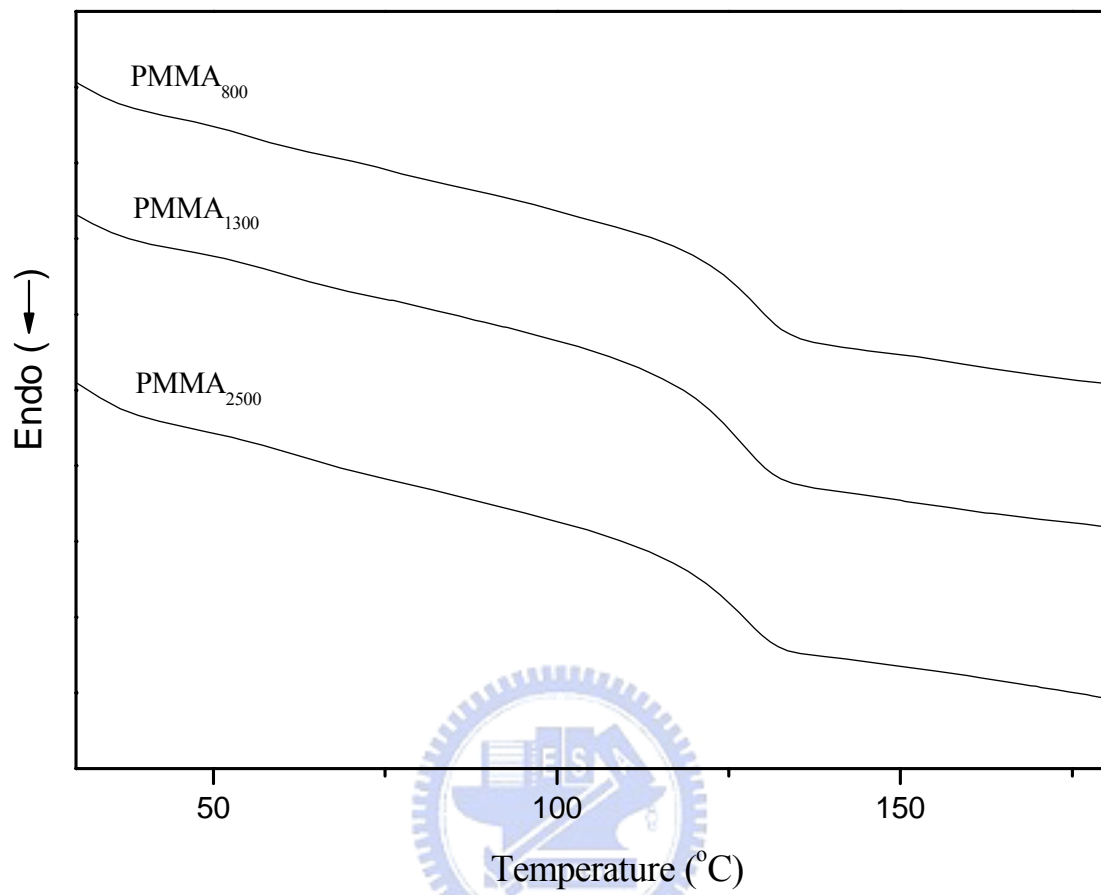
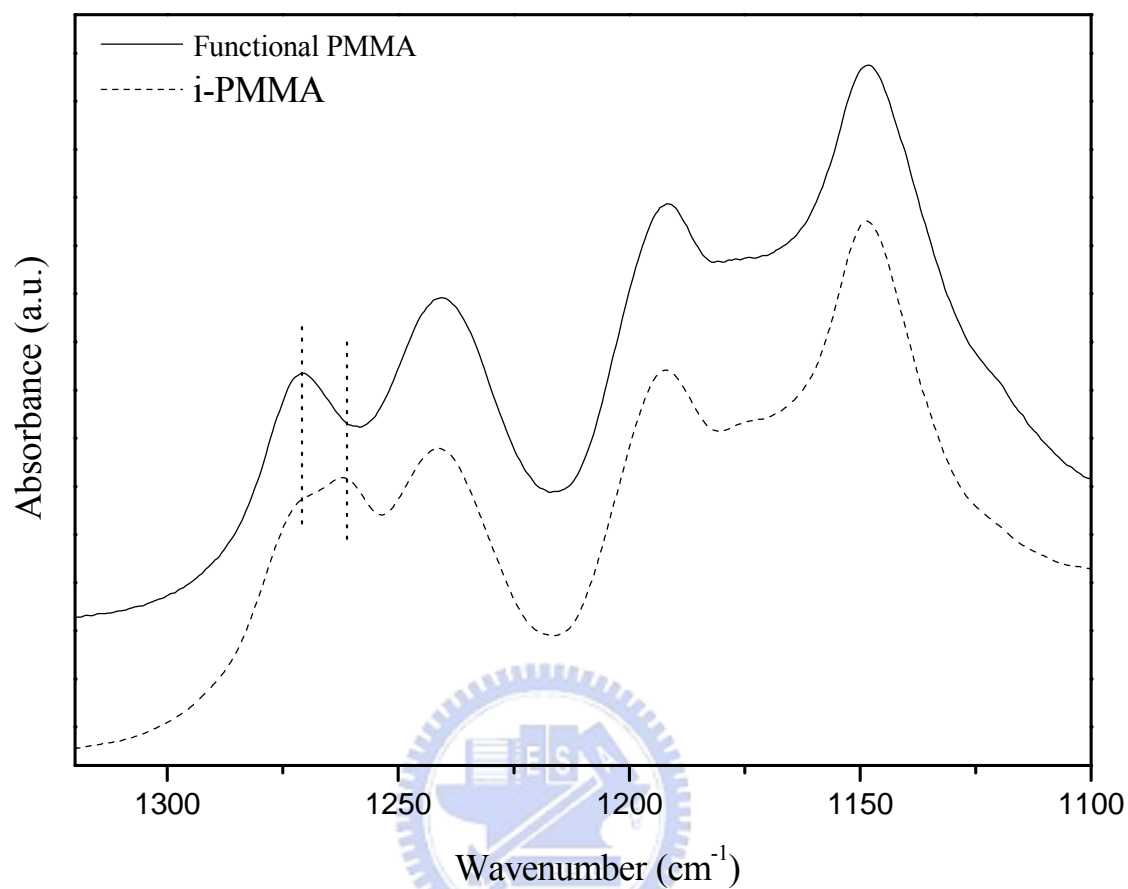Figure 3-1: DSC scans of PMMAs having various degrees of polymerization

Figure 3-2: Infrared absorbances of PMMAs having different tacticities. The curve having the solid line represents the syndiotactic-like methyl ketone-terminated PMMA; the dashed line represents that of the isotactic-like PMMA. (The isotactic-like PMMA was synthesized in our laboratory through the use of a different initiator for ATRP.)
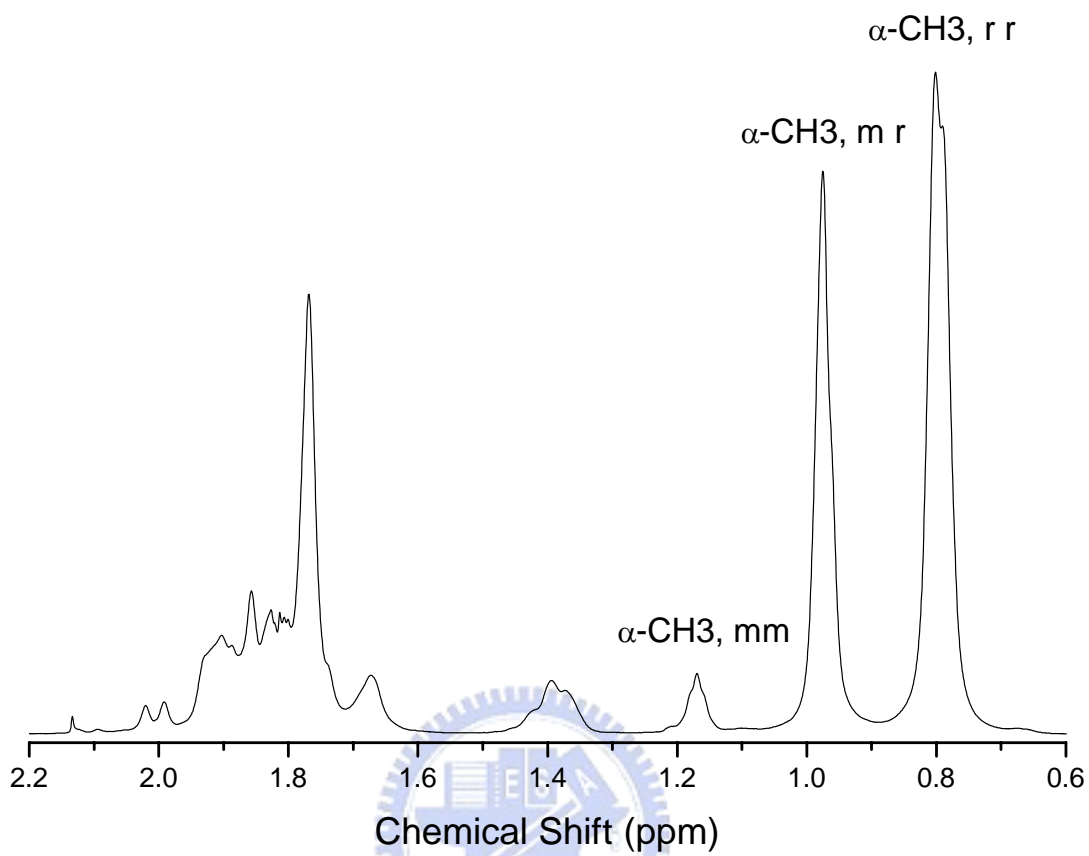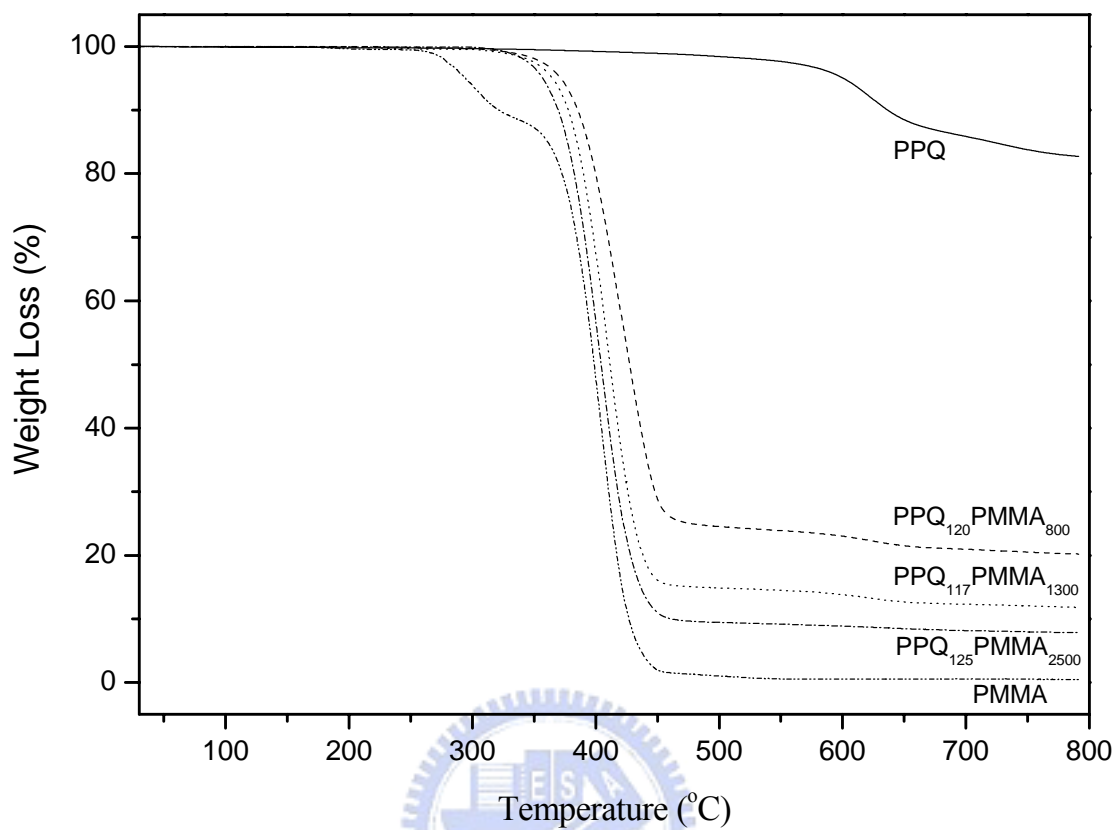
Figure 3-3: ^{1}H NMR spectrum of the PMMA$_{1300}$.

Figure 3-4: TGA thermograms of PPQ, methyl ketone-terminated PMMA, and rod–coil diblock copolymers under a flow of N_2 at 20 °C/min.

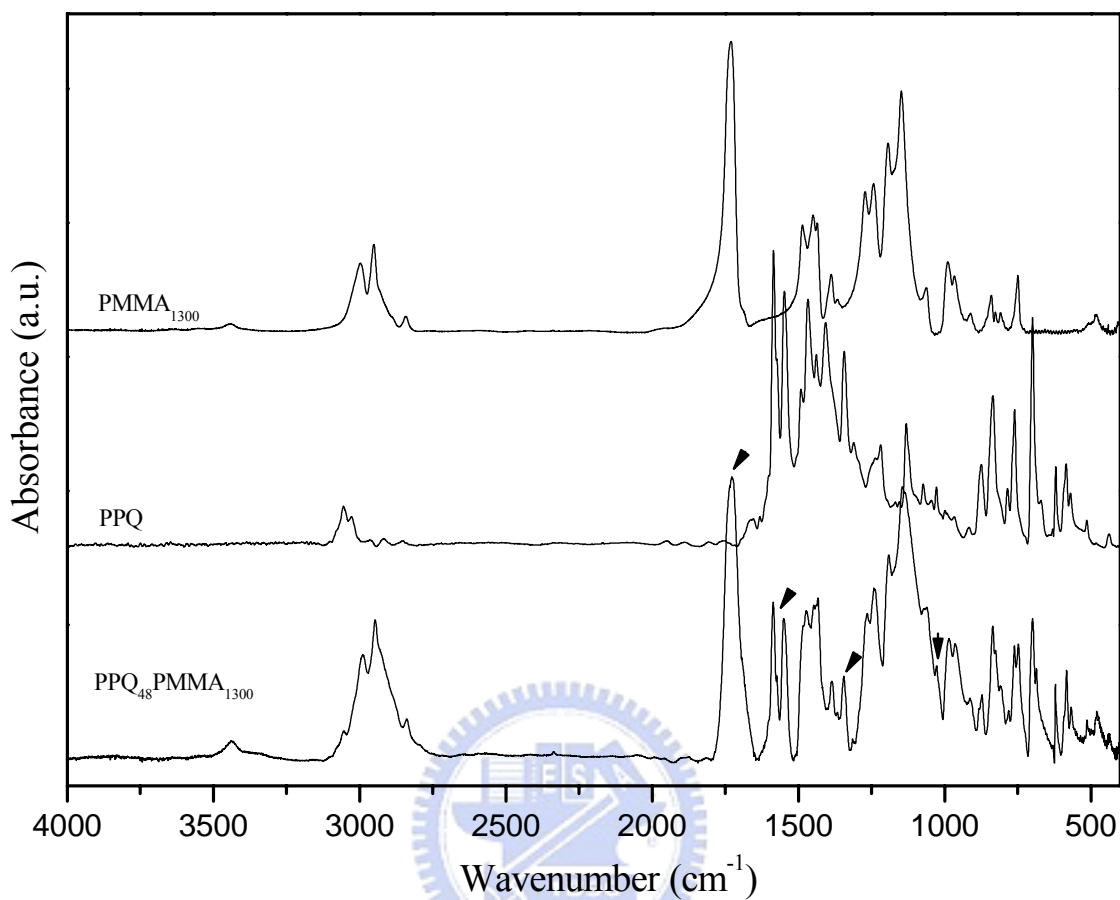Figure 3-5: FTIR spectra of methyl ketone-terminated PMMA, the PPQ homopolymer, and the rod－coil diblock copolymer. The arrows indicate the characteristic absorption peaks of the diblock copolymer.
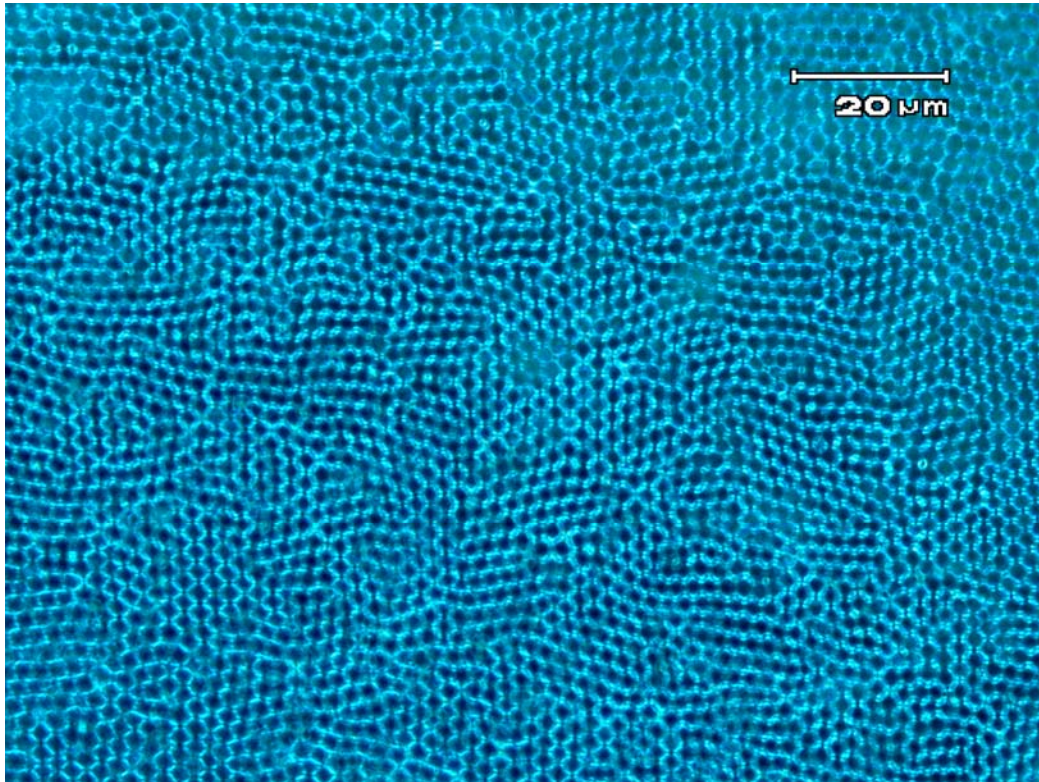
Figure 3-6: POM images prepared by dichloromethane solution of PPQ$_{52}$PMMA$_{2500}$ at concentration of 0.5 wt% under humidity of 73 %.

Figure 3-7: SEM images prepared when using dichloromethane solutions of $PPQ_{52}PMMA_{2500}$ at different concentrations. (a) 0.1 wt%; (b) 0.5 wt%; (c) 1 wt%; (d) 0.005 wt%.
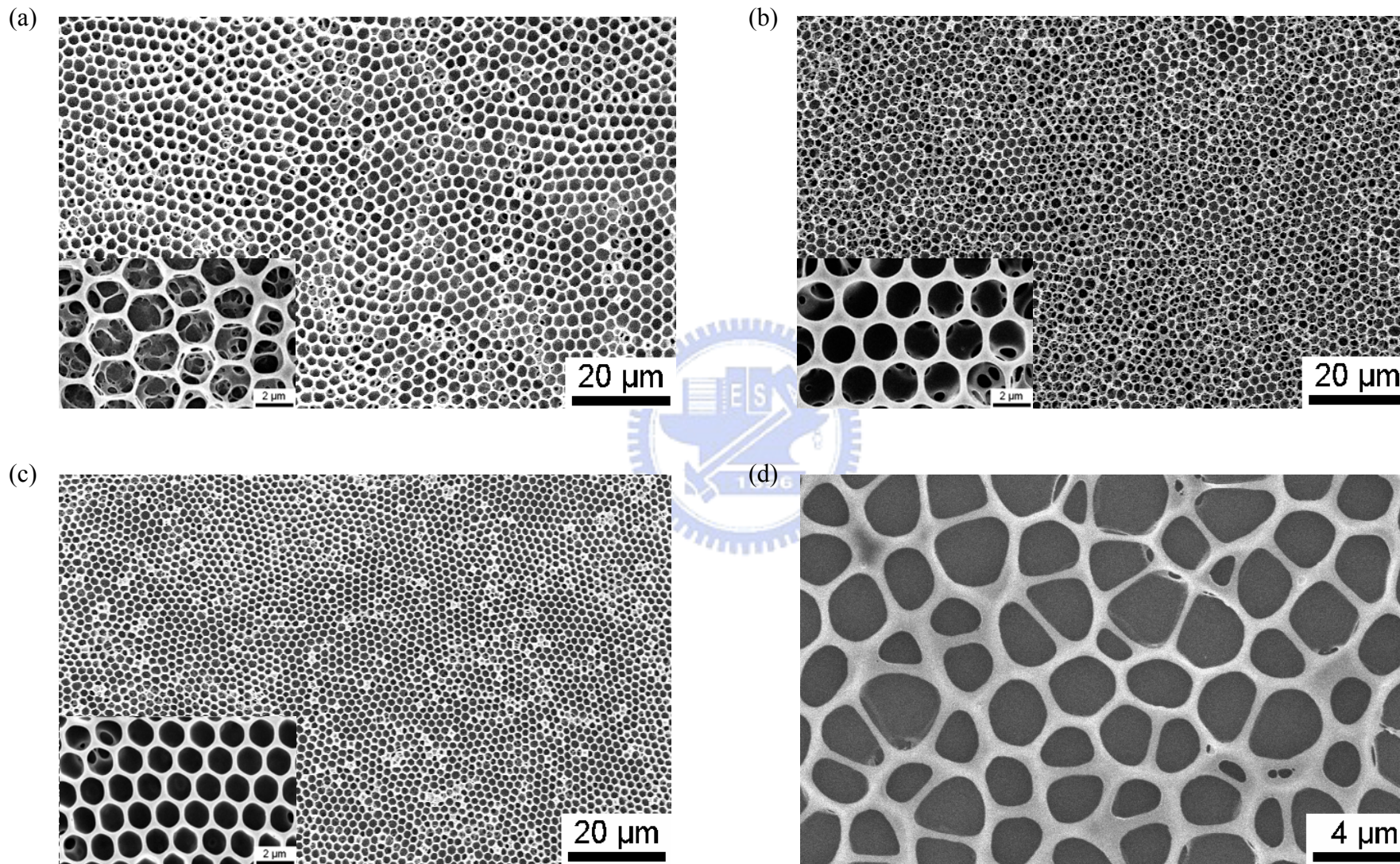
Figure 3-8: SEM images prepared when using the same concentration (1 wt%) of different diblock copolymers. (a) $PPQ_{48}PMMA_{1300}$; (b) $PPQ_{52}PMMA_{2500}$; (c) $PPQ_{50}PMMA_{800}$.

(a)

(b)

(c)
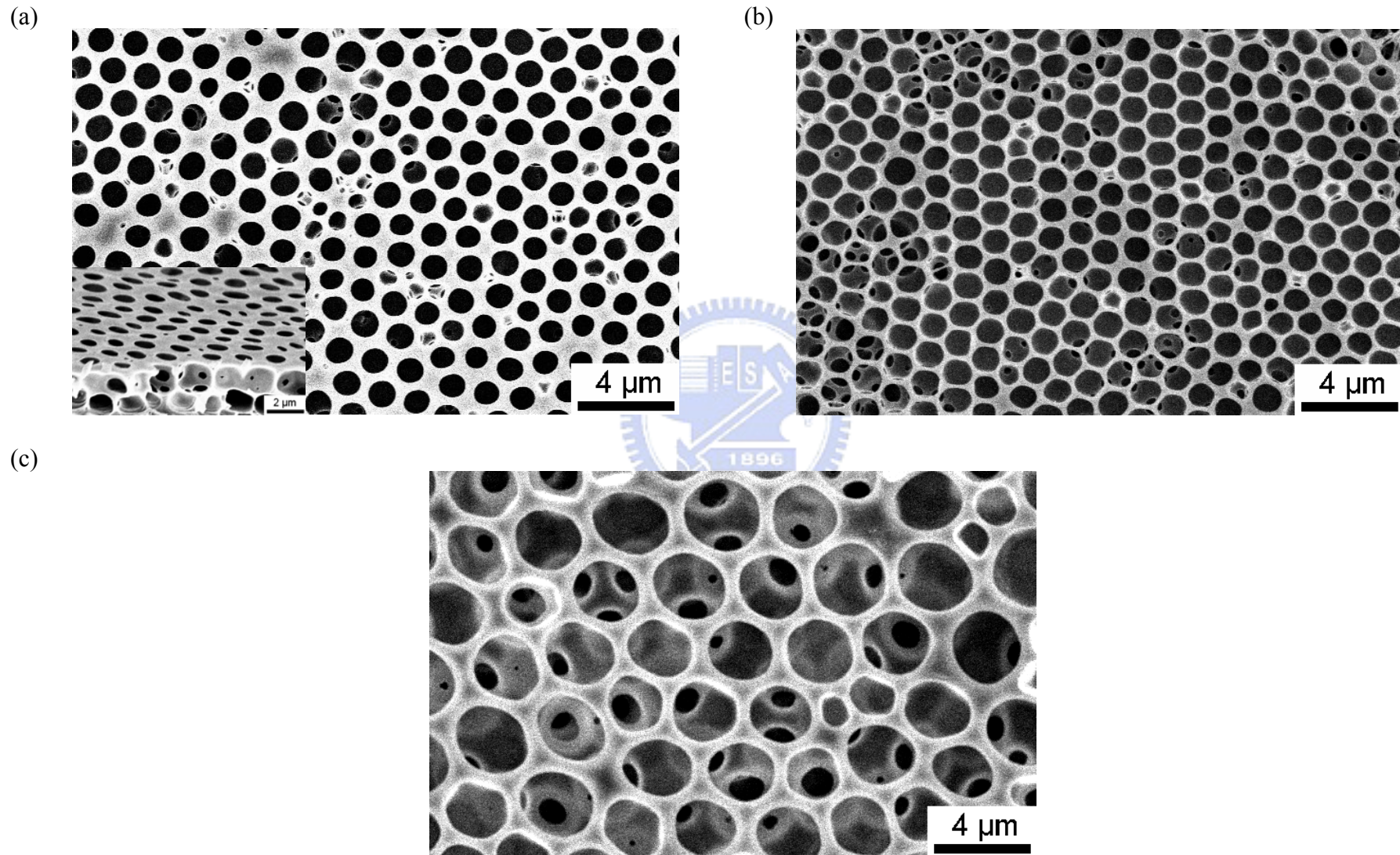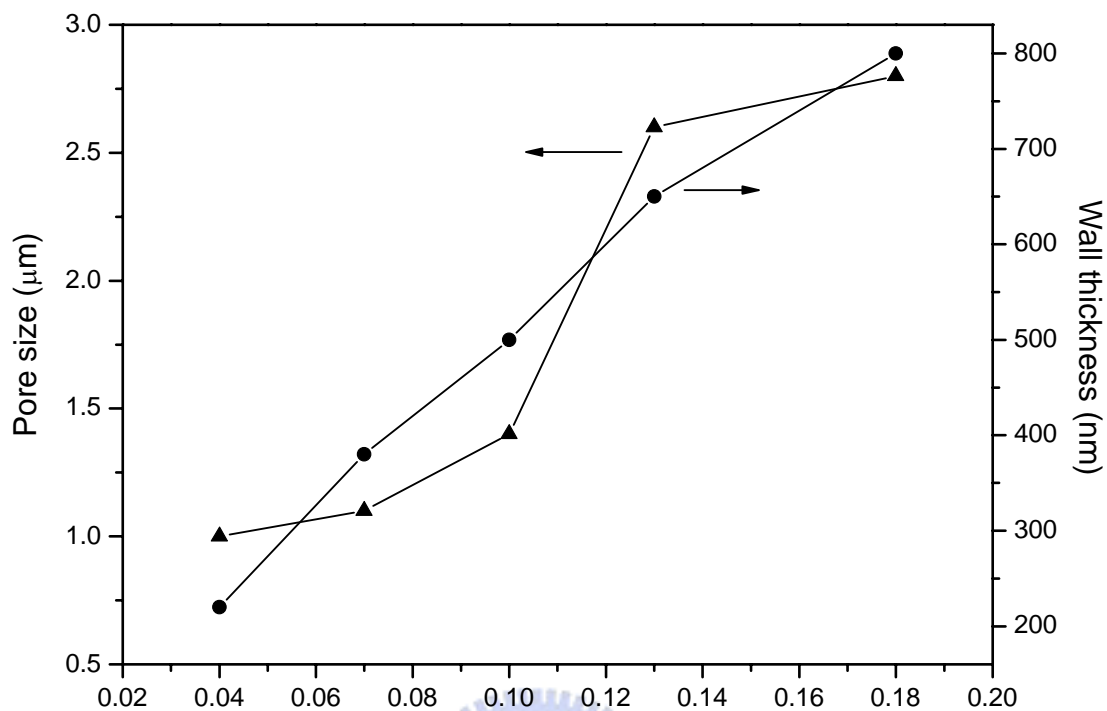
Figure 3-9: The plot of pore size and wall thickness versus relative molecular mass

(M_r) at constant polymer concentration of 1 wt%. Only five ratios are plotted,

because the solubility of $PPQ_{120}PMMA_{800}$ is too poor to form the regular porous

film.

Chapter 4

Sequence Distribution and Polydispersity Index Affect the Hydrogen Bonding Strength of Poly (vinylphenol-co-methyl methacrylate) Copolymers

Abstract

A series of poly(vinylphenol-*co*-methyl mehacrylate) (PVPh-*co*-PMMA) block and random copolymers were prepared through anionic and free radical polymerizations, respectively, of 4-*tert*-butoxystyrene and methyl methacrylate and subsequent selective hydrolysis of the 4-tert-butoxystyrene protective groups. Analysis of infrared spectra suggests that the random copolymer possesses a higher fraction of hydrogen-bonded carbonyl groups and a larger inter-association equilibrium constant relative to those of a block copolymer containing similar vinylphenol content because of the different sequence distribution that may arise from the so-called intramolecular screening effect. In contrast, the glass transition temperature of the block copolymer, which has the lower polydispersity index, is higher than that of the random copolymer at the same composition.

4-1 Introduction

A vast majority of the studies aimed at enhancing the miscibility of polymer blends have involved incorporating local centers into the blend components that are capable of participating in strong noncovalent interactions,[1-3] e.g., ion-ion interactions, ion-dipole interactions, and hydrogen bonding interactions. In particular, several papers have emphasized the use of hydrogen bonding as a miscibility enhancer.[4-7] These studies indicate that the favorable hydrogen bonding interactions are those that are stronger than the dispersive interactions that are also present; indeed, immiscible blends may be converted to single phase materials upon introducing quite low levels of hydrogen bonding. It is well known that the strength and extent of hydrogen bonding in copolymers or polymer blends are depended on their respective affinities[8-10] between the hydrogen bond donors and acceptors.

Over the years, the most widely studied hydrogen bonding polymer blend system has been the poly(vinylphenol)/poly(methyl methacrylate) (PVPh/PMMA) blend.[11-22] Sermal et al.[11] used DSC analyses to study the phase behavior of PVPh blended with PMMA and found them to be miscible; they determined the inter-association equilibrium constant (K_A) between the hydroxyl group of PVPh and the carbonyl group of PMMA to be 37.4. At the same time, however, Zhang et al.[12] reported the immiscibility of PVPh/PMMA blends from a study using the cross polarization/magic angle spinning (CP/MAS) solid state ^{13}C NMR spectroscopy. These contradictory observations may have arisen from the different solvents employed in the different blend preparation. The implication here is that miscibility may be achieved when methyl ethyl ketone (MEK) is used as the solvent, miscibility may be achieved, but a tetrahydrofuran (THF) cast blend is immiscible. This phenomenon can be explained by considering that the compositional heterogeneities arise from the different solvent

molecules.

Painter and Coleman proposed[23] that "intramolecular screening and functional group accessibility effects" have a significant effect on the number of hydrogen bonded functional groups. They used the FT-IR spectroscopy to measure the fraction of hydrogen bonded carbonyl groups present in miscible blends of poly(vinylphenol) (PVPh) with poly(ethyl methacrylate) (PEMA) as a function of composition and temperature. These results have been compared to analogous ethyl methacrylate-*random*-vinylphenol (EMAVPh) copolymers, polymer solutions of PVPh and ethyl isobutyrate (EIB), and low molecular weight model mixtures of 4-ethylphenol (EPH) and EIB.[24] The authors found that there were significant differences in the equilibrium fractions of intermolecular hydrogen bonded carbonyl groups that formed at identical concentrations and temperature.[24] Furthermore, according to the Painter-Coleman association model,[2] the inter-association equilibrium constant of the EMAVPh random copolymer ($K_A = 67.4$) is higher than that of the PVPh/PEMA blend ($K_A = 37.4$), which can be interpreted as arising from the difference in the degree of rotational freedom that results from intramolecular screening and spacing effects.[23] In this study, we concentrated on the effect of sequence distribution of PVPh-*co*-PMMA copolymer on the hydrogen bonding strength. Based on our knowledge, only a few researchers[25, 26] have compared the effects of different sequence distributions and the related hydrogen bonding strengths of copolymers.

Katime et al.[25] studied the hydrogen bond strength of the poly(vinyl acetate-*co*-vinyl alcohol) (ACA) copolymer prepared from acidic hydrolysis; this polymer is more randomly distributed than the one obtained from basic solution. The specific interaction between the acetate carbonyl and vinyl alcohol hydroxyl groups competes with self-association of hydroxyl groups. The sequence distribution effect

has been proven to be the main factor responsible for the distribution of hydrogen bonds in the copolymer. Similarly, we prepared poly(vinylphenol-*co*-acetxoystyrene) copolymers of different sequence distributions through partial hydrolyses of poly(acetoxystyrene) in acidic and basic solutions. Higher glass transition temperature, higher fraction of hydrogen-bonded carbonyl groups and a higher inter-association equilibrium constant were observed for copolymers at same composition prepared from the acidic hydrolysis than those from the basic hydrolysis because the sequence distribution of the former is relatively more random than that of the latter.[26] However, in these previous studies,[25-26] the different sequence distribution copolymers only prepared from the different hydrolyses, the real block copolymers were not available for comparison. In this study, we describe the preparation, through anionic polymerization, of the poly(vinylphenol-*b*-methyl methacrylate) block copolymer and, through free radical polymerization, the corresponding random copolymer. We used these two copolymers to compare the specific interactions that exist within them.

4-2 Experimental Section

4-2.1 Materials.

MMA (SHOWA, 99%) and 4-*tert*-butoxystyrene (*t*BOS, Aldrich, 99%) were distilled from finely ground CaH_2 before use. 2, 2'-Azobis-isobutyronitrile (AIBN, SHOWA, 99%) and benzene (TEDIA, 99%) were used without further purification.[27] *Sec*-Butyllithium (Acros, 1.3 M in cyclohexane) was used as the initiator for anionic polymerization. Tetrahydrofuran, which was used as polymerization solvent for anionic polymerization, was purified by distillation under argon from the red solution obtained by diphenylhexyllithium (produced by the reaction of 1,1-diphenylethylene and *n*-BuLi).

4-2.2 Synthesis of Poly(vinylphenol-*block*-methyl methacrylate) by Anionic Polymerization

The reactions used for the preparation of poly(vinylphenol-*block*-methyl methacrylate) (PVPh-*b*-PMMA) are shown in Scheme 4-1. A poly(4-*tert*-butoxystyrene-*block*-methyl methacrylate) (P*t*BOS-*b*-PMMA) diblock copolymer was synthesized by sequential living anionic polymerization under inert atmosphere[28] in THF using *sec*-butyl lithium as the initiator and degassed methyl alcohol as the terminator at -78 °C. 4-*tert*-butoxystyrene monomer was polymerized first for 2 h; an aliquot of poly(4-*tert*-butoxystyrene) was isolated for analysis after termination with degassed methanol. Methyl methacrylate monomer was then introduced into the reactor and the reaction was terminated with degassed methanol after 2 h.

The P*t*BOS-*b*-PMMA copolymer was converted to

poly(vinylphenol-*block*-methyl methacrylate) (PVPh-*b*-MMA) through hydrolysis. The block copolymer was dissolved in dioxane and then a 10-fold excess of 37 wt% hydrochloric acid was added. The mixture was reacted overnight at 80 ^{o}C under an atmosphere of argon and then the product was precipitated into methanol/water mixture (3:7, v/v).[29] After neutralization with 10 wt% NaOH solution to a pH value of 6-7, the polymer was filtered off. The resulting polymer underwent two dissolve (THF)/ precipitate (methanol/water) cycles and purified by the Soxhlet extraction with water for 72 h before being dried under vacuum at 80 ^{o}C.

Using a living anionic polymerization procedure similar to the one described above, the homopolymer of poly(vinylphenol) was synthesized to compare the thermal properties of the homopolymer with those of copolymers. In additional, the homopolymer of PMMA was polymerized at -78 ^{o}C using, as the initiator, *n*-BuLi reacted with 1,1-diphenylethylene.

4-2.3 Synthesis of Poly(vinylphenol -*random*-methyl methacrylate) by Free Radical Polymerization

Solution copolymerization of methyl methacrylate with 4-*tert*-butoxystyrene in benzene was performed in glass reaction flasks containing condensers at 70 ^{o}C under an argon atmosphere. AIBN was employed as an initiator and the mixture was stirred for ca. 12 h. To determine reactivity ratios, samples of the copolymers were taken from the reaction flasks in the early stage of copolymerization when the degree of conversion was low (4-9%). The copolymer was purified by repeatedly dissolving in THF and precipitating in methanol/water mixture (3:7, v/v). The synthesized poly(4-*tert*-butoxystyrene-*random*-methyl methacrylate) (P*t*BOS-*r*-PMMA) was dissolved in dioxane at a concentration of 10% (w/v). The solution was then refluxed

overnight in the presence of 37% HCl to remove the *tert*-butoxy groups. Before

vacuum drying, the poly(vinylphenol-*random*-methyl methacrylate) (PVPh-*r*-PMMA)

was precipitated repeatedly from THF solution into methanol/water and purified by

the Soxhlet extraction with water for 72 h to remove any residual HCl.

4-2.4 Blend Preparation

Blends of various binary PVPh/PMMA blend compositions were prepared by

solution casting. Methyl ethyl ketone (MEK) solution containing 5 wt% polymer

mixture was stirred for 6-8 h and then it was cast onto a Teflon dish. The solution was

left to evaporate slowly at room temperature for 1 day. The blend films were then

dried at 50 $^{\circ}$C for 2 days.

4-2.5 Measurements.

Molecular weights and molecular weight distributions were determined through

GPC using a Waters 510 HPLC equipped with a 410 differential refractometer, a UV

detector, and three Ultrastyragel columns (100, 500, and 10^3 Å) connected in series

and THF as eluent at a flow rate of 0.6 mL/min and 35 $^{\circ}$C. The molecular weight

calibration curve was obtained using polystyrene standards. ^{1}H NMR and ^{13}C NMR

spectra were obtained using an INOVA 500 instrument; acetone-d_6 was the solvent.

All infrared spectra were recorded at 25 $^{\circ}$C at a resolution of 1cm^{-1} on a Nicolet

AVATAR 320 FTIR spectrometer and degassed with nitrogen. Each sample was

dissolved in methyl ethyl ketone (MEK) and than cast directly onto KBr pellets. All

films were vacuum–dried and were thin enough to be within the absorbance range

where the Beer-Lambert law is obeyed. Thermal analysis was performed on a DSC

instrument from Du-Pont (DSC-9000) at a scan rate of 20 $^{\circ}$C/min over a temperature

range from 20 to 250 ^{o}C. The sample was quenched to 20 ^{o}C from the melt state for the first scan and then rescanned between 20 ^{o}C and 250 ^{o}C at 20 ^{o}C/min. The glass transition temperature was obtained at the inflection point of the jump heat capacity.

4-3 Results and Discussion

4-3.1 Synthesis of poly(vinylphenol-*block*-methyl methacrylate) copolymer by anionic polymerization

The block copolymer, PVPh-*b*-PMMA, was designed and prepared by living anionic polymerization and subsequent hydrolytic deprotection. The GPC trace of the PVPh-*b*-PMMA block copolymer obtained after polymerization and hydrolysis shown in Figure 4-1 displays a narrow molecular weight distribution. Although this diblock copolymer system has not been investigated previously, living anionic polymerization of the protected hydroxystyrene monomer[29-31] and methyl methacrylate monomer[32,33] are well documented. To obtain a monodisperse PVPh block, it is necessary to protect the hydroxyl group prior to polymerization to avoid the termination of the living chain end. Various protecting groups, including *tert*-butyl ether[31] and *tert*-butyldimethylsilyl[30] groups, have been used for hydroxyl group protection during anionic polymerization. In this study, the *tert*-butyl ether protected monomer was used because of its simple hydrolysis and ready availability.

The complete elimination of the protective groups and the regeneration of the phenolic hydroxyl groups were demonstrated by ^{1}H and ^{13}C NMR spectroscopy. Figure 4-2 displays typical ^{1}H NMR spectra of the diblock copolymer recorded before (bottom) and after (top) deprotection. A chemical shift at 1.29 ppm corresponds to the *tert*-butyl group of the P*t*BOS-*b*-PMMA copolymer (in acetone-d_6). The spectrum of the hydrolyzed block copolymer is essentially disappeared on those peaks corresponding to the *tert*-butyl group, only polymer backbone protons appear in the chemical shift region of 1-2 ppm. In addition, a peak (8.0 ppm) corresponding to the proton of the hydroxyl group appears after hydrolysis reaction. Figure 4-3 displays the ^{13}C NMR spectra of the

P*t*BOS-*b*-PMMA and PVPh-*b*-PMMA copolymers. The signal of the quarternary carbon atoms of the *tert*-butyl group in the P*t*BOS segment is located at 78.0 ppm. After hydrolysis reaction, no signal remains for the *tert*-butyl group (Figure 4-3b). Scheme 4-1 displays all of the other peak assignments presented in Figure 4-2 and Figure 4-3. As mentioned above, the *tert*-butyl group was deliberately chosen as a protective group in this study because it was expected to be selectively and readily removed from the parent copolymers without hydrolyzing the methacrylate ester groups.[34-36] The FT-IR spectrum (Figure 4-4) of the resulting block copolymer after hydrolysis clearly shows the carbonyl stretching vibration band of PMMA segment in the region from 1690 and 1750 cm^{-1}. The broad peak at 3450 cm^{-1} in Figure 4-4c indicates the presence of the hydroxyl groups. The molecular weight fraction of the PVPh-b-PMMA block copolymer was measured by ^{1}H NMR spectroscopy by analyzing their relative signal intensities of the protons of the PMMA and PVPh segments. The calculation was performed by comparing the signals of the aromatic protons of the PVPh segment (6.4–6.8 ppm) and the signal of the methyl ester groups of the PMMA segment (3.6 ppm). Table 4-1 lists these calculated molecular weight fractions and the total molecular weights determined by GPC; the number "*n*" beside the descriptor "PVPh-*b*-PMMA" reflects the molecular weight fraction.

4-3.2 Synthesis of poly(vinylphenol-*random*-methyl methacrylate) copolymer through free radical polymerization

The random copolymer was prepared in benzene at 70 ^{o}C under argon using AIBN as initiator (Scheme 4-2). A series of random copolymers were prepared containing different MMA and *t*BOS monomer concentrations. As mentioned above, the total molecular weight of copolymer was determined by GPC and the chemical

composition of the copolymer was characterized by ^{1}H NMR. The complete elimination of the protective groups and the regeneration of the phenolic hydroxyl groups were also demonstrated by ^{1}H and ^{13}C NMR spectroscopies using a method similar to that used for block copolymer (for brevity, not shown here) and these respective values are summarized in Table 4-2. Here, we assume that the PtBOS precursor and ensuing PVPh copolymer possessed the same degree of polymerization in both block and random copolymers.

To estimate copolymer composition, we used the Kelen–Tüdös method to determine the reactivity ratios (r_1 and r_2) for MMA and tBOS.[37,38] The values of $r_1 = k_{11}/k_{12}$ and $r_2 = k_{22}/k_{21}$ are the ratios of homo-propagation/cross-propagation rate constants for each monomer species. All polymerizations were performed in benzene under the same conditions described in the Experimental Section and terminated them below 10% monomer conversion to minimize errors due to changes in the feed ratio. This method derives the reactivity ratio from the well-known 'copolymerization equation' which contains two parameters, η and ξ, as described in previous literatures.[39,40] The results are displayed graphically for the PtBOS-co-PMMA copolymer in Figure 4-5 from which values of $r_{PMMA} = 0.8$ and $r_{PtBOS} = 0.28$ are calculated. The apparent linear relationship suggests that the copolymerization of these two comonomers follows the simple two-parameter (terminal) model. The product of the reactivity ratios falls with the range 0.18-0.25, which indicates that these two monomers are introduced into the polymer chain in an essentially random fashion with a slight tendency towards alternation. Hence, these copolymers synthesized by free radical polymerization are essentially random copolymers.

4-3.3 FT-IR analyses

Several regions within the infrared spectra of PVPh-co-PMMA copolymers are influenced by hydrogen-bonding interaction. Figure 4-6 shows the infrared spectra in the 2700-3800 cm^{-1} range for different sequence distributions of PVPh-*co*-PMMA copolymers prepared from (a) free radical and (b) anionic polymerizations in addition to (c) the PVPh/MMA blend system. Clearly, the hydroxyl stretching intensities of both copolymers and polymer blend shift to lower wavenumber upon increasing the vinylphenol content. In the meantime, the hydroxyl stretching band broadens as a result of being composed of contributions arising from the different environments surrounding the hydroxyl groups. These data suggest that there are many different types of hydroxyl groups present in PVPh-*co*-PMMA copolymers and PVPh/PMMA blends. The spectrum of pure PVPh shown in Figure 4-6 is characterized by a very broad band centered at 3350 cm^{-1}, indicating that these hydroxyl groups are hydrogen bonded to other hydroxyl groups as dimmers and chain-like multimers. A second narrower band, observed at 3525 cm^{-1} as a shoulder on the high frequency side of the broad hydrogen bonded band, is assigned to free hydroxyl groups.[2] The inter-association hydrogen bonding between hydroxyl and carbonyl groups is at the middle wavenumber (depending on the sequence distribution and compositions in copolymer and compositions in polymer blend).

Taking into account the effect of composition, the carbonyl groups of methyl methacrylate units compete with self-associated hydroxyl groups for hydrogen bonding and cause the shift of the hydroxyl band toward higher wavenumbers at lower vinylphenol content. In this situation, majority of only one type of hydroxyl group from the hydrogen–carbonyl inter-association is expected, and thus the

hydroxyl stretching band is relatively narrower. In the cases of block copolymers and blend systems, this shift is less pronounced. On the contrary, the free, dimmer, or multimer hydrogen bonded hydroxyl groups will exist at higher vinylphenol contents, resulting in broader absorptions. Thus the self-association hydrogen bonding of hydroxyl group dominates at higher vinylphenol contents.

In Figure 4-7, the spectra in the hydroxyl stretching region for two different sequence distributions of PVPh-*c*o-PMMA copolymers and the PVPh/PMMA binary blend are displayed. There is a clear difference between the spectra of these two copolymers and the blend system; even through they possess similar vinylphenol content. The random copolymer prepared from free radical polymerization presents its hydroxyl stretching band shifted to higher wavenumber. In contrast, the hydroxyl bands of block copolymer and binary blend are relatively closer to that of pure PVPh. This can be explained in terms of different environments experienced by these hydroxyl groups. In block copolymer and binary blend, the hydroxyl environment is closer to that of PVPh, where these hydroxyl groups are surrounded mostly by other hydroxyl groups, and thus multiple self-associations are favored. It is well known that multiple hydrogen bonding between hydroxyl groups leads to lower its wavenumber. In addition, for the random PVPh-*r*-PMMA copolymers, the absorption peak of the broad band representing the self-associated hydroxyl-hydroxyl units shifts to higher wavenumber upon increasing PMMA content (Figure 4-6a). Therefore, it is reasonable to assign the band at 3440 cm^{-1} to the hydroxyl groups interacting with carbonyl groups because the small number of the hydroxyl groups tends to interact completely with carbonyl group. Moreover, the appearance of the hydroxyl band of the random copolymer was narrower than those of block copolymer and binary blend because the existence of nearly only one type of inter-association of hydroxyl-carbonyl in the

PVPh-*r*-PMMA copolymer.

The carbonyl stretching band for PMMA appears at 1730 cm^{-1}. For PVPh-*co*-PMMA copolymers, Figure 4-8 indicates that the location of this band changes widely depending on the composition and sequence distribution of its repetitive units. The spectra of PVPh-*r*-PMMA, PVPh-*b*-PMMA and PVPh/PMMA blend were measured at room temperature over the region from 1670 to 1760 cm^{-1}. Again, the peaks at 1730 cm^{-1} and 1705 cm^{-1}, corresponding to the free carbonyl and hydrogen bonded carbonyls can be fitted well to the Gaussian function. As expected, a higher content of vinylphenol units results in a higher number of hydrogen bonded carbonyl groups. To obtain the fraction of the hydrogen bonded carbonyl group, the known absorptivity ratio for hydrogen bonded and free carbonyl contributions is required. We employed a value of $\alpha_{HB}/\alpha_F = 1.5$ which was previously calculated by Moskala et al.[41] Table 4-3 summarizes the fractions of hydrogen-bonded carbonyl groups that are calculated through curve fitting of the data from both the copolymers and the binary blends. The fraction of hydrogen bonded carbonyl groups increased upon increasing the PVPh content for both two PVPh-*co*-PMMA copolymers and PVPh/PMMA blend system. Moreover, the fraction of hydrogen bonded carbonyl groups of these two copolymers was always higher than that of blend system at similar PVPh contents. This observation can be explained in terms of the difference in degree of rotational freedom between polymer blend and copolymers. The polymer chain architecture of a homopolymer is significantly different to a copolymer as a result of intramolecular screening and functional group accessibility caused by the chain connectivity.[42-46] The PVPh segments in the PVPh/PMMA blend has more contacts with segments of its own type than exist in the corresponding copolymer because of chain connectivity and intramolecular screening effect. Intramolecular screening results from an increase in the number of

same-chain contacts due to the polymer chains bending back upon themselves. This "screening" reduces the number of intermolecular hydrogen bonds that are formed in a polymer blend. Thus the density of inter-association hydrogen bonds of a polymer blend is relatively lower than that of a corresponding copolymer. Moreover, the spacing between functional groups along a homopolymer chain and the presence of bulky side group are also responsible for the observed less inter-association hydrogen bond density in terms of the so-called functional group accessibility effect. This effect occurs as the result of steric crowding and shielding.[45] As a result; the density of the hydrogen bonded carbonyl group in the PVPh/PMMA blend is relatively lower than that in the corresponding PVPh-co-PMMA copolymer at the same composition as would be expected.

Now, we turn our attention to different sequence distribution of PVPh-co-PMMA. The fraction of hydrogen bonded carbonyl of the PVPh-r-PMMA is observed to be higher than that of the block copolymer over the entire compositions. A random distributed PVPh-r-PMMA copolymer provides greater opportunity for hydrogen bond formation between the hydroxyl group of PVPh and the carbonyl group of PMMA than does a block copolymer. On the basis of the Painter-Coleman association model, the inter-association equilibrium constants of PVPh-co-PMMA copolymers prepared through both free radical and anionic polymerization were determined. The inter-association equilibrium constants (K_A) of PVPh-r-PMMA and the PVPh/PMMA blend have been reported[23] to be 67.4 and 37.4, respectively. To calculate the inter-association equilibrium constant of PVPh-b-PMMA copolymer, the methodology of a least-square method has been described in the previous study.[47] Table 4-4 lists all of the thermodynamic parameters in these copolymer and polymer blend systems. K_2 and K_B represent the hydrogen-bonded dimer and multimer of the self-association equilibrium constants

of PVPh, respectively. The K_A is the equilibrium constant describing the inter-association of PMMA with PVPh. Accordingly, the inter-association constant of the PVPh-*b*-PMMA is obtained as 47.1 when using least-squares fit based on the fraction of hydrogen bonded carbonyl group experimentally obtained.

Using values of K_A together with the PVPh self-association equilibrium constants (K_2 and K_B), we can calculate the theoretical curves for the number of hydrogen bonded carbonyl group at 25 ^{o}C as a function of the weight fraction of PVPh content, and the results are displayed in Figure 4-9. At first sight, the shape of the calculated curve reproduces the trend in the experimental data very well. However, the fit between calculated and experimental results at high and low fractions of PVPh, i.e., at weight fractions less than 0.4, is not quite as good it is in the central region. This derivation is reasonable because the most accurate range for determining fraction of hydrogen bonded carbonyl groups spectroscopically is that from 0.4 to 0.7, where the bands for both free and hydrogen bonded carbonyl groups are well separated with significant absorbance.[43] Outside this range of 0.4 ~ 0.7, one of the bands is buried under the other and appears as a less defined shoulder. Moreover, it can be seen from Figure 4-9 that the fraction of hydrogen bonded carbonyl groups is most sensitive to the magnitude of K_A at PVPh weight fraction of > 40%. Below this weight fraction, the variation of fraction of hydrogen bonded carbonyl groups with K_A is relatively few sensitive.

From Table 4-4, the observed inter-association equilibrium constants from the PVPh-*r*-PMMA copolymer (67.4) and the self-association constant of PVPh homopolymer (66.8) are fairly close. The competition between self-associating and inter-associating bonds is complicated and numbers of self-association and inter-association hydrogen bonds depend upon the component fraction in the copolymer. In addition, the inter-association equilibrium constant of the

PVPh-*b*-PMMA is substantially less than that of the self-association equilibrium constant of the PVPh homopolymer (47.1 vs 66.8), which implies that the tendency toward forming hydrogen bonds between two hydroxyl groups dominates over hydroxyl – carbonyl interactions in PVPh-*b*-PMMA copolymer. Most importantly, the K_A value of PVPh-*r*-PMMA is greater than that of PVPh-*b*-PMMA copolymer, implying that the hydroxyl groups in the random copolymer have a better opportunity to interact with carbonyl groups than they do in the block copolymer. As mentioned above, and previously in the literature,[42,48] intramolecular screening effect arises as a consequence of chain connectivity, the covalent linkages between polymer segments from a copolymer induces greater number of same chain contacts than that calculated on the basis of a simple random mixing of segments. Hence, Painter and Coleman modified their Painter – Coleman association model (PCAM). A parameter, γ, was introduced, defined as the fraction of same chain contacts that originate from the polymer chain bending back upon itself, primarily through local, but also through long range connectivity effects. In brief, the equilibrium constants, $\tilde{K}_B$ and $\tilde{K}_A$ were substituted for K_B and K_A and defined as

$$\tilde{K}_B = K_B \left[\frac{\gamma + (1-\gamma)\Phi_B}{\Phi_B} \right] \tag{1}$$

$$\tilde{K}_A = K_A \left[\frac{1 - (\gamma + (1-\gamma)\Phi_B)}{\Phi_A} \right] = K_A (1-\gamma) \tag{2}$$

where Φ_B and Φ_A are the volume fraction of self-association species B (PVPh) and non-self-association species A (PMMA), respectively. γ is the fraction of intrachain contacts, as mentioned above. This means that $\tilde{K}_A$ is the "effective" equilibrium constant. To adjust for intramolecular screening, Painter and Coleman employed equations 1 and 2 with a value of γ = 0.30 which appears most appropriate for amorphous polymer melt.[42] When a value of $\tilde{K}_A$ of 47.1 is employed for

PVPh-*b*-PMMA in Eq. 2, the value of K_A is obtained to be 67.3 (i.e., $K_A = \tilde{K}_A/\gamma = 47.1/0.7$). In other words, $K_A = 67.3$ of PVPh-*b*-PMMA can be considered to be the characteristic of an inter-association equilibrium constant in the absence of intramolecular screening. It is interesting to notice that this value of $K_A = 67.3$ is very close to the value of 67.4 obtained experimentally from the PVPh-*r*-PMMA copolymer. Accordingly, it implies that the $\tilde{K}_A$ value of a block copolymer containing both hydrogen bonded donor and acceptor segments may be able to be estimated from the "effective" equilibrium constant of its corresponding random copolymer. While additional work is necessary to ensure the validity of such an approach, this result is not simply a fortuitous one, and it does offer the tantalizing possibility that the value of the inter-association equilibrium constant may be transformable.

4-3.4 Thermal Analyses

Differential scanning calorimetry (DSC) is a convenient method to observe thermal characteristics arising from different interactions between copolymers and polymer blends. Figure 4-10 shows the DSC thermograms of both PVPh-*co*-PMMA copolymers and PVPh/PMMA blend, revealing that essentially all DSC traces possess only one glass transition temperature. Single glass transition temperature strongly suggests that these systems are fully miscible and possess a homogeneous amorphous phase. The values of glass transition temperatures and T_g breadths obtained form systems are listed in Table 4-5. In general, a miscible polymer blend generally gives a broader DSC transition, while those of copolymer systems are relatively narrower. The random copolymer usually exhibits the narrowest T_g breadth because of the more adjacent units of segments A and B. As a result, a

random copolymer has greater homogeneity at the molecular scale than a block copolymer.

At the first sight, the glass transition temperatures in all systems increase upon increasing the content of vinylphenol because PVPh has a higher T_g. In another aspect, the PVPh/PMMA blend system typically has the lowest T_g at every composition. It is quite unexpected to notice that the glass transition temperature of the block copolymer is higher than that of the random copolymer containing the same PVPh content even though the fraction of hydrogen bonded carbonyl and the value of K_A obtained from PVPh-*r*-PMMA copolymers are higher than these obtained from the PVPh-*b*-PMMA copolymers, the T_g relationship between two copolymer containing different sequence distribution does not obey the conventional trend. In general, the glass transition temperature is not only dependent on the specific interactions, but also upon the physical and chemical nature of the polymer molecules such as molecular weight, poydispersity, chain segment flexibility, branching and crosslinking. It has been well documented that, for a constant polydispersity, as the molecular weight of a polymer is increased there is a subsequent increase in glass transition temperature.[49] However, once a sufficiently high molar mass is obtained, the T_g remains essentially constant. This phenomenon can be rationalized by the reduction in free volume as the number of chain ends decreases with increasing molar mass. As expected a similar trend is observed in these synthesized PVPh homopolymers (Table 4-6). From Table 4-6, it can be seen that the T_g reaches a plateau value above a molecular weight of 6000. Furthermore, these copolymers used in this study have the similar molecular weight. The influence of molecular weight would not be the significant factor for the property of glass transition temperature. Thus such unexpectedly result may arise from the different polydispersity between the random and the block copolymer.

It is well known that block copolymers prepared from anionic polymerization

have a lower polydispersity (ca. 1.05–1.2) than do those obtained through conventional free radical copolymerization. Higher polydispersity may result in additional interaction energy arising from the longer chain and higher radius of gyration, both of which influence polymer packing to increase in free volume and result in lower glass transition temperature.[50,51] To confirm this assumption, we purposely synthesized (see the next Section) PVPh-b-PMMA block copolymers of higher polydispersity by using atom transfer radical polymerization (ATRP). The synthesized PVPh-b-PMMA copolymer by ATRP indeed has greater polydispersity index (near the magnitude of 1.6) than that from anionic polymerization because of the purity of monomers. Although the ATRP block copolymer and anionic block copolymer were hydrolyzed under different conditions, the PtBOS and PAS segments were completely hydrolyzed and purified by the Soxhlet extraction to remove any residual NaOH or HCl. We supposed that the different hydrolysis reactions would not influence the glass transition temperature of different block copolymers.

Figure 4-11 shows the glass transition temperatures of each system. Again, the PVPh-b-PMMA copolymer obtained through anionic polymerization has the largest T_g among all of these PVPh-co-PMMA copolymers, even though its f_b and K_A are less than those of PVPh-r-PMMA copolymer. As mentioned previously, glass transition temperature of a polymer is strongly depended on the polydispersity index. When the PVPh-r-PMMA prepared by free radical polymerization and PVPh-b-PMMA prepared by ATRP have the similar polydispersity index, the typical trend of large value of f_b resulting in a higher value of T_g remains valid. However, the PVPh-b-PMMA with similar composition and molecular weight but the lowest polydispersity index results in the highest glass transition temperature.

4-4 Synthesis of Poly(vinylphenol-*block*-methyl methacrylate) Copolymer by

Atom Transfer Radical Polymerization

4-4.1 Materials

The methyl methacrylate (MMA, 99 %) was distilled from calcium hydride and the 4-acetoxystyrene (AS, 95 %) was used as received without any purified procedure. Copper (I) bromide (CuBr) was stirred continuously in glacical acetic acid overnight, filtered, and then rised with absolute ethanol under a blanket of argon, and dried under vacuum at 80 °C for three days. The solvent, xylenes, was distilled prior to use. Amberlite IR-120 (H form) cation exchange resin, *N,N,N′,N′,N′′*-pentamethyldiethylenetriamine (PMDETA) was used as received and (1-bromoethyl)benzene was used as initiator. The syntheses of PMMA-Br, PMMA-*b*-PAS and PMMA-*b*-PVPh were shown in Scheme 4-3.

4-4.2 Preparation of PMMA-Br Macroinitiator

A typical polymerization is as follows: CuBr (1 mmol) was placed into a dry 100 mL round-bottom flask equipped with a stirrer bar. Deoxygenated xylenes (25 mL), MMA (100 mmol) and ligand (1 mmol) were added sequentially and the solution was stirred for 60 min to form the Cu complex. The initiator (1 mmol) was then added. This whole process took place in a nitrogen-filled dry box. The reaction mixture turned dark green immediately and became progressively more viscous. Upon completion of the reaction controlled at 80 °C for 12 hr, the mixture was diluted with five-fold of tetrahydrofuran (THF) and stirred with of Amberlite IR-120 (H form) cation-exchange resin (3–5 g) for 30–60 min to remove the catalyst. The mixture was then passed through an alumina column and precipitated into methanol (500 mL). The resulting polymers were filtered and dried overnight at 60 °C under

vacuum.

4-4.3 Preparation of PAS-*b*-PMMA by ATRP of 4-acetoxystyrene with PMMA-Br Macroinitiator.

The macroinitiator PMMA-Br (0.04 mmol) and CuBr (0.4 mmol) was placed in a dry 50 mL round-bottom flask equipped with a stirrer bar. Deoxygenated solvent (xylenes, 2 mL), monomer (4-acetoxystyrene, 32 mmol) and ligand (0.4 mmol) were added sequentially and the solution was stirred for 30 min to form the Cu complex. This whole process took place in a nitrogen-filled dry box. The reaction mixture turned dark green immediately and became progressively more viscous. Upon completion of the reaction controlled at 110 °C for 96 hr, the mixture was diluted five-fold with tetrahydrofuran (THF) and stirred with of Amberlite IR-120 (H form) cation-exchange resin (3–5 g) for 30–60 min to remove the catalyst. The mixture was then precipitated into methanol (300 mL). The resulting polymer was filtered and dried overnight at 60 °C under vacuum.

4-4.4 Deacetylation of Poly(PAS-*b*-PMMA)

To a mixture of PMMA-b-PAS in 1,4-dioxane under N_2, the appropriate amount of NaOH (0.3 N) was added dropwisely over 15 min. After addition, the reaction mixture was reflux at 90 °C for 5 h. The reaction is then cooled to room temperature, and the polymer product was isolated by precipitation into diethyl ether. Furthermore, the final product was purified by the Soxhlet extraction with water for 72 h to remove the residual NaOH, and then dried in a vacuum oven overnight at 80 °C.

4-5 Analysis of PVPh-*b*-PMMA Copolymer

4-5.1 ^{1}H NMR Analyses

Figure 4-12a shows the ^{1}H NMR spectrum of the PMMA-Br macroinitiator, showing the minor resonances of the benzene ring terminal group in the range of 7.0~7.3 ppm. Polymerization of acetoxystyrene to form the PAS-*b*-PMMA block copolymer (Figure 4-12b), which reveals characteristic resonances for both poly(methyl methacrylate) and poly(acetoxystyrene) blocks. Figure 4-12c shows the ^{1}H NMR spectrum of the PVPh-*b*-PMMA after hydrolysis of the PAS-*b*-PMMA. Therefore, the ^{1}H NMR spectra confirm that the incorporation of acetoxystyrene into the poly(methyl methacrylate) and the formation of the PVPh-*b*-PMMA copolymer after hydrolysis.

4-5.2 GPC Analyses

The molecular weight and polydispersity of the PVPh-*b*-PMMA copolymers were characterized by GPC. The synthesized PVPh-*b*-PMMA copolymer by ATRP has larger polydispersity index (near the magnitude of 1.6) due to the purity of monomer which contains vinylphenol. We performed additional molecular weight measurement by ^{1}H NMR spectroscopy by analyzing the relative signal intensities of the protons of the initiator (7.0~7.3 ppm) and the PMMA (3.55 ppm) (Figure 4-12a). Molecular weights of PAS-*b*-PMMA and PVPh-*b*-PMMA were calculated by comparing the acetate group of PAS (Figure 4-12b, 2.24 ppm) and the phenyl group of PVPh (Figure 4-12c, 6.74 ppm) with the methyl ester group of the PMMA (3.55 ppm) segment. The molecular weights and polydispersity index for PMMA, PAS-*b*-PMMA and PVPh-*b*-PMMA were summarized in Table 4-7 and Table 4-8.

4-5.3 FT-IR Analyses

Figure 4-13 shows the infrared spectra of (a) PMMA, (b) PAS-*b*-PMMA and (c) PVPh-*b*-PMMA at room temperature ranging from 600-4000 cm^{-1}. The most notable differences in these copolymers are carbonyl group and hydroxyl group. The carbonyl

stretching for the pure PMMA is at 1730 cm^{-1}, and for the PAS-*b*-PMMA is at 1765 cm^{-1} and 1730 cm^{-1}, respectively. It clearly indicates that the PAS was indeed covalently bonded onto the PMMA-Br chain. Thereafter, the PVPh-*b*-PMMA was obtained after the hydrolysis of PAS. The absorption bands at 3445 cm^{-1}, corresponding to the overtone of PMMA carbonyl groups, were observed in Figures 4-13a and 4-13b. A broad hydroxyl group absorption band was obtained after hydrolysis of the PAS as shown in Figure 4-13c.

4-5.4 DSC analysis

Figure 4-14 shows the DSC thermograms of PVPh-*b*-PMMA, revealing that all DSC traces have only one glass transition temperature. Single glass transition temperature strongly suggests that these are fully miscible with a homogeneous amorphous phase. The values of glass transition temperatures and T_g breadths obtained form each system are listed in Table 4-8.
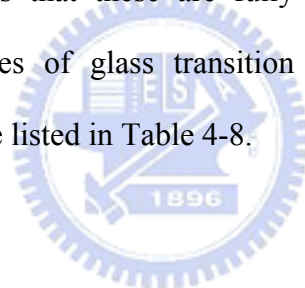
4-6 Conclusions

The block copolymer PVPh-*b*-PMMA and random copolymer PVPh-*r*-PMMA were designed and synthesized by anionic and free radical copolymerization of 4-*tert*-butoxystyrene and methyl methacrylate and the *tert*-butoxy protective group was selectively removed through hydrolysis reaction. These two PVPh-*co*-PMMA copolymers, which possess the same composition but different sequence distributions, exhibit different properties. Moreover, the fractions of hydrogen bonded carbonyl groups and glass transition temperatures of two copolymers are higher than those of the PVPh/PMMA blend system at similar PVPh content. This observation can be attributed to the difference in degrees of rotational freedom between polymer blend and copolymer. Meanwhile, the polymer chain architecture of a homopolymer is significantly different to that of copolymers due to intramolecular screening and functional group accessibility caused by the covalent bond connectivity. In addition, the inter-association equilibrium constant of PVPh-*r*-PMMA copolymer obtained from curve fitting method of f_b and based on PCAM is larger than that of PVPh-*b*-PMMA copolymer. $K_A = 67.3$ of the PVPh-*b*-PMMA without intramolecular screening is very close to the value of 67.4 obtained experimentally from the PVPh-*r*-PMMA copolymer. This result provides us with a hint that the effective inter-association equilibrium constant may be transformed between block copolymer and random copolymer that contained the same hydrogen bonded donor and acceptor segment. The block copolymer has the highest T_g value because it has the lowest polydispersity index.

References

(1) Utracki, L. A. *Polymer Alloys and Blends: Thermodynamics and Rheology*, Carl Hanser Verlag: Munich, **1989**.

(2) Coleman, M. M.; Graf, J. F.; Painter, P. C. "*Specific Interactions and the Miscibility of Polymer Blends. Technomic Publishing*", Lancaster, PA, **1991**.

(3) Coleman, M. M.; Painter, P. C. *Prog. Polym. Sci.* **1995**, *20*, 1.

(4) Coleman, M. M.; Lee, J. Y.; Serman, C. J.; Wang, Z.; Painter, P. C. *Polymer* **1989**, *30*, 1298.

(5) Serman, C. J.; Xu, Y.; Painter, P. C.; Coleman, M. M. *Polymer* **1991**, *32*, 516.

(6) Kuo, S. W.; Chang, F. C. *Macromolecules*, **2001**, *34*, 4089.

(7) Kuo, S. W.; Chang, F. C. *Macromolecules*, **2001**, *34*, 5224.

(8) He, Y.; Zhu, B.; Inoue, Y. *Prog. Polym. Sci.* **2004**, *29*, 1021.

(9) Kuo, S. W.; Huang, C. F.; Chang, F. C. *J. Polym. Sci., Polym. Phys.* **2001**, *39*, 1348.

(10) Kuo, S. W.; Lin, C. L.; Chang, F. C. *Polymer* **2002**, *43*, 3943.

(11) Serman, C. J.; Painter, P. C.; Coleman, M. M., *Polymer* **1991**, *32*, 1049.

(12) Zhang, X.; Takegoshi, K.; Hikichi, K., *Macromolecules* **1991**, *24*, 5756.

(13) Li, D.; Brisson, J., *Macromolecules* **1996**, *29*, 868.

(14) Dong, J.; Ozaki, Y., *Macromolecules* **1997**, *30*, 286.

(15) Serman, C. J.; Xu, Y.; Painter, P. C.; Coleman, M. M. *Macromolecules* **1989**, *22*, 2015.

(16) Li, D.; Brisson, J. *Polymer* **1998**, *39*, 793.

(17) Li, D.; Brisson, J. *Polymer* **1998**, *39*, 801.

(18) Hsu, W. P. *J. Appl. Polym. Sci.* **2002**, *83*, 1425.

(19) Jong, L.; Pearce, E. M.; Kwei, T. K. *Polymer* **1993**, *34*, 48.

(20) Hsu, W. P.; Yeh, C. F. *J. Appl. Polym. Sci.* **1999**, *73*, 431.

(21) Xu, Y.; Graf, J.; Painter, P. C.; Coleman, M. M. *Polymer* **1991**, *32*, 3103.

(22) Wang, L. F.; Pearce, E. M.; Kwei, T. K., *J. Polym. Sci., Polym. Phys. Ed.* **1991,** *29*, 619.

(23) Painter, P. C.; Coleman, M. M. *Polymer Blends*; Paul, D. R., Ed.; John Wiley & Sons: New York, **2000**; Vol. 1.

(24) Coleman, M. M.; Xu, Y.; Painter, P. C. *Macromolecules* **1994**, *27*, 127.

(25) Isasi, J. R.; Cesteros, L. C.; Katime, I. *Macromolecules* **1994**, *27*, 2200.

(26) Kuo, S. W.; Liu, W. P.; Chang, F. C. *Macromolecules* **2003**, *36*, 5165.

(27) Sybert, P. D.; Beever, W. H.; Stille, J. K. *Macromolecules* **1981**, *14*, 493.

(28) Ndoni, S.; Papadakis, C. M.; Bates, F. S.; Almdal, K. *Rev. Sci. Instrum.* **1995**, *66*, 1090.

(29) Li, M.; Douki, K.; Goto, K.; Li, X.; Coenjarts, C.; Smilgies, D. M.; Ober, C. K. *Chem. Mater.* **2004**, *16*, 3800.

(30) Zhao, J. Q.; Pearce, E. M.; Kwei, T. K.; Jeon, H. S.; Kesani, P. K.; Balsara, N. P. *Macromolecules* **1995**, *28*, 1972.

(31) Se, K.; Miyawaki, K.; Hirahara, K.; Takano, A.; Fujimoto, T. *J. Polym. Sci., Polym. Chem.* **1998**, *36*, 3021.

(32) Hadjichristidis, N.; Iatrou, H.; Pispas, S.; Pitsikalis, M. *J. Polym. Sci., Polym. Chem.* **2000**, *38*, 3212.

(33) Jérôme, R.; Teyssié, Ph.; Vuillemin, B.; Zundel, T.; Zune, C. *J. Polym. Sci., Polym. Chem.* **1999**, *37*, 1.

(34) Kurita, K.; Inoue, M.; Harata, M. *Biomacromolecules* **2002**, *3*, 147.

(35) Mecerreyes, D.; Moineau, G.; Dubois, P.; JeÂroÃme, R.; Hedrick, J. L.; Hawker, C. J.; Malmström, E. E.; Trollsas, M. *Angew. Chem. Ind. Ed.* **1998**, *37*, 1274.

(36) Heise, A.; Hedrick, J. L.; Frank. C. W.; Miller, R. D. *J. Am. Chem. Soc.* **1999**, *121*, 8647.

(37) Kennedy, J. P.; Kelen, T.; Tüdös, F. *J. Polym. Sci., Polym. Chem. Ed.* **1975**, *13*, 2277.

(38) Kelen, T.; Tüdös, F. *J. Macromol. Sci. Chem.* **1975**, *A9*, 1.

(39) Kuo, S. W.; Chang, F. C. *Polymer* **2001**, *42*, 9843.

(40) Xu, Y.; Painter, P. C.; Coleman, M. M. *Polymer*, **1993**, *34*, 3010.

(41) Moskala, E. J.; Howe, S. E.; Painter, P. C.; Coleman, M. M. *Macromolecules* **1984**, *17*, 1671.

(42) Painter, P. C.; Veytsman, B.; Kumar, S.; Shenoy, S.; Graf, J. F.; Xu, Y.; Coleman, M. M. *Macromolecules* **1997**, *30*, 932.

(43) Coleman, M. M.; Pehlert, G. J.; Painter, P. C. *Macromolecules* **1996**, *29*, 6820.

(44) Pehlert, G. J.; Painter, P. C.; Veytsman, B.; Coleman, M. M. *Macromolecules* **1997**, *30*, 3671.

(45) Pehlert, G. J.; Painter, P. C.; Coleman, M. M. *Macromolecules* **1998**, *31*, 8423.

(46) Coleman, M. M.; Guigley, K. S.; Painter, P. C. *Macromol. Chem. Phys.* **1999**, *200*, 1167.

(47) Kuo, S. W.; Chang, F. C. *Macromol. Chem. Phys.* **2001**, *202*, 3112.

(48) Coleman, M. M.; Painter, P. C. *Macromol. Chem. Phys.* **1998**, *199*, 1307.

(49) Fox, A.; Loshaek, S. *J. Polym. Sci.* **1955**, *15*, 371.

(50) Sperling, L. H. *"Introduction to Physical Polymer Science"*, 3rd edition, John Wiley & Sons, Inc, NY, **2001**.

(51) Barclay, G. G.; Hawker, C. J.; Ito, H.; Orellana, A.; Malenfant, P. R. L.; Sinta, R. F. *Macromolecules* **1998**, *31*, 1024.

Table 4-1. Characterization of poly(vinylphenol-*block*-methyl methacrylate) prepared by anionic polymerization.

copolymer	Mn,PMMA (g/mol)[a]	Mn,PVPh (g/mol)[a]	Total Mn (g/mol)[b]	Composition of PVPh (wt%)[a]	M_w/M_n[b]	T_g (^{o}C)
PMMA	10300	-	10300	0	1.17	105
PVPh30-*b*-PMMA70	11200	4800	16000	30	1.11	148
PVPh40-*b*-PMMA60	9600	6400	16000	40	1.15	159
PVPh55-*b*-PMMA45	13500	16500	30000	55	1.10	168
PVPh75-*b*-PMMA25	5500	16500	22000	75	1.13	181
PVPh	-	20000	20000	100	1.07	181

[a] Obtained from ^{1}H NMR measurement. [b] Obtained from GPC analysis.

Table 4-2. Characterization of poly(vinylphenol-*random*-methyl methacrylate) prepared by free radical polymerization.

copolymer	Monomer feed (mol%)[a]		Polymer Composition (mol%)[a]		Mn (g/mol)[b]	M_w/M_n[b]	T_g (^{o}C)
	tBOS	MMA	tBOS	MMA			
PtBOS30-r-PMMA70	19.6	80.4	21.0	79.0	20600	1.64	110
PtBOS58-r-PMMA42	36.2	64.8	53.1	46.9	24200	1.68	104
PtBOS76-r-PMMA24	57.0	43.0	72.4	27.6	24000	1.51	101
PtBOS92-r-PMMA8	83.6	16.4	91.1	8.9	23000	1.67	71

copolymer	$M_{n,PMMA}$ (g/mol)[a]	$M_{n, PVPh}$ (g/mol)[a]	Composition of PVPh (wt%)[a]	Mn (g/mol)[b]	M_w/M_n[b]	T_g (^{o}C)
PVPh30-r-PMMA70	12600	5400	30	18000	1.62	143
PVPh58-r-PMMA42	8000	11000	58	19000	1.63	160
PVPh76-r-PMMA24	4200	13400	76	17600	1.49	169
PVPh92-r-PMMA8	1300	14700	92	16000	1.63	179

[a] Obtained from ^{1}H NMR measurement. [b] Obtained from GPC analysis.

Table 4-3. Results of curve-fitting the data for PVPh-*co*-PMMA and PVPh/PMMA

blends at room temperature.

PVPh-*random*-PMMA	H-bonded C=O			free C=O			f_b[a]
	v, cm^{-1}	$W_{1/2}$, cm^{-1}	A_b, %	v, cm^{-1}	$W_{1/2}$, cm^{-1}	A_f, %	
30-70	1707	24	35.6	1731	19	64.4	26.9
58-42	1705	26	59.3	1731	19	40.7	49.3
76-24	1704	25	75.7	1730	19	24.3	65.6
92-8	1703	24	82.3	1729	18	17.7	75.7

PVPh-*block*-PMMA	H-bonded C=O			free C=O			f_b
	v, cm^{-1}	$W_{1/2}$, cm^{-1}	A_b, %	v, cm^{-1}	$W_{1/2}$, cm^{-1}	A_f, %	
30-70	1709	23	32.8	1732	20	67.2	24.6
40-60	1709	24	42.1	1732	19	57.9	32.6
55-45	1708	24	58.3	1733	19	41.7	43.5
75-25	1709	25	65.8	1732	18	34.2	56.2

PVPh/PMMA blend	H-bonded C=O			free C=O			f_b
	v, cm^{-1}	$W_{1/2}$, cm^{-1}	A_b, %	v, cm^{-1}	$W_{1/2}$, cm^{-1}	A_f, %	
30-70	1707	23	24.8	1732	20	75.2	18.1
50-50	1707	25	49.7	1733	19	50.3	37.7
70-30	1707	26	58.7	1733	20	41.3	48.6
90-10	1705	24	68.5	1732	18	31.5	59.2

[a] f_b: fraction of hydrogen bonded carbonyl group.

Table 4-4. Summary of the self-association and interassociation parameters of PVPh-*co*-PMMA copolymer and PVPh/PMMA blend systems

polymer	molar volume (ml/mol)	molecular weight (g/mol)	solubility parameter (cal/ml)$^{0.5}$	self-association equilibrium constant		interassociation equilibrium constant K_A		
				K_2	K_B	random copolymer	block copolymer	polymer blend
PVPh	100.0	120.0	10.6	21.0	66.8			
PMMA	84.9	100.0	9.1			67.4	47.1	37.4

Table 4-5. The values of T_g and T_g breadth obtained from PVPh-*co*-PMMA copolymer and PVPh/PMMA blend systems

PVPh-*random*-PMMA	T_g (^{o}C)	$\triangle T_g$ (^{o}C)
0/100	105	12.6
30/70	143	7.3
58/42	160	6.0
76/24	169	7.0
92/8	179	7.0
100/0	181	14.6
PVPh-*block*-PMMA		
0/100	105	12.6
30/70	149	10.0
40/60	159	8.6
55/45	168	8.6
75/25	181	7.8
100/0	181	14.6
PVPh/PMMA blend		
0/100	105	12.6
30/70	133	14.8
50/50	142	14.4
70/30	151	12.7
90/10	165	12.3
100/0	181	14.6

Table 4-6. The values of T_g obtained from the narrow polydispersity of PVPh

Mn (g/mol)	M_w/M_n	T_g (^{o}C)
3200	1.12	174
6000	1.14	178
20000	1.07	181
30000	1.06	183
150000	1.09	186

Table 4-7: Molecular weight information of polymers

Copolymer	Conditions $[M]_0/[I]_0/[CuBr]_0/[PMDETA]_0$	Yield (%)	Mn
functionalized PMMA	100/1/1/1	89	10100^a (PDI=1.22) $10,900^b$
PMMA-*b*-PAS	800/1/10/10	42	38900^b (PAS, Mn=28,800)

a: measured by GPC (RI detector)

b: measured by ^{1}H NMR (based on PMMA(Mn=10,900))

Table 4-8. Characterization of poly(vinylphenol-*block*-methyl methacrylate) prepared by ATRP polymerization

copolymer	Mn,PMMA (g/mol)[a]	Mn,PVPh (g/mol)[a]	Total Mn (g/mol)[b]	Composition of PVPh (wt%)[a]	M_w/M_n[b]	T_g (^{o}C)
PVPh32-*b*-PMMA68	10100	21500	31600	32	1.61	130.6
PVPh46-*b*-PMMA54	10100	11800	21900	46	1.58	140.1
PVPh62-*b*-PMMA38	10100	6200	16300	62	1.63	151.0
PVPh75-*b*-PMMA25	10100	3400	13500	75	1.64	165.2

[a] Obtained from ^{1}H NMR measurement. [b] Obtained from GPC analysis.

Scheme 4-1. Synthesis of poly(vinylphenol-*block*-methyl methacrylate) copolymer by anionic polymerization
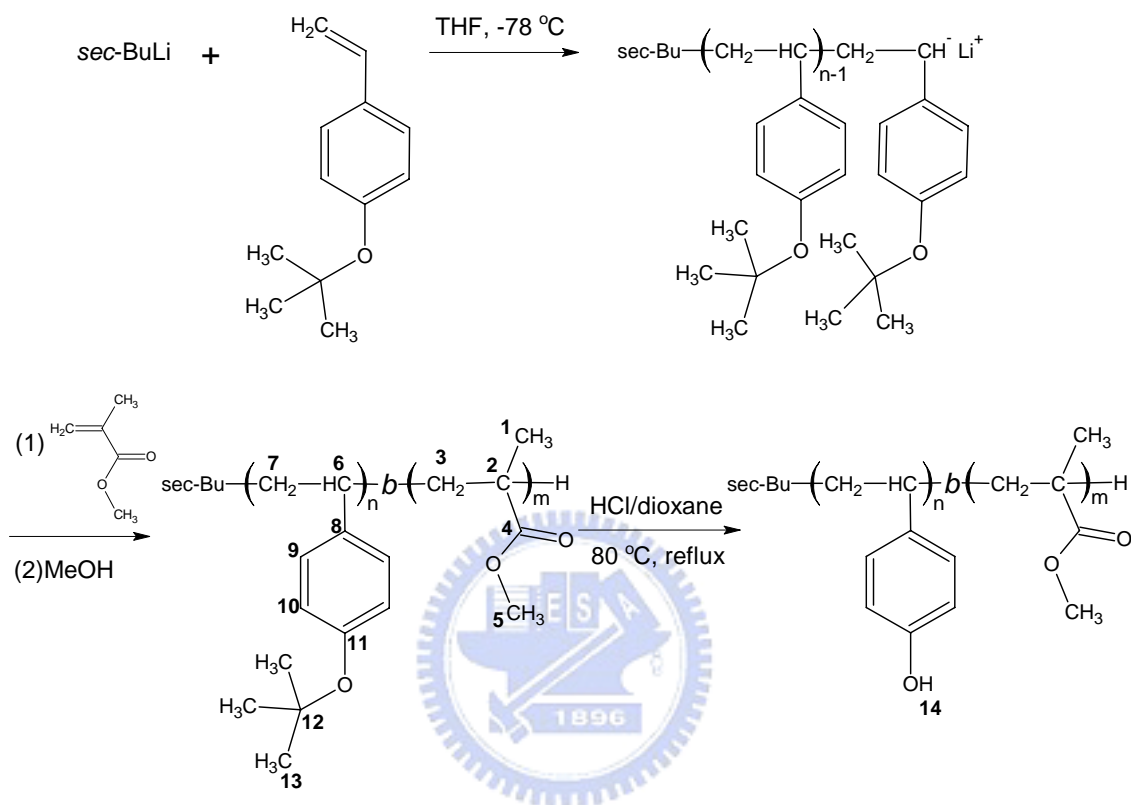
Scheme 4-2. Synthesis of poly(vinylphenol-*random*-methyl methacrylate) copolymer through free radical polymerization
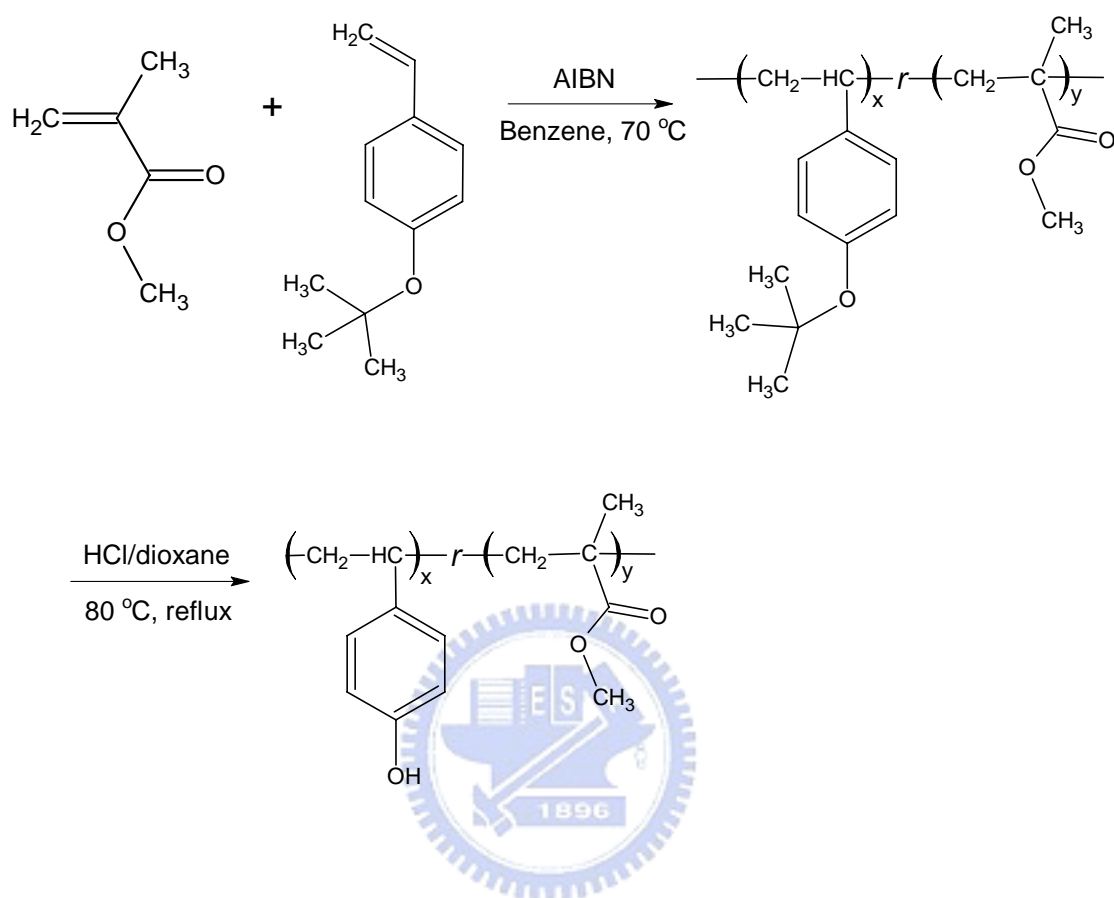
Scheme 4-3. Synthesis of poly(vinylphenol-*random*-methyl methacrylate) copolymer through atom transfer radical polymerization

PMMA

PMMA-*b*-PAS

PMMA-*b*-PVPh
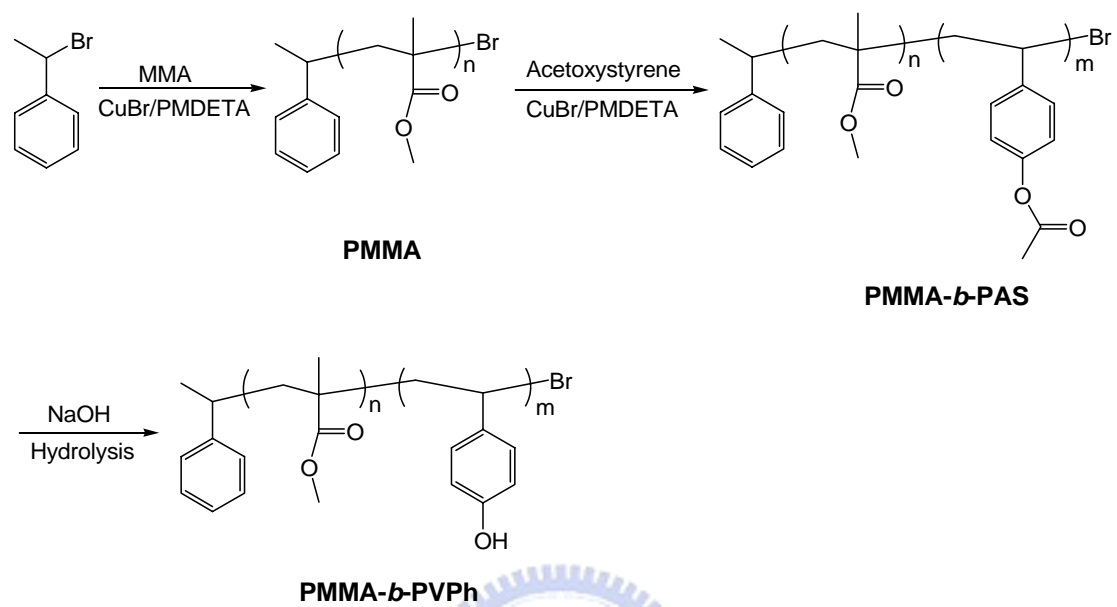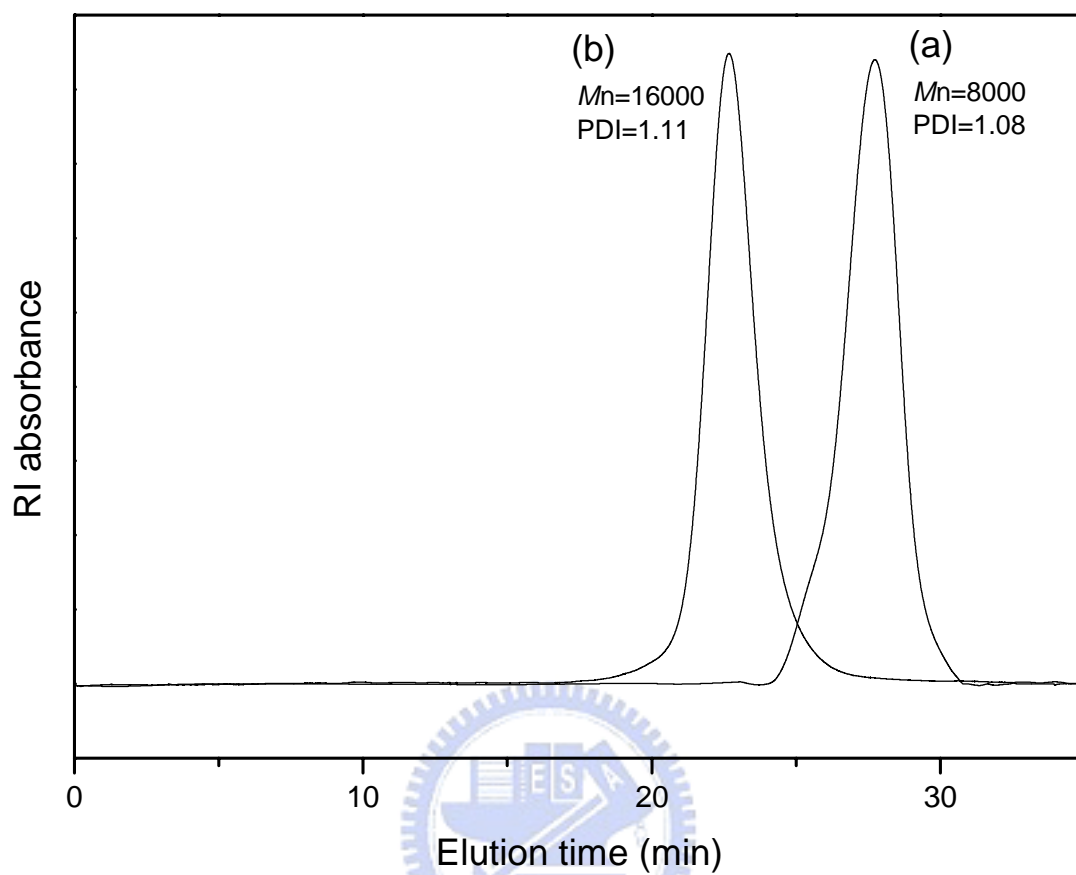
Figure 4-1: GPC traces of PVPh-*b*-PMMA block copolymers. (a) First block poly(*tert*-butoxystyrene) (P*t*BOS), *M*n = 8000 g/mol, PDI = 1.08; (b) poly(vinylphenol-*b*-methyl methacrylate) (PVPh-*b*-PMMA), *M*n = 16000 g/mol, PDI = 1.11.
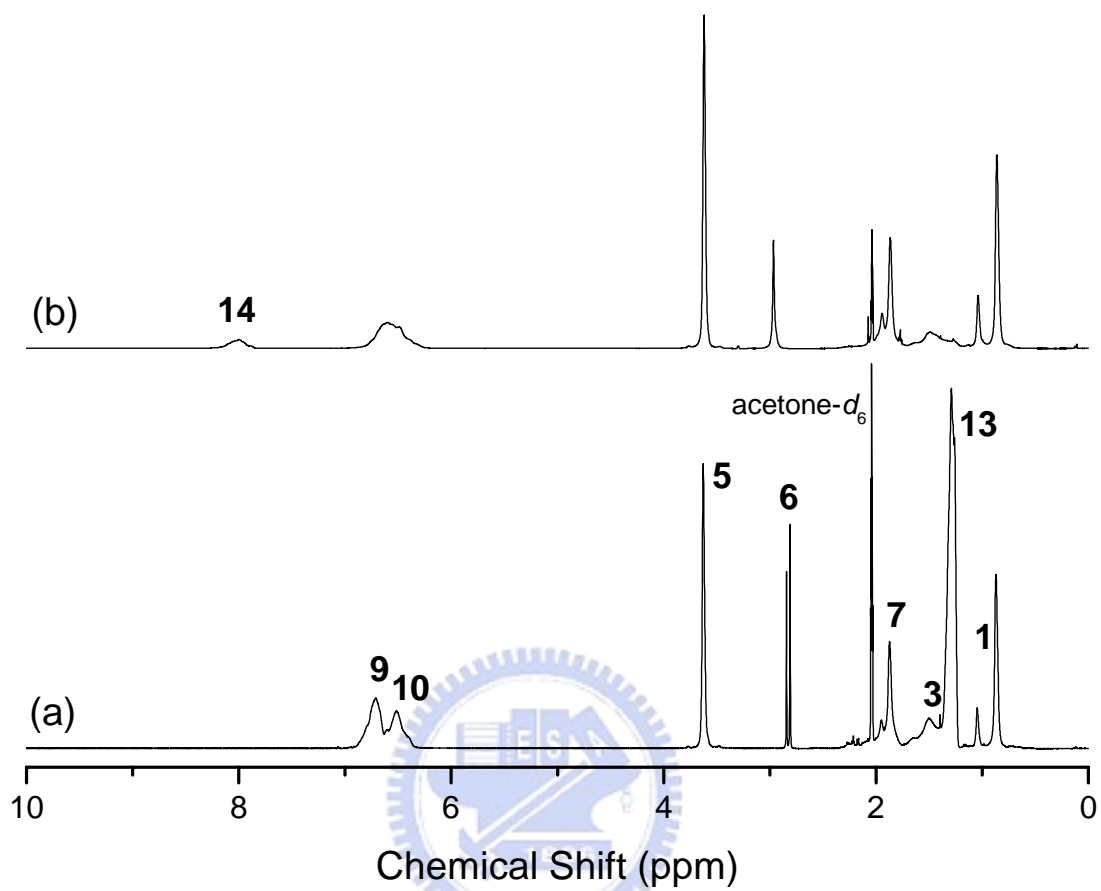
Figure 4-2: ^{1}H NMR spectra of (a) before hydrolysis, P*t*BOS-*b*-PMMA, and (b) after hydrolysis, PVPh-*b*-PMMA.
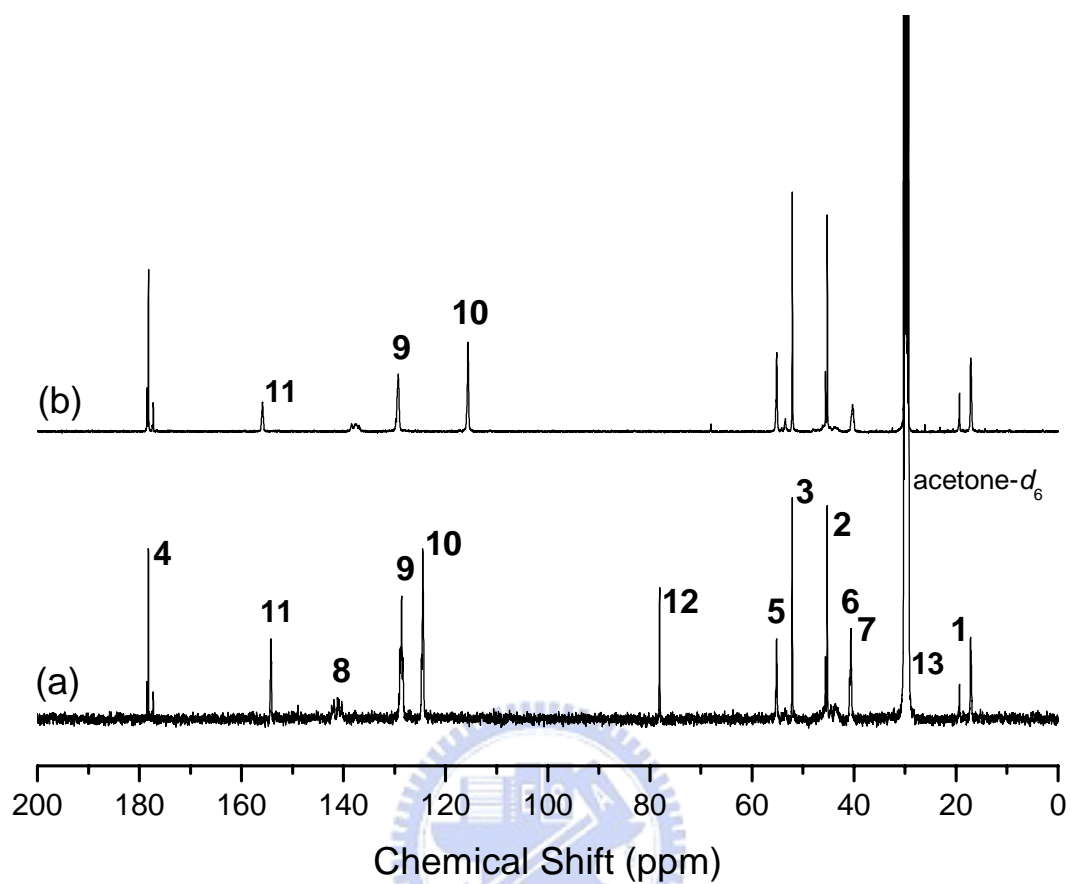
Figure 4-3: ^{13}C NMR spectra of (a) before hydrolysis, P*t*BOS-*b*-PMMA, and (b) after hydrolysis, PVPh-*b*-PMMA.
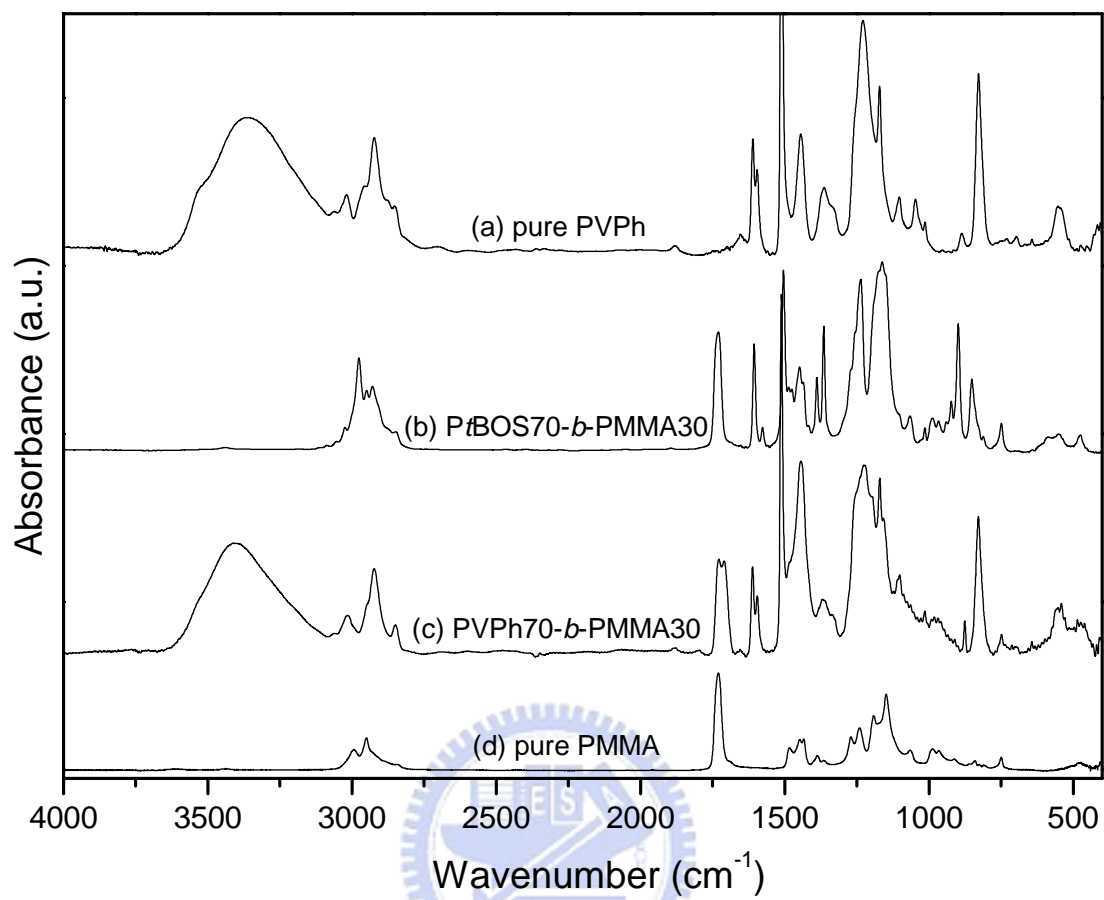
Figure 4-4: IR spectra of (a) pure PVPh, (b) P*t*BOS-*b*-PMMA, (c) PVPh-*b*-PMMA, and (d) pure PMMA at room temperature ranging from 400 – 4000 cm⁻¹.
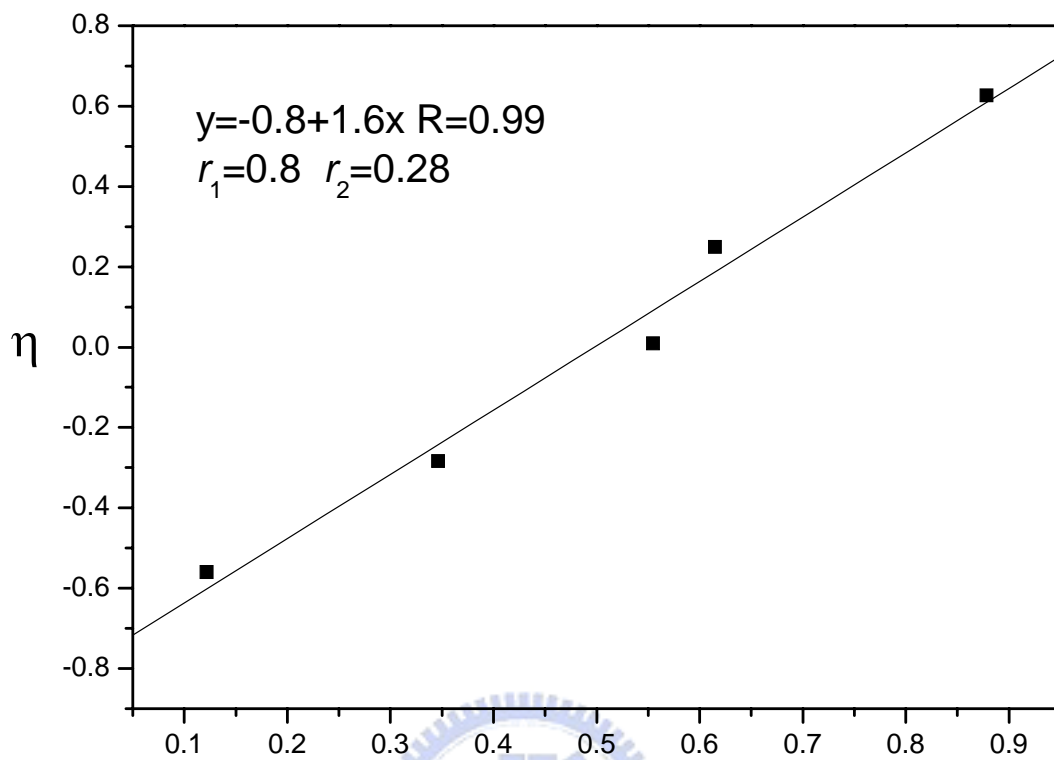
Figure 4-5: Kelen-Tüdös plot for the P*t*BOS-*r*-PMMA copolymers.
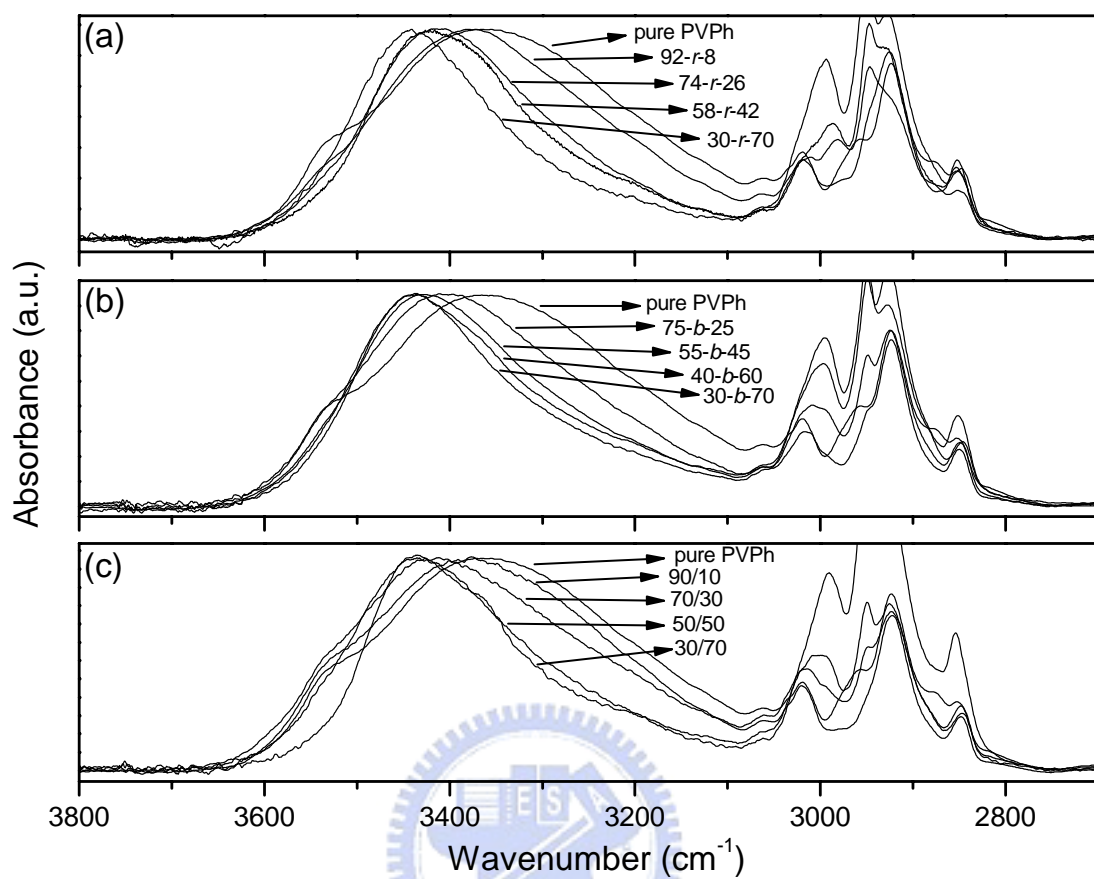
Figure 4-6: FT-IR spectra in the 2700 – 3800 cm^{-1} region for (a) random copolymer,

(b) block copolymer, and (c) polymer blend.
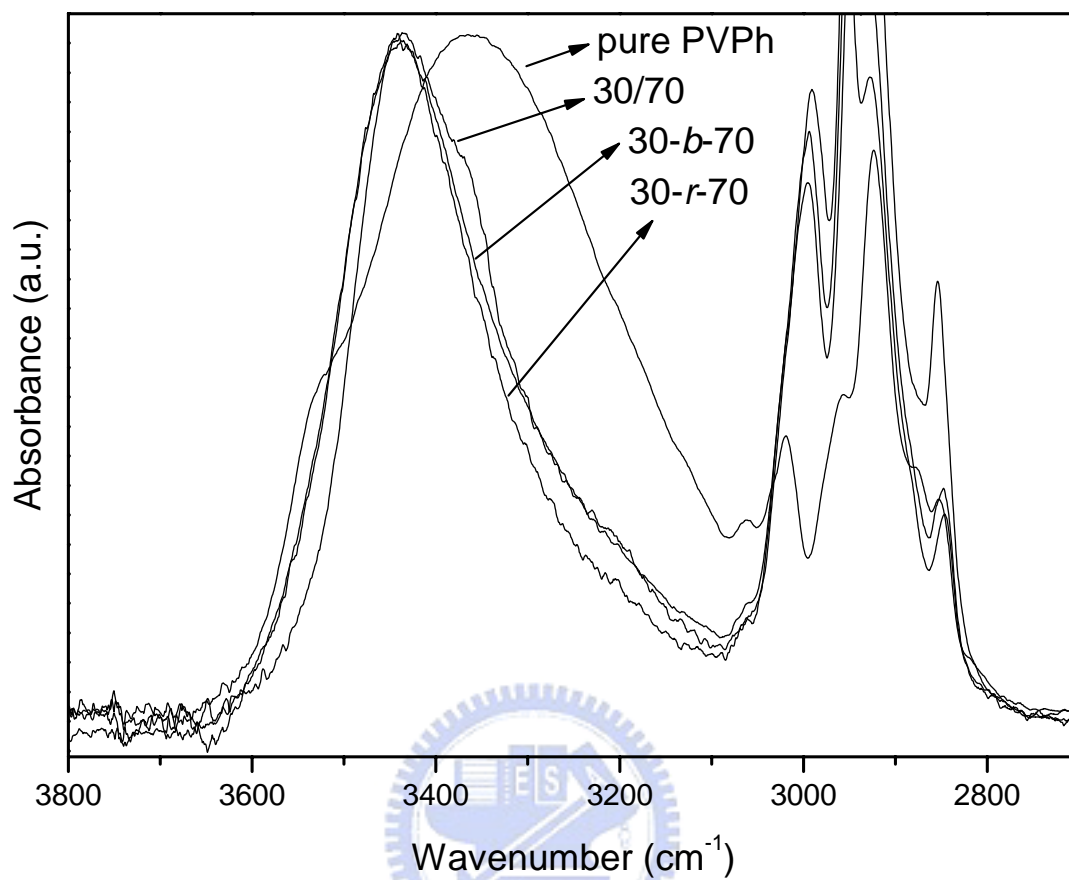
Figure 4-7: Comparison between the FTIR spectra (2700–3800 cm^{-1}) of samples having similar PVPh contents.
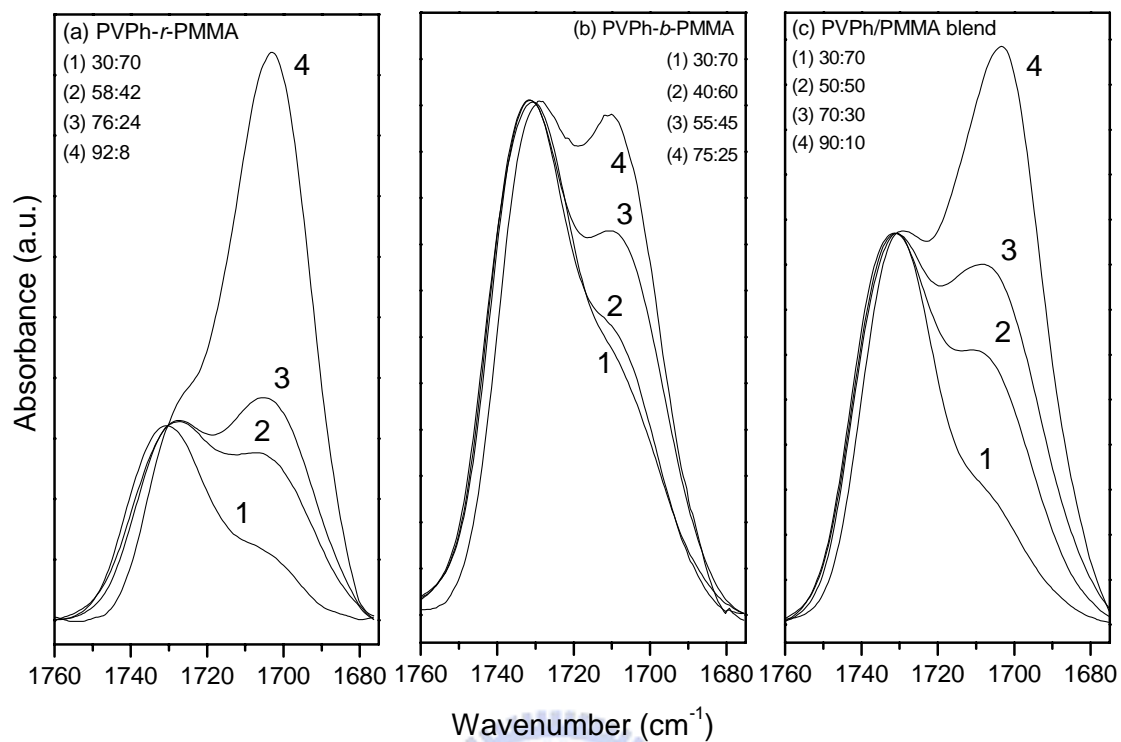
Figure 4-8: FT-IR spectra (1670 – 1760 cm^{-1}) of a (a) random copolymer, (b) block copolymer, and (c) polymer blend.
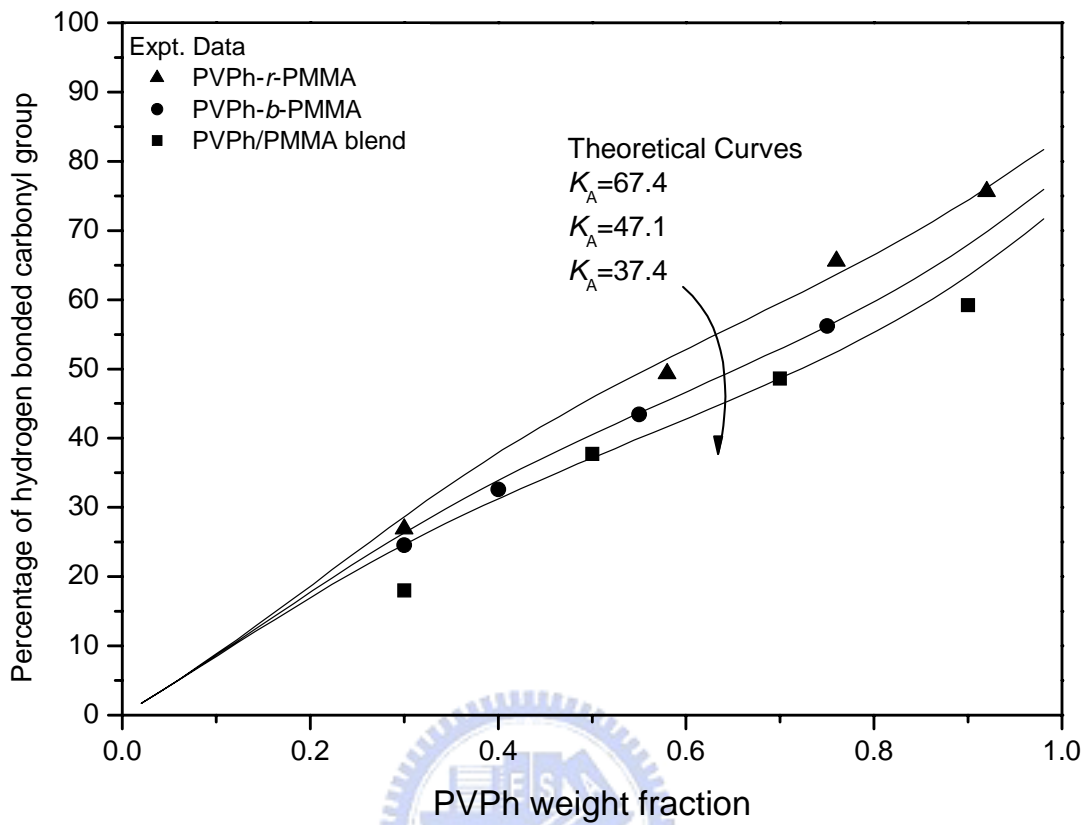
Figure 4-9: Plots of the fraction of hydrogen-bonded carbonyl groups vs. the PVPh

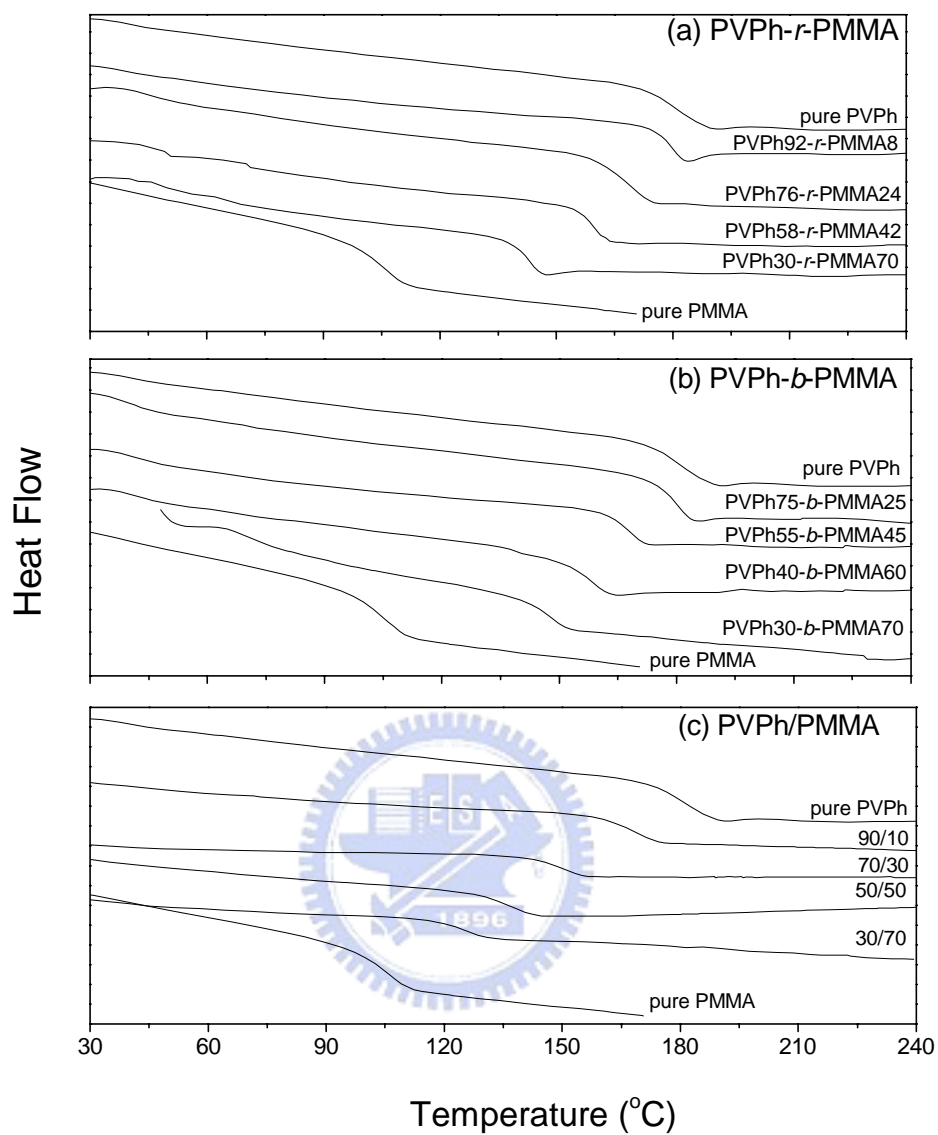fraction for a random, block copolymer, and polymer blend.

Figure 4-10: DSC traces of (a) PVPh-*r*-PMMA copolymers, (b) PVPh-*b*-PMMA copolymers and (c) PVPh/PMMA blend.
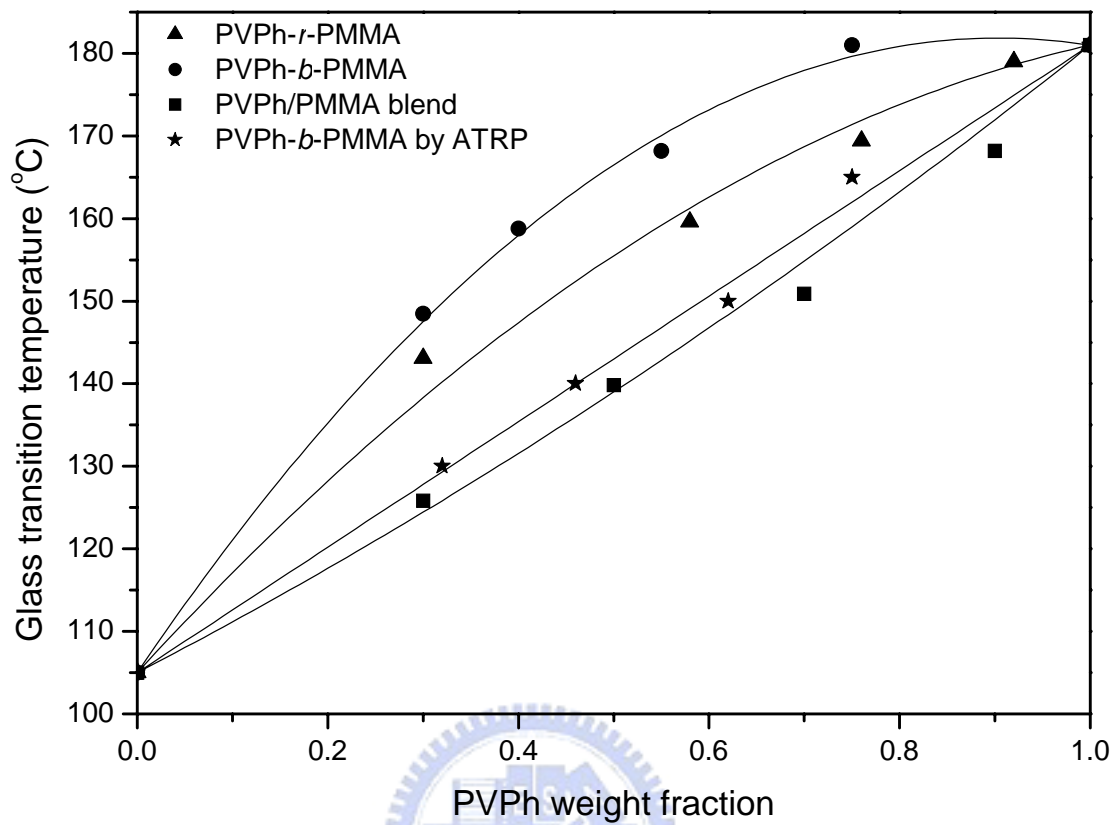
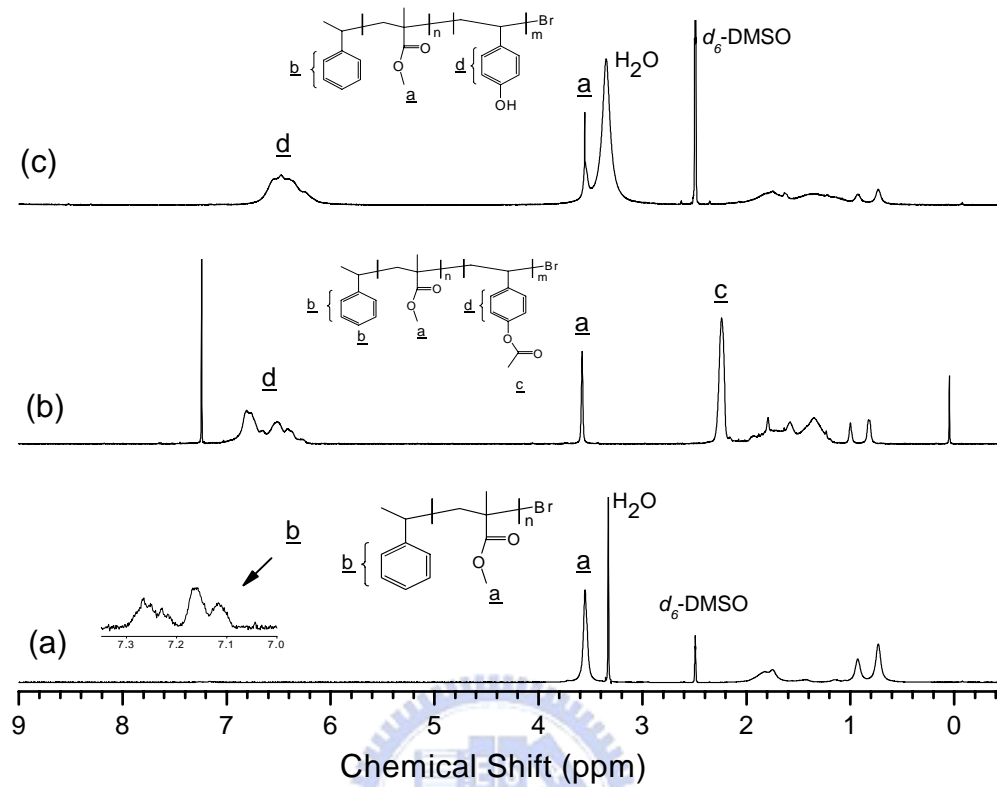Figure 4-11: Plots of T_g vs, composition based on (symbol) experimental data.

Figure 4-12: ^{1}H NMR spectra of (a) PMMA (d_6-DMSO), (b) PAS-b-PMMA (CDCl$_3$), and (c) PVPh-b-PMMA (d_6-DMSO).
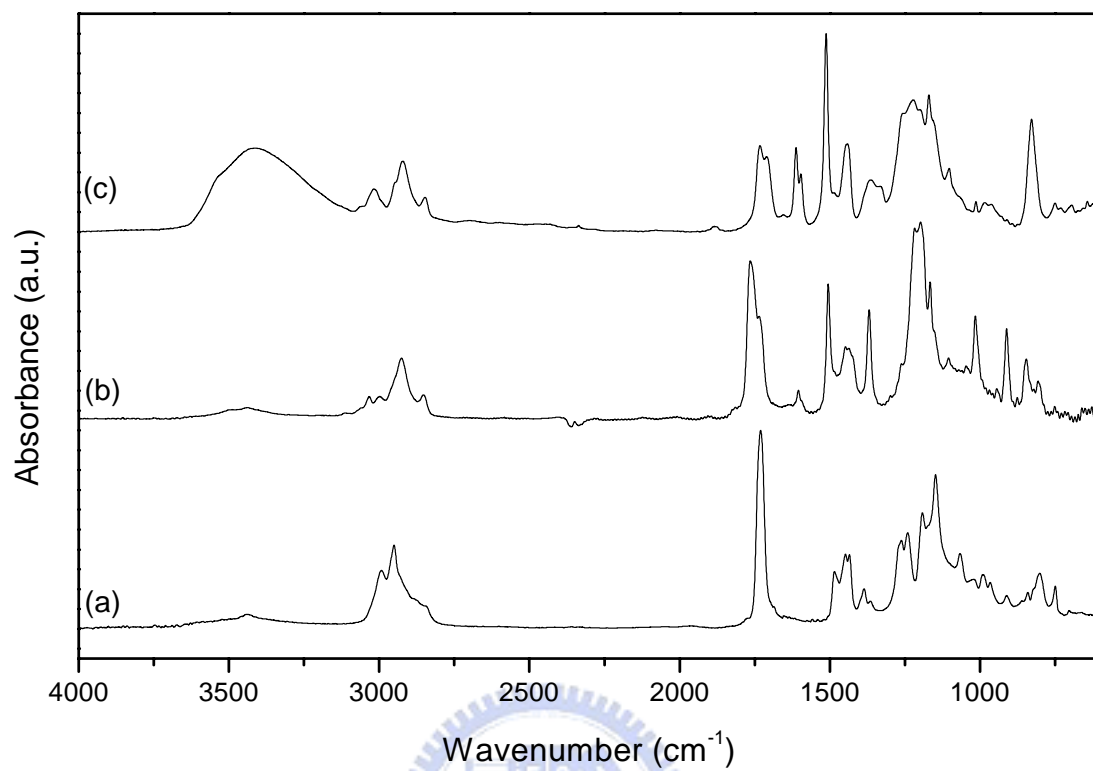
Figure 4-13: FT-IR spectra of (a) PMMA, (b) PMMA-*b*-PAS, and (c) PMMA-*b*-PVPh recorded at room temperature between 600-4000 cm⁻¹.
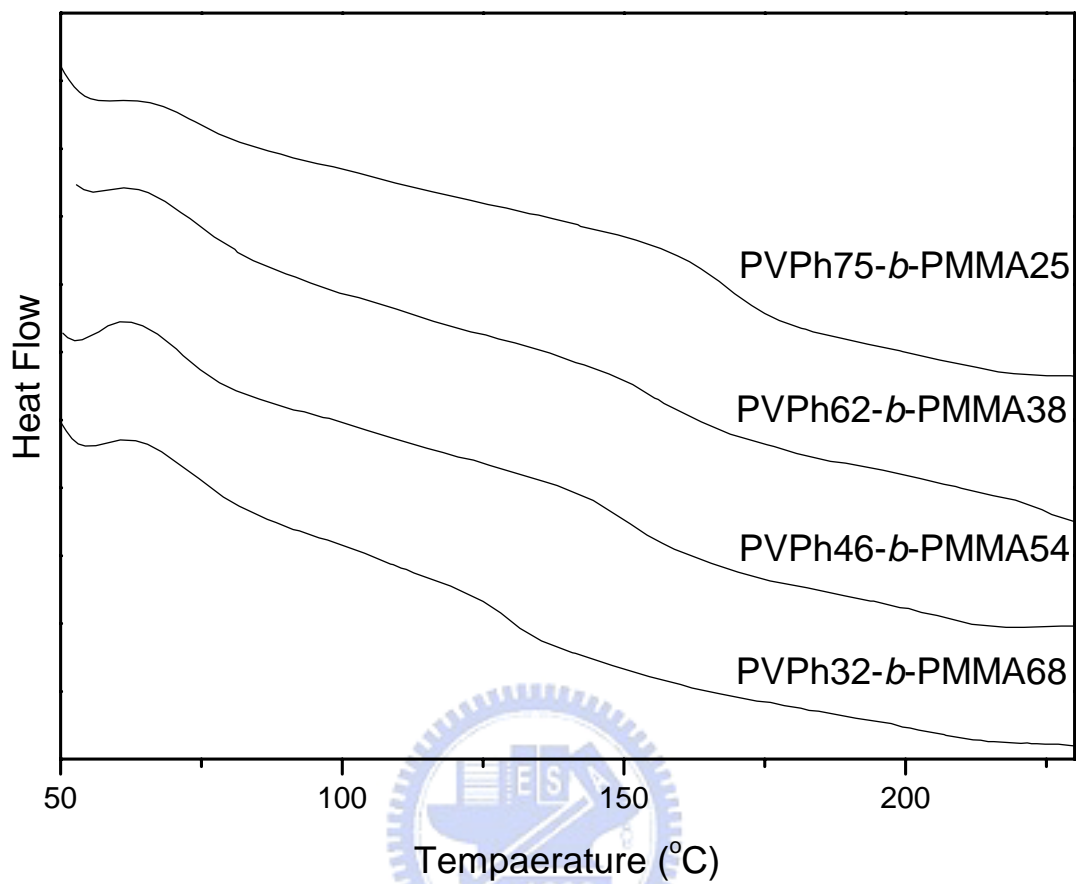
Figure 4-14 : DSC traces of PVPh-*b*-PMMA copolymers through ATRP.

Chapter 5

Sequence Distribution Affect the Phase Behavior and Hydrogen Bonding Strength in Blends of Poly(vinylphenol-*co*-methyl methacrylate) with Poly(ethylene oxide)

Abstract

Experimental results indicate that PEO was miscible with PVPh-*r*-PMMA as shown by the existence of single composition-dependent glass transition temperature over the entire composition. However, the PVPh-*b*-PMMA blend with PEO shows a closed loop immiscible region in the ternary polymer blend system. Furthermore, FTIR reveals that at least three competing equilibrium are present in these blends; self-association of PVPh-*co*-PMMA copolymer (hydroxyl-hydroxyl), interassociation of hydroxyl-carbonyl, and hydroxyl-ether interassociation between PVPh and PEO. Based on the Painter-Coleman Association Model (PCAM), a value for K_C = 300 is obtained in PVPh-*b*-PMMA/PEO blend system at room temperature. Although the relative ratio of interassociation equilibrium constant of PEO to PMMA is larger in PVPh-*b*-PMMA/PEO blend system, the PVPh-*r*-PMMA/PEO blend system has greater $\Delta\nu$ and greater homogeneity at the molecular scale than the PVPh-*b*-PMMA/PEO blend system because of the ΔK effect.

5-1 Introduction

Polymer blends are one of the most important topics in polymer science during the last decade. For macromolecules, the Gibbs free energy of mixing is mainly controlled by its enthalpic contribution because the entropic term is usually favorable but very small. Therefore, polymer pairs with complementary chemical structures favoring specific interactions (and, thus a negative enthalpy of mixing) usually lead to miscible systems.[1-4] Ideally, one polymer should possess donor sites and the other possesses acceptor sites on their respective chains. The most commonly observed interactions are of the acid-base type, i.e., hydrogen bonding,[5] dipole-dipole, and charge-transfer interactions. On the contrary, when only dispersive forces can be expected between components, a positive (unfavorable) contribution of the enthalpic term is expected and as a consequence these systems are usually immiscible.

In order to obtain miscible polymer blends with desirable properties, it is very important to understand factors affecting the miscibility of polymer mixtures. The miscibility of homopolymer/copolymer blends has been successfully described by the binary interaction model.[6-8] According to this model, the mutual repulsive force between dissimilar segments in the copolymer can lead to negative heat of mixing necessary to attain miscibility. Paul et al.,[9-11] Karasz et al.,[12,13] and Jo et al.[14] have further extended the above binary interaction model to several types of blends containing copolymers and applied the model to interpret the effect of the copolymer composition in the miscibility of blends. Nevertheless, the effect of the copolymer microstructures is not always explained in terms of neighboring repulsions. In the case of poly(vinyl acetate-*co*-vinyl alcohol) (ACA)[15] or poly(vinylphenol-*co*-methyl methacrylate) (PVPh-*co*-PMMA),[16] the specific interaction between carbonyl groups

and hydroxyl groups competes with hydroxyl self-association. Therefore, the monomer sequential distribution in these copolymers must play an important role in determining resulted hydrogen bond distribution. The possibility of hydrogen bond formation between hydroxyl groups and neighboring carbonyl groups in the copolymer attributes to a short scale competition of specific interactions. In addition, the sequential distribution of the copolymer in a homopolymer/copolymer blend will also affect the charge distribution and the probability of contact between interaction sites, and consequently affect the miscibility of the blend.[17]

In the ternary polymer blend, however, when all three binary pairs (B-A, B-C, and A-C) are individually miscible, a completely homogeneous or a closed immiscibility loop phase diagram has been observed.[18] The phase separation is caused by the difference in the interaction energy of the binary system, the so-called "$\Delta\chi$" effect and "ΔK" effect in ternary polymer blends such as phenoxy/PMMA/PEO,[19] poly(vinylphenol) (PVPh)/poly(vinyl acetate) (PVAc)/PEO,[20] and poly(styrene-*co*-acrylic acid)/PMMA/PEO.[21] According to previous literature,[5,22-24] binary pairs of PVPh/PMMA and PVPh/PEO are totally miscible over the entire compositions in the amorphous phase due to the formation of the interassociation hydrogen bonding between the hydroxyl group of PVPh and the carbonyl group of PMMA and the ether group of PEO, respectively. PEO is a highly crystalline polymer that is miscible with several weakly interacting polymers, such as PMMA,[25-28] PVAc,[29] and poly(vinylpyrrolindone).[30] Miscible blends of PEO with PMMA have been well investigated in the literature, and the results indicate that the blend components are miscible in the melt and in the amorphous phase. PEO can act as a Lewis base since the oxygen atom bears a partial negative charge, while the carbonyl carbon atom of PMMA possesses a partially positive charge. In this study, we intend to the effect of different sequential distribution of a copolymer on

the miscibility in homopolymer/copolymer blend by FTIR and DSC analyses. In addition, the ΔK effect was found to play a key role resulting in different phase behaviors.

5-2 Experimental Section

5-2.1 Materials.

The poly(vinylphenol-*co*-methyl methacrylate) (PVPh-*co*-PMMA) copolymers studied in this work were prepared by different synthetic routes as described elsewhere.[16] The block copolymer PVPh-*b*-PMMA and random copolymer PVPh-*r*-PMMA were synthesized by anionic and free radical copolymerization of 4-*tert*-butoxystyrene and methyl methacrylate, respectively. The *tert*-butoxy protective group was selectively removed through hydrolysis reaction. Table 1 shows the sequential distributions and molecular weights of several PVPh-*co*-PMMA copolymers employed in this study. Poly(ethylene oxide) (PEO) with Mn = 20 000 was obtained from Aldrich Co.

5-2.2 Blend Preparation

Blends of various (PVPh-*co*-PMMA)/PEO compositions were prepared by solution casting. Tetrahydrofuran (THF) solution containing 5 wt% polymer mixtures was stirred for 6-8 h and then cast onto a Teflon dish and was left to evaporate slowly at room temperature for 1 day. The blend film was then dried at 50 ^{o}C for 2 days.

5-2.3 Measurements.

All infrared spectra were recorded at 25 ^{o}C at a resolution of 1cm^{-1} on a Nicolet AVATAR 320 FTIR spectrometer. Each sample was dissolved in THF and then cast directly onto KBr pellets. All films were vacuum–dried and were thin enough to be within the absorbance range where the Beer-Lambert law is obeyed. Since these samples containing hydroxyl groups that are water sensitive, a pure nitrogen flow was used to purge the IR optical box in order to maintain sample films dryness. Thermal analysis was performed on a DSC instrument from Du-Pont (DSC-9000) at

a scan rate of 20 ^{o}C/min over a temperature ranging from 20 to 250 ^{o}C. The sample was quenched to -120 ^{o}C from the melt state for the first scan and then rescanned between -120 ^{o}C and 250 ^{o}C at 20 ^{o}C/min. The glass transition temperature was obtained at the inflection point of the jump heat capacity.

5-3 Results and Discussion

5-3.1 Thermal Analyses

The PVPh is totally miscible with PEO and PMMA in the amorphous phase due to the formation of the interassociation hydrogen bonding between the hydroxyl group of the PVPh and the carbonyl group of the PMMA or the ether group of the PEO. In addition, PEO and PMMA are also fully miscible in the amorphous phase. In general, differential scanning calorimetry (DSC) is one of the convenient methods to determine the miscibility in polymer blends. Meanwhile, a single compositionally dependent glass transition is an indication of full miscibility at a dimensional scale between 20 and 40 nm. Figure 1 shows the conventional second run DSC thermograms of PVPh-r-PMMA/PEO blends of various compositions; it reveals that each blend composition has only single glass transition temperature. A single value of T_g strongly suggests that the PVPh-r-PMMA/PEO blend system is fully miscible in the homogeneous amorphous phase. Table 2 summarizes the thermal properties of PVPh-r-PMMA, PEO, and their blends. At higher PEO contents, PEO crystallizes from the molten mixture of PEO and PVPh-r-PMMA copolymer. The melting temperature of the PEO component decreases with increasing the PVPh-r-PMMA copolymer content in the blend. The melting temperature also decreases with increasing the PVPh content in the PVPh-r-PMMA copolymer at the same blend ratio. This phenomenon suggests that the PVPh-r-PMMA copolymer in the blend hinders the crystallization of PEO, which is a typical phenomenon of a miscible blend in which the glass transition temperature of an amorphous polymer is higher than that of a crystalline component. Furthermore, the dependence of T_g on the composition of the miscible PVPh-r-PMMA/PEO blends is shown in Figure 2A. Clearly, the value of T_g of each PVPh-r-PMMA/PEO blend shift to lower

temperatures as the PEO content increases in the blend. However, the upturn of the values of T_g at higher PEO content is due to the crystallization of PEO during quenching. This phenomenon suggests that not only the crystallization of PEO in the blends can change the amorphous phase but also the crystal of PEO is able to act as a physical cross-linking point that may hinder the molecular mobility of amorphous phase.[31,32]

Figure 3 displays the second run DSC thermograms of PVPh-*b*-PMMA/PEO blends. Again, the binary PVPh/PMMA, PVPh/PEO, and PMMA/PEO blends are all fully miscible in the amorphous phase. However, the DSC thermograms of 30-*b*-70/PEO = 8/2, 7/3, and 40-*b*-60/PEO = 8/2 show two T_g's, implying that they are immiscible in the amorphous phase. The thermal properties of PVPh-*b*-PMMA/PEO blends were summarized in Table 3 and the dependence of T_g on the composition of the miscible PVPh-*b*-PMMA/PEO blends is shown in Figure 2B. It is observed that the thermal behavior of PVPh-*b*-PMMA/PEO blends have the similar tendency to the PVPh-*r*-PMMA/PEO blends.

5-3.2 FT-IR analyses

Infrared spectroscopy has been used to detect the existence of specific interactions in polymer blends. This tool can be used to study the mechanism of interpolymer miscibility through the bond formation both qualitatively and quantitatively. Several regions within the infrared spectra of PVPh-*co*-PMMA/PEO blends are influenced by the hydrogen-bonding interaction.

Figure 4A shows infrared spectra in the 2700-3800 cm^{-1} range for the pure PVPh. This broad band can be considered to be composed of narrow contributions corresponding to hydroxyl groups surrounded by different environments: hydroxyl

groups hydrogen bonded with other hydroxyl groups in the same or vicinal chains (forming dimmers, trimers, etc.), and non-hydrogen bonded hydroxyl groups.[33] In addition, the spectra of the miscible 92-*r*-8/PEO blends show significant changes in this region, suggesting a redistribution in the arrangement of the hydroxyl group association. These data indicate that there are many different types of hydroxyl groups present in PVPh-*r*-PMMA copolymers and PVPh-*r*-PMMA/PEO blends. In the meantime, the spectrum of pure PVPh shown in Figure 4A is characterized by a very broad band centered at 3350 cm^{-1}, indicating that these hydroxyl groups are hydrogen bonded to other hydroxyl groups as dimmers and chain-like multimers. A second narrower band, observed at 3525 cm^{-1} as a shoulder on the high frequency side of the broad hydrogen bonded band, is assigned to free hydroxyl groups.[5] Taking into account the effect of composition, the carbonyl groups of methyl methacrylate units compete with self-associated hydroxyl groups for hydrogen bonding and cause the shift of the hydroxyl band toward higher wavenumbers at lower vinylphenol content. In this situation, majority of only one type of hydroxyl group from the hydrogen–carbonyl inter-association is expected, and thus the hydroxyl stretching band is relatively narrower. On the contrary, the free, dimmer, or multimer hydrogen bonded hydroxyl groups will exist at higher vinylphenol contents, resulting in broader absorptions. Therefore, the spectrum of 30-*r*-70 copolymer shown in Figure 4B is reasonable to assign the band at 3440 cm^{-1} to the hydroxyl groups interacting with carbonyl groups because the small number of the hydroxyl groups tend to interact completely with carbonyl groups. When comparing the spectra corresponding to the same system as a function of composition, a progressive shift of this band toward lower wavenumber is observed for increasing content of ether oxygen of PEO (Figure 4). This behavior suggests that a significant part of the hydroxyl groups involved in the association processes previously

described for PVPh-*r*-PMMA copolymer are now hydrogen bonded to ether oxygen groups in PEO.

In the case of PVPh-*b*-PMMA/PEO blends (Figure 5), infrared spectra show a clear shift of the hydroxyl band toward lower wavenumbers, relative to that of the pure PVPh-*b*-PMMA copolymer. As the PEO content in the blend increases, the band gradually shift to lower frequencies, providing additional evidence for the existence of hydrogen bonding interaction between the PEO ether group and the hydroxyl group of PVPh. The frequency difference between the free hydroxyl absorbance and the hydrogen bonded hydroxyl (Δv) is a measure of the average strength of the intermolecular interactions.[34,35] For instance, we use the position of the free hydroxyl stretching vibration at 3525 cm^{-1} as a reference, then the median frequency difference for hydroxyl-hydroxyl self-association in PVPh is about 175 cm^{-1} while that of the interassociation between hydroxyl groups of PVPh and carbonyl groups of PMMA is 85 cm^{-1}. Figure 6 displays the frequency difference (Δv) in FTIR of all PVPh-*r*-PMMA/PEO and PVPh-*b*-PMMA/PEO blends at room temperature vs. PEO content. The Δv of PVPh-*r*-PMMA/PEO and PVPh-*b*-PMMA/PEO blend system exhibits the same increasing trend as the PEO content is increased. In the 30-r-70/PEO = 4/6 blend, there is no evidence for the presence of free hydroxyl and the concentration of hydroxyl-hydroxyl interactions appears insignificant. Therefore, it is reasonable to assign the band at 3150 cm^{-1} to the hydroxyl groups of PVPh hydrogen bonded to ether oxygens of the PEO in the PVPh-*r*-PMMA/PEO system. The frequency difference between the free hydroxyl band and the band attributed to hydroxyl groups hydrogen bonded to ether oxygens is about 375 cm^{-1}. This is somewhat greater than that observed for PVPh-*b*-PMMA/PEO system (c.a. 350 cm^{-1}) and presumably reflects a moderate increase in the relative strength of the PVPh-*r*-PMMA/PEO intermolecular

interaction; a reasonable conclusion considering the enhanced affinity for hydrogen bonding of the hydroxyl groups in PVPh-*r*-PMMA compared to that in PVPh-*b*-PMMA. However, these values of $\Delta\nu$ in all copolymer/PEO blends also imply that the interassociation between PVPh and PEO is considerably stronger than either the self-association of hydroxyl groups in PVPh or the interactions between hydroxyl groups in PVPh and carbonyl groups in PMMA.

The CH_2 wagging region of the pure PEO and its blends with PVPh-*co*-PMMA copolymer is now examined. Figure 7 and Figure 8 show infrared spectra in the 1320-1380 cm^{-1} region of the pure PEO, and various PVPh-*co*-PMMA/PEO blends at room temperature. The pure PEO has two bands at 1360 and 1343 cm^{-1} that represent the crystalline phase of the PEO.[36] These bands decrease as the PVPh-*co*-PMMA content is increased. These crystalline bands disappear on PVPh-*r*-PMMA/PEO = 4/6 and PVPh-*b*-PMMA/PEO = 5/5 blends and are replaced by a broad band roughly centered at 1350 cm^{-1} corresponding to the amorphous phase. That means the PEO crystallization is being retarded or even inhibited by adding the amorphous PVPh-*co*-PMMA copolymer. As a result, we can confirm that the hydroxyl group of PVPh is more favorable to form the interassociation with ether group of PEO than with carbonyl group of PMMA. However, the difference in crystallization behaviors was investigated by DSC and FTIR on 30-*r*-70/PEO = 4/6 and 30-*b*-70/PEO = 5-5 blends. In general, the polymer crystallinity measured by FTIR is from direct sample measurement, and no thermal history is involved in preparing the sample. On the contrary, the polymer crystallinity detected by DSC depends on the thermal history because recrystallization may occur during cooling or heating scan.
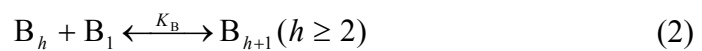
We now turn our attention to Figure 6 again. The frequency difference ($\Delta\nu$) increases with increasing PEO content and approaches a maximum for the blend

containing 60 wt% PEO except the 92-*r*-8/PEO and 75-*b*-25/PEO blends, in which they show Δν decrease with further increase of the PEO content. The observed slight decrease in Δν at higher PEO content (80 wt%) can be explained by the fact that these blend systems possess PEO crystalline phase. Consequently, the hydroxyl-ether interassociation tends to decrease between the PVPh and PEO segments due to reduced chain mobility in the PEO crystalline phase.[37] In another aspect, since more hydroxyl groups are present at the interface between PVPh-*co*-PMMA copolymer and PEO crystalline phase in the 92-*r*-8/PEO = 2/8 and 75-*b*-25/PEO = 2/8 blends, the hydroxyl stretching bands do not shift back to higher wavenumber.

The carbonyl stretching band for PMMA appears at 1730 cm^{-1}. Figure 9 and Figure 10 show the infrared spectra of the carbonyl stretching measured at room temperature ranging from 1670 to 1770 cm^{-1} of PVPh-*co*-PMMA and PVPh-*co*-PMMA/PEO blends. The carbonyl stretching of the pure PVPh-*co*-PMMA is split into two bands, absorption by free and hydrogen bonded carbonyl groups at 1730 and 1705 cm^{-1}, respectively. Obviously, the relative contribution of these two types of carbonyl groups must be dependent on copolymer composition. As has been observed in infrared spectra, we can expect a higher fraction of hydrogen bonded carbonyl groups for copolymers rich in vinylphenol units where carbonyl groups are more surrounded by the donor medium. As can be seen in Figure 9 and Figure 10, the presence of ether groups in these blend leads to a competition with carbonyl groups for hydrogen bonding with hydroxyl groups. This competition is evident in the evolution of the carbonyl band in the blend. Thus for a particular PVPh-*co*-PMMA copolymer, the hydrogen bonded carbonyl groups (progressive decrease of the shoulder at relatively lower wavenumber) decrease with the increase of the PEO content in the blend increases. In other word, the hydroxyl-ether

association prevails over the hydroxyl-carbonyl association. This result agrees with the evolution previously reported for the hydroxyl stretching region.

These bands can be readily decomposed into two Gaussian peaks, the free carbonyl (1730 cm^{-1}) and the hydrogen bonded carbonyl (1705 cm^{-1}) absorptions. Using the known respective absorptivity coefficients, fractions of these two types carbonyl groups can be calculated from the relative intensities of these two bands. To obtain the fraction of the hydrogen bonded carbonyl group, a known absorptivity ratio for hydrogen bonded and free carbonyl is required. We employed a value of $\alpha_{HB}/\alpha_F = 1.5$ which was previously calculated by Moskala et al.[38] Table 4 and Table 5 summarize fractions of hydrogen-bonded carbonyl calculated through curve fitting of the data from both copolymers and their blends. Table 4 and Table 5 show that the fraction of hydrogen bonded carbonyl decreases with increasing the relative ratio of PEO to PMMA. This result implies that the interassociation equilibrium constant of hydroxyl-ether is greater than the interassociation equilibrium constant of hydroxyl-carbonyl and the self-association equilibrium constant of hydroxyl-hydroxyl at room temperature. In our previous study,[37,39] we have used three competing functional groups to predict the fraction of hydrogen bonded carbonyl group. According to the Painter-Coleman Association Model (PCAM), we designate B, A, and C as PVPh, PMMA, and PEO, respectively. K_2, K_B, K_A, and K_C are their respective association equilibrium constants.

$$B_1 + B_1 \xleftrightarrow{\;K_2\;} B_2 \tag{1}$$

$$B_h + B_1 \xleftrightarrow{\;K_B\;} B_{h+1}\,(h \geq 2) \tag{2}$$

$$B_h + C_1 \xleftrightarrow{\;K_c\;} B_h C \tag{3}$$

$$B_h + A_1 \xleftrightarrow{\;K_A\;} B_h A \tag{4}$$

These four equilibrium constants can be expressed as follows in terms of volume fractions

$$\Phi_B = \Phi_{B1}\Gamma_2\left[1 + \frac{K_A\Phi_{A1}}{r_A} + \frac{K_C\Phi_{C1}}{r_C}\right] \tag{5}$$

$$\Phi_A = \Phi_{A1}\left[1 + K_A\Phi_{B1}\Gamma_1\right] \tag{6}$$

$$\Phi_C = \Phi_{C1}\left[1 + K_C\Phi_{B1}\Gamma_1\right] \tag{7}$$

where

$$\Gamma_1 = \left(1 - \frac{K_2}{K_B}\right) + \frac{K_2}{K_B}\left(\frac{1}{1 - K_B\Phi_{B1}}\right) \tag{8}$$

$$\Gamma_2 = \left(1 - \frac{K_2}{K_B}\right) + \frac{K_2}{K_B}\left(\frac{1}{\left(1 - K_B\Phi_{B1}\right)^2}\right) \tag{9}$$

Φ_B, Φ_A, and Φ_C are the volume fractions of repeat units in the blend, Φ_{B1}, Φ_{A1}, and Φ_{C1} are the volume fractions of isolated units in the blend, and $r_A = V_A/V_B$ and $r_C = V_C/V_B$ are the ratios of segmental molar volumes.

The self-association constant of PVPh (hydroxyl-hydroxyl), the interassociation constant between PMMA and PVPh (carbonyl-hydroxyl), and the interassociation constant between PEO and PVPh (ether-hydroxyl) in PVPh-r-PMMA/PEO blend have been reported in the literature.[16,40,41] The interassociation constant of PEO in PVPh-b-PMMA/PEO blend is determined indirectly from a least-squares fitting procedure. If these equilibrium constants (K_2, K_B, K_A), segment molar volume, and the fraction of hydrogen bonded carbonyl group are known, the K_C value can be calculated from eqs 5-9 by using a least-squares fitting based on the fraction of hydrogen bonded carbonyl group experimentally obtained. We obtained the value for $K_C = 300$ in PVPh-b-PMMA/PEO blend system at room temperature, implying that the interassociation equilibrium constant for hydroxyl-ether is indeed greater than the

144

interassociation equilibrium constant of hydroxyl-carbonyl and self-association equilibrium constant of PVPh at room temperature. Table 6 lists all the parameters required by the Painter-Coleman Association Model to estimate thermodynamic properties for these PVPh-*co*-PMMA/PEO blends. These results give a good agreement between the experimental and theoretical fractions of the hydrogen bonded carbonyl groups corresponding based on PVPh-*r*-PMMA/PEO and PVPh-*b*-PMMA/PEO blends by using a fixed volume fractions of PEO ($\Phi_C = 0.2$) as illustrated in Figure 11. The observed difference in K_C values between these two PVPh-*co*-PMMA/PEO blends can be attributed to the "screening" or locally nonrandom mixing driven primarily by intramolecular connectivity effects.[41,42] The covalent linkages within polymer segments of a copolymer result in greater numbers of same-chain contacts than that calculated from a random mixing of segments.

The interassociation equilibrium constant of PEO ($K_C = 231$ obtained from PVPh-*r*-PMMA/PEO blends and $K_C = 300$ obtained from PVPh-*b*-PMMA/PEO blends) is greater than the interassociation equilibrium constant (hydroxyl-carbonyl) of PVPh-*r*-PMMA ($K_A = 67.4$) or PVPh-*b*-PMMA ($K_A = 47.1$). When PEO is mixed with PVPh-*co*-PMMA, its ether oxygen competes for the PVPh hydroxyl and f_b of PMMA in both copolymer/PEO blends inevitably decreases. Meanwhile, the fraction of hydrogen bonded carbonyl of PVPh-*r*-PMMA/PEO blend is greater than that of PVPh-*b*-PMMA/PEO blend under the similar composition based on higher K_A (67.4 vs. 47.1). The f_b listed in Table 4 and Table 5 indeed show the expected trend. In another aspect, someone may speculate that the observed higher $\Delta\nu$ of PVPh-*b*-PMMA/PEO blend than that of PVPh-*r*-PMMA/PEO blend is due to the relative ratio of interassociation equilibrium constant of PEO to PMMA is larger in PVPh-*b*-PMMA/PEO blend system. However, we have displayed the opposed experiment results in Figure 6. This phenomenon can be rationalized by the

so-called $\Delta\chi$ effect and ΔK effect in a ternary blend.

The phase behavior of a ternary polymer blend system is primarily governed by the magnitude of the individual binary interaction parameters (χ_{ij}) if no strong specific interaction is present. There is a driving force towards phase separation if the difference in the interaction parameter values is significantly high and results in a $\Delta\chi$ effect, which is unfavourable "physical" interaction. When there is hydrogen bonding interactions present in a polymer blend, higher difference in interassociation equilibrium constant tends to induce phase separation. The ΔK effect reflects the difference in the "chemical" interaction between the self-association polymer and the other polymers in the mixture. While the presence of specific intermolecular interactions enhances the probability of forming a homogeneous ternary polymer blend, they can concurrently exacerbate the situation through the ΔK effect, which tends to promote phase separation. By taking into account these two effects simultaneously, it is difficult to find ternary polymer blends that exist homogeneously over a wide composition range.[43]

The phase diagrams of both PVPh-*co*-PMMA/PEO blends are shown in Figure 12(A) and 12(B) based on DSC results listed in Table 2 and Table 3. For comparison, the phase diagram of PVPh/PMMA/PEO ternary polymer blend is also displayed in Figure 12(C) and its thermal properties are listed in Table 7. As can been seen, the PVPh-*r*-PMMA/PEO blend system exhibits a single phase over the entire compositions. On the other hand, there exists a closed-looped of phase separated region in the phase diagrams of PVPh-*b*-PMMA/PEO and PVPh/PMMA/PEO due to the so-called $\Delta\chi$ and ΔK effects in ternary polymer blends. The non-hydrogen bonded solubility parameters of the specific repeat units for these two PVPh-*co*-PMMA/PEO blend systems are the same, implying that the contribution to the free energy of mixing from physical force in the two blend

146

systems is essentially identical. Furthermore, ΔK is related to the ratio of the two interassociation equilibrium constants, K_C/K_A. Consequently, the closed-loop of heterogeneous region is formed in PVPh-b-PMMA/PEO blend system caused by greater ΔK effect. In addition, the PVPh-r-PMMA/PEO blend system has greater homogeneity at the molecular scale than that of the PVPh-b-PMMA/PEO blend system. The strength of the hydrogen bond formed between the hydroxyl and ether in PVPh-r-PMMA/PEO blends is higher than that in PVPh-b-PMMA/PEO blends. As a result, the $\Delta \nu$ of PVPh-r-PMMA/PEO blend is higher than that of PVPh-b-PMMA/PEO blend, implying that the ΔK effect plays a more important role in dictating the ability of hydrogen bond formation and the miscibility in the ternary polymer blend.

5-4 Conclusions

The PVPh-*r*-PMMA/PEO blending system is completely miscible in an amorphous phase over the entire composition range. On the contrary, the PVPh-*b*-PMMA/PEO blend system shows a closed-looped phase separated region in the phase diagram due to $\Delta\chi$ and ΔK effects in the ternary polymer blend. FTIR was employed to study the specific interaction at various compositions and various inter and intramolecular hydrogen bonding. Based on the frequency difference ($\Delta\nu$) from both copolymer/PEO blends, the interassociation between hydroxyl in PVPh and ether in PEO is considerably stronger than either the self-association of hydroxyl in PVPh or the interactions between hydroxyl groups in PVPh and carbonyl groups in PMMA. Based on the Painter-Coleman Association Model (PCAM), a value for K_C = 300 is obtained in PVPh-*b*-PMMA/PEO blend system at room temperature. This result gives a good agreement between the experimental and theoretical fraction of hydrogen bonded carbonyl groups for the two sets of copolymer/PEO blends based on a fixed volume fractions of PEO (Φ_C = 0.2). Although the relative ratio of interassociation equilibrium constant of PEO to PMMA is larger in PVPh-*b*-PMMA/PEO blend system, the PVPh-*r*-PMMA/PEO blend system has greater $\Delta\nu$ and greater homogeneity at the molecular scale than the PVPh-*b*-PMMA/PEO blend system because of the ΔK effect.

References

(1) Huglin, M. B.; Rego, J. M. *Polymer* **1990**, *21*, 1269.

(2) Lee, J. Y.; Painter, P. C.; Coleman, M. M. *Macromolecules* **1988**, *21*, 954.

(3) Meaurio, E.; Velada, J. L.; Cesteros, L. C.; Katime, I. *Macromolecules* **1996**, *29*, 4598.

(4) Dai, J.; Goh, S. H.; Lee, S. Y.; Siow, K. S. *Polymer* **1995**, *35*, 2174.

(5) Coleman, M. M.; Graf, J. F.; Painter, P. C. "*Specific Interactions and the Miscibility of Polymer Blends. Technomic Publishing*", Lancaster, PA, **1991**.

(6) Kambour, R. P.; Bendler, J. T.; Bopp, R. C. *Macromolecules* **1983**, *16*, 753.

(7) Paul, D. R.; Barlow, J. W. *Polymer* **1984**, *25*, 487.

(8) Roe, R. J.; Rigby, D. *In Advances in Polymer Science 82*; Springer-Verlag: Berlin, 1987.

(9) Woo, E. M.; Barlow, J. W.; Paul, D. R. *Polymer* **1985**, *26*, 763.

(10) Fernandes, A. C.; Barlow, J. W.; Paul, D, R. *J. Appl. Polym. Sci.* **1986**, *32*, 5357.

(11) Fowler, M. E.; Barlow, J. W.; Paul, D. R. *Polymer* **1987**, *28*, 1177.

(12) ten Brinke, G.; Karasz, F. E.; MacKnight, W. J. *Macromolecules* **1983**, *16*, 1827.

(13) Shiomi, T.; Karasz, F. E.; MacKnight, W. J. *Macromolecules* **1986**, *19*, 2274.

(14) Jo, W. H.; Lee, S. C. *Macromolecules* **1990**, *23*, 2261.

(15) Isasi, J. R.; Cesteros, L. C.; Katime, I. *Macromolecules* **1994**, *27*, 2200.

(16) Lin, C. L.; Chen, W. C.; Liao, C. S.; Su, Y. C.; Huang, C. F.; Kuo, S. W.; Chang, F. C. Macromoleculus in press.

(17) Jo, W. H.; Choi, K. *Macromolecules* **1997**, *30*, 1509.

(18) Coleman, M. M.; Painter, P. C. *Prog. Polym. Sci.* **1995**, *20*, 1.

(19) Hong, B. K.; Kim, J. K.; Jo, W. H.; Lee, S. C. *Polymer* **1997**, *38*, 4373.

(20) Manestrel, C. L.; Bhagwagar, D. E.; Painter, P. C.; Coleman, M. M.; Graf, J. F. *Macromolecules* **1992**, *25*, 7101.

(21) Jo, W. H.; Kwon, Y. K.; Kwon, I. H. *Macromolecules* **1991**, *24*, 4708.

(22) Jack, K. S.; Whittaker, A. K. *Macromolecules* **1997**, *30*, 3560.

(23) Serman, C. J.; Painter, P. C.; Coleman, M. M., *Polymer* **1991**, *32*, 1049.

(24) Dong, J.; Ozaki, Y., *Macromolecules* **1997**, *30*, 286.

(25) Li, X.; Hsu, S. L. *J. Polym. Sci., Polym. Phys. Ed.* **1984**, *22*, 1331.

(26) Ito, H.; Russell, T. P.; Wignall, G. D. *Macromolecules* **1987**, *20*, 2213.

(27) Zawada, J. A.; Ylitalo, C. M.; Fuller, G. G.; Colby, R. H.; Long, T. E. *Macromolecules* **1992**, *25*, 2896.

(28) Wastlund, C.; Maurer, F. H. J. *Macromolecules* **1997**, *30*, 5870.

(29) Chen, X.; An. L.; Yin, J.; Sun, Z. *Macromolecules* **1999**, *32*, 5905.

(30) Feldstein, M. M.; Shandryuk, G. A.; Kuptsov, S. A.; Plate, N. A. *Polymer* **2000**, *41*, 5327.

(31) Kuo, S. W.; Chang, F. C. *Macromol. Chem. Phys.* **2001**, *202*, 3112.

(32) Kuo, S. W.; Huang, W. J.; Huang, C. F.; Chan, S. C.; Chang, F. C. *Macromolecules* **2004**, *37*, 4164.

(33) Schmulbach, C. D.; Drago, R. S. *J. Phys. Chem.* **1960**, *64*, 1956.

(34) Purcell, K. F.; Drago, R. S. *J. Am. Chem. Soc.* **1968**, *89*, 2874.

(35) Moskala, E. J.; Varnell, D. F.; Coleman, M. M. *Polymer* **1985**, *26*, 228.

(36) Chintapalli, S.; Frech, R. *Macromolecules* **1996**, *29*, 3499.

(37) Kuo, S. W.; Chang, F. C. *Macromolecules* **2001**, *34*, 4089.

(38) Moskala, E. J.; Howe, S. E.; Painter, P. C.; Coleman, M. M. *Macromolecules* **1984**, *17*, 1671.

(39) Kuo, S. W.; Lin, C. L.; Chang, F. C. *Macromolecules* **2002**, *35*, 278.

(40) Coleman, M. M.; Xu, Y.; Painter, P. C. *Macromolecules* **1994**, *27*, 127.

(41) Painter, P. C.; Veytsman, B.; Kumar, S.; Shenoy, S.; Graf, J. F.; Xu, Y.; Coleman, M. M. *Macromolecules* **1997**, *30*, 932.

(42) Coleman, M. M.; Painter, P. C. *Macromol. Chem. Phys.* **1998**, *199*, 1307.

(43) Zhang, H.; Bhagwagar, D. E.; Graf, J. F.; Painter, P. C.; Coleman, M. M. *Polymer* **1994**, *35*, 5379.

Table 5-1. Characterization of PVPh-*r*-PMMA prepared by free radical polymerization and PVPh-*b*-PMMA synthesized by anionic polymerization

PVPh-*r*-PMMA	M_n (g/mol)	Composition of PVPh (wt%)	M_w/M_n	PVPh-*b*-PMMA	M_n (g/mol)	Composition of PVPh (wt%)	M_w/M_n
30-*r*-70	18000	30	1.62	30-*b*-70	16000	30	1.11
58-*r*-42	19000	58	1.63	40-*b*-60	16000	40	1.15
76-*r*-24	17600	76	1.49	55-*b*-45	30000	55	1.10
92-*r*-8	16000	92	1.63	75-*b*-25	22000	75	1.13

Table 5-2. Thermal properties of PVPh-*r*-PMMA/PEO blends

Copolymer	PEO content (wt%)	T_g (^{o}C)	T_m (^{o}C)
30-*r*-70	0	143	
	20	58	
	40	0	
	50	-32	
	60	-39	58.7
	80	-6	62.5
	100	-67	69.2
58-*r*-42	0	160	
	20	78	
	40	11	
	50	-18	
	60	-35	58.1
	80	-11	61.8
76-*r*-24	0	169	
	20	81	
	40	14	
	50	-18	
	60	-32	56.9
	80	-17	61.4
92-*r*-8	0	179	
	20	87	
	40	21	
	50	-9	
	60	-20	
	80	-17	61.0

Table 5-3. Thermal properties of PVPh-*b*-PMMA/PEO blends

Copolymer	PEO content (wt%)	T_g (°C)		T_m (°C)
30-*b*-70	0	149		
	20	28	116	
	30	3	119	
	40	-19		
	50	-39		60.3
	60	-40		60.2
	80	-36		63.5
	100	-67		69.2
40-*b*-60	0	159		
	20	37	111	
	30	30		
	40	-19		
	50	-28		58.1
	60	-39		57.8
	80	-1		60.2
55-*b*-45	0	168		
	20	51	111	
	30	30		
	40	10		
	50	-18		
	60	-33		62.0
	80	-16		62.3
75-*b*-25	0	181		
	20	89		
	30	28		
	40	22		
	50	-7		
	60	-8		
	80	-14		61.6

Table 5-4. Results of curve-fitting the data for PVPh-*r*-PMMA and PVPh-*r*-PMMA/PEO blends at room temperature

PVPh-*random*-PMMA/PEO	H-bonded C=O			free C=O			f_b^a
	ν, cm^{-1}	$W_{1/2}$, cm^{-1}	A_b, %	ν, cm^{-1}	$W_{1/2}$, cm^{-1}	A_f, %	
92-*r*-8	1703	24	82.3	1729	18	17.7	75.7
92-*r*-8/PEO_8/2	1703	21	55.9	1727	17	44.1	45.8
92-*r*-8/PEO_6/4	1702	20	27.3	1726	17	72.7	20.0
92-*r*-8/PEO_5/5	1704	20	14.4	1726	17	85.6	10.1
92-*r*-8/PEO_4/6	1706	19	11.9	1726	17	88.1	8.2
92-*r*-8/PEO_2/8	1705	19	5.2	1726	17	94.8	3.5
76-*r*-24	1704	25	75.7	1730	19	24.3	65.6
76-*r*-24/PEO_8/2	1704	22	43.8	1728	17	56.2	34.2
76-*r*-24/PEO_6/4	1704	21	19.1	1727	18	80.9	13.6
76-*r*-24/PEO_5/5	1703	21	11.0	1727	18	89.0	7.6
58-*r*-42	1705	26	59.3	1731	19	40.7	49.3
58-*r*-42/PEO_8/2	1704	24	35.1	1729	19	64.9	26.5
58-*r*-42/PEO_6/4	1703	23	16.5	1728	19	83.5	11.6
30-*r*-70	1707	24	35.6	1731	19	64.4	26.9
30-*r*-70/PEO_8/2	1705	23	16.8	1730	19	83.2	11.8

[a] f_b: fraction of hydrogen bonded carbonyl group.

Table 5-5. Results of curve-fitting the data for PVPh-*b*-PMMA and PVPh-*b*-PMMA/PEO blends at room temperature

PVPh-*block*-PMMA/PEO	H-bonded C=O			free C=O			f_b
	v, cm^{-1}	$W_{1/2}$, cm^{-1}	A_b, %	v, cm^{-1}	$W_{1/2}$, cm^{-1}	A_f, %	
75-*b*-25	1709	25	65.8	1732	18	34.2	56.2
75-*b*-25/PEO_8/2	1708	21	36.3	1732	18	63.7	27.5
75-*b*-25/PEO_7/3	1707	20	17.3	1731	18	82.7	12.2
75-*b*-25/PEO_6/4	1704	19	5.1	1731	18	94.9	3.5
55-*b*-45	1708	24	58.3	1733	19	41.7	43.5
55-*b*-45/PEO_8/2	1706	22	24.2	1731	19	76.8	17.5
55-*b*-45/PEO_7/3	1704	22	8.8	1731	19	91.2	6.0
40-*b*-60	1709	24	42.1	1732	19	57.9	32.6
40-*b*-60/PEO_8/2	1706	23	14.6	1731	19	85.4	10.2
40-*b*-60/PEO_7/3	1704	22	7.0	1731	19	93.0	4.8
30-*b*-70	1709	23	32.8	1732	20	67.2	24.6
30-*b*-70/PEO_8/2	1704	23	11.1	1731	19	88.9	7.7

Table 5-6. Summary of the self-association and interassociation parameters of PVPh-*co*-PMMA copolymers and PVPh-*co*-PMMA/PEO blends

polymer	molar volume (ml/mol)	molecular weight (g/mol)	solubility parameter (cal/ml)$^{0.5}$	self-association equilibrium constant		interassociation equilibrium constant					
						random copolymer		block copolymer		ternary polymer blend	
				K_2	K_B	K_A	K_C	K_A	K_C	K_A	K_C
PVPh	100.0	120.0	10.6	21.0	66.8						
PMMA	84.9	100.0	9.1			67.4[a]		47.1[b]		37.4[a]	
PEO	38.1	44.1	9.4				231[c]		300		490[d]

[a] Reference 40. [b] Reference 16. [c] Reference 41. [d] Reference 20.

Table 5-7. Thermal properties of PVPh/PMMA/PEO ternary polymer blends

PVPh/PMMA/PEO (wt%)	T_g (^{o}C)		T_m (^{o}C)
100/0/0			
0/100/0	105		
0/0100	-67		69.2
10/72/18	-28	123	62.8
10/54/36	8	114	65.9
10/36/54			66.0
10/18/72			66.1
30/56/14	31	98	
30/42/28	15	112	
30/28/42	-21	110	62.0
30/14/56	-24	114	64.1
50/40/10	7	104	
50/30/20	44	96	
50/20/30	11		
50/10/40	-24		
70/24/6	138		
70/18/12	102		
70/12/18	21		
70/6/24	18		
80/16/4	138		
80/12/8	137		
80/8/12	98		
80/4/16	84		
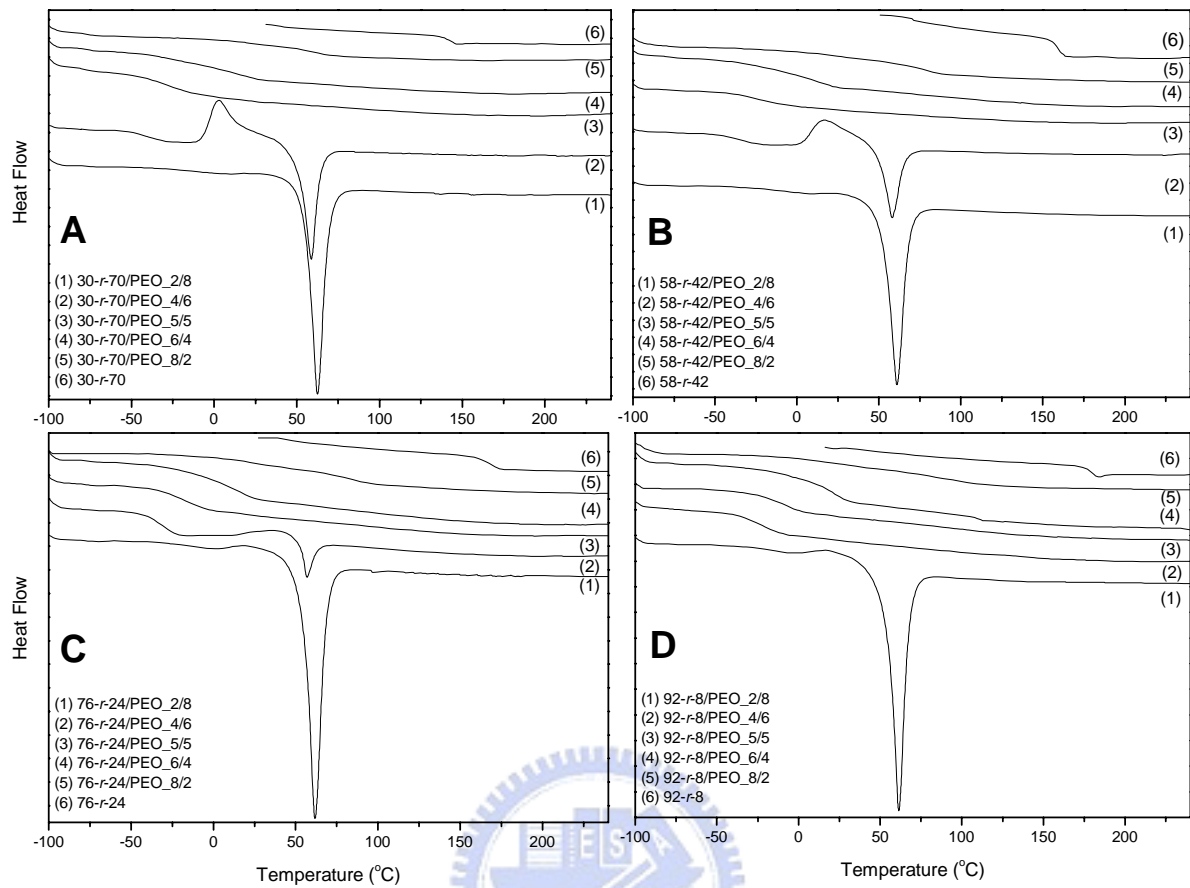
Figure 5-1: DSC thermograms of PVPh-*r*-PMMA/PEO blends having different compositions for (A) 92-*r*-8/PEO, (B) 76-*r*-24/PEO, (C) 58-*r*-42/PEO, and (D) 30-*r*-70/PEO.
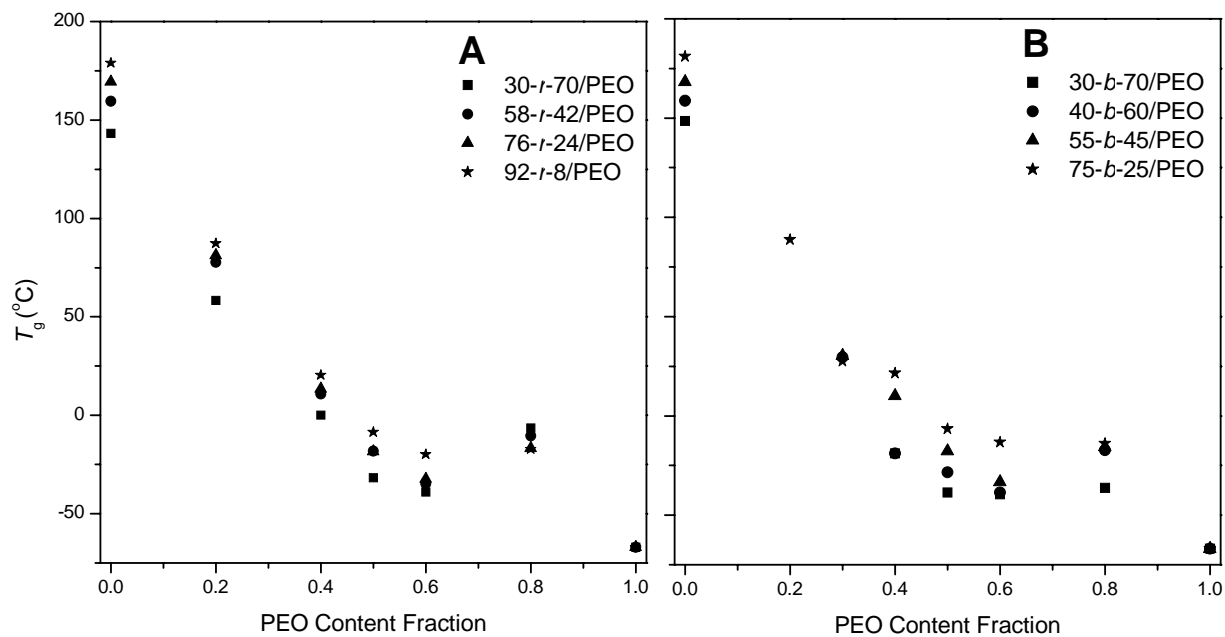
Figure 5-2: Plots of T_g vs weight of PEO for the copolymer/PEO: (A) PVPh-*r*-PMMA/PEO and (B) PVPh-*b*-PMMA/PEO blends.
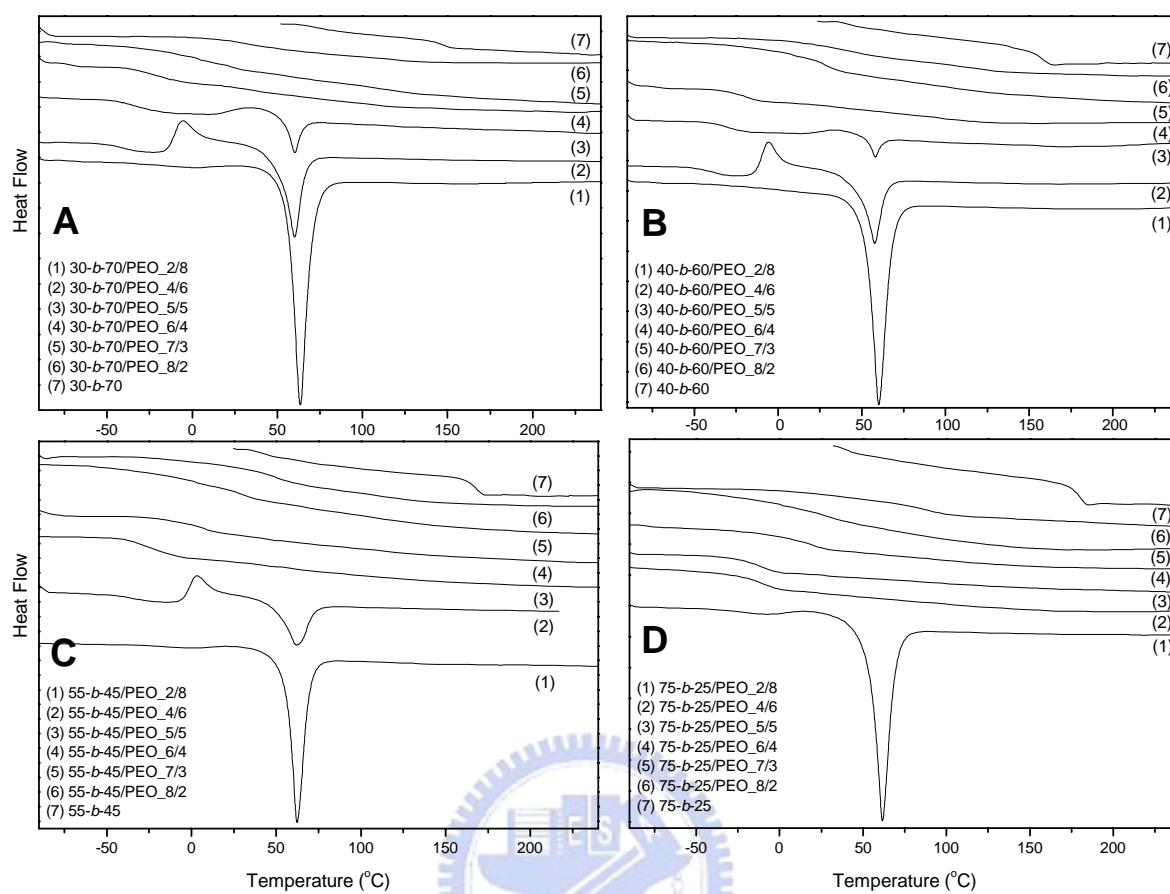
Figure 5-3: DSC thermograms of PVPh-*b*-PMMA/PEO blends having different compositions for (A) 75-*b*-25/PEO, (B) 55-*b*-45/PEO, (C) 40-*b*-60/PEO, and (D) 30-*b*-70/PEO.
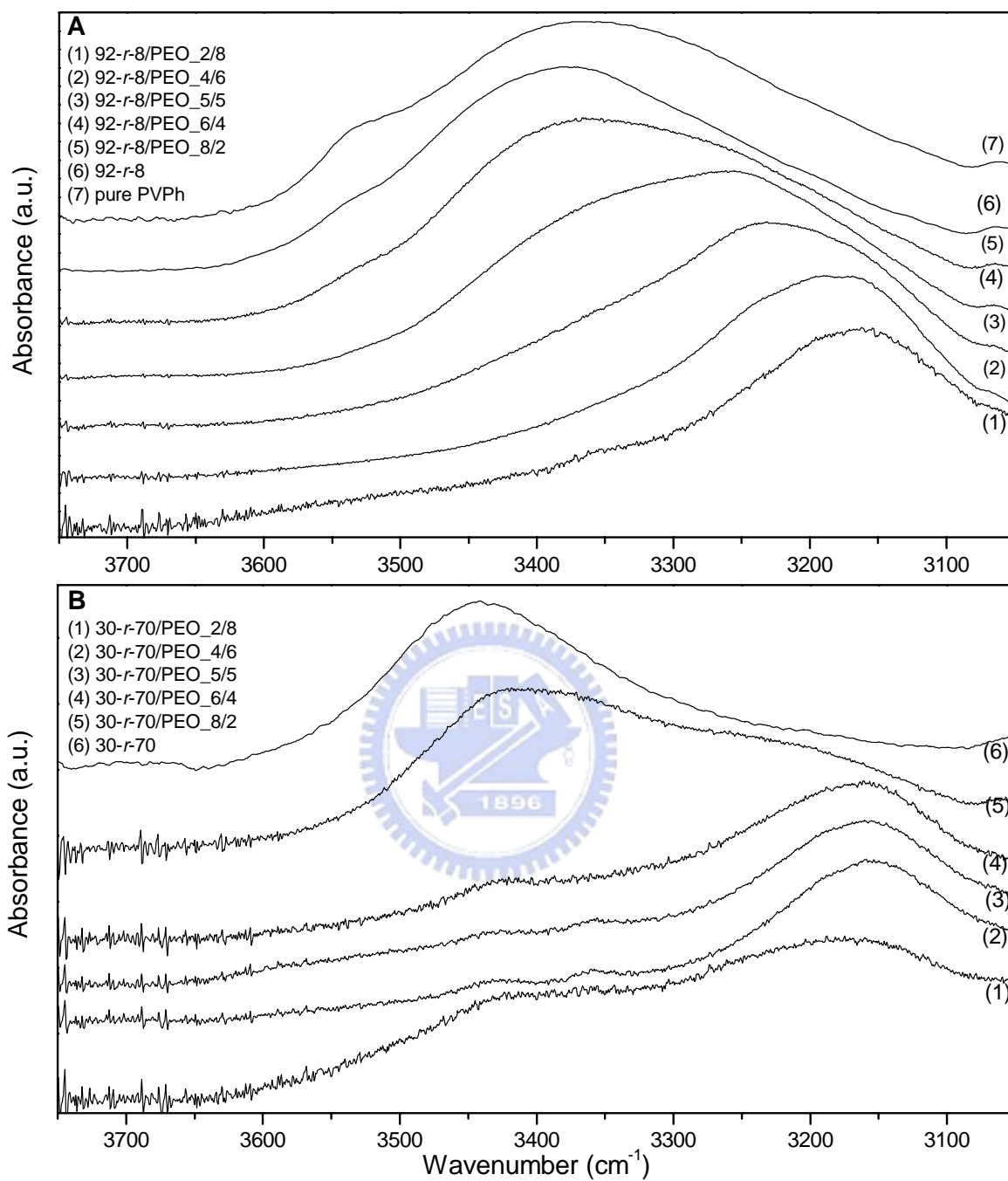
Figure 5-4: FTIR spectra in the 3050 – 3750 cm^{-1} region for (A) 92-*r*-8/PEO and (B) 30-*r*-70/PEO.
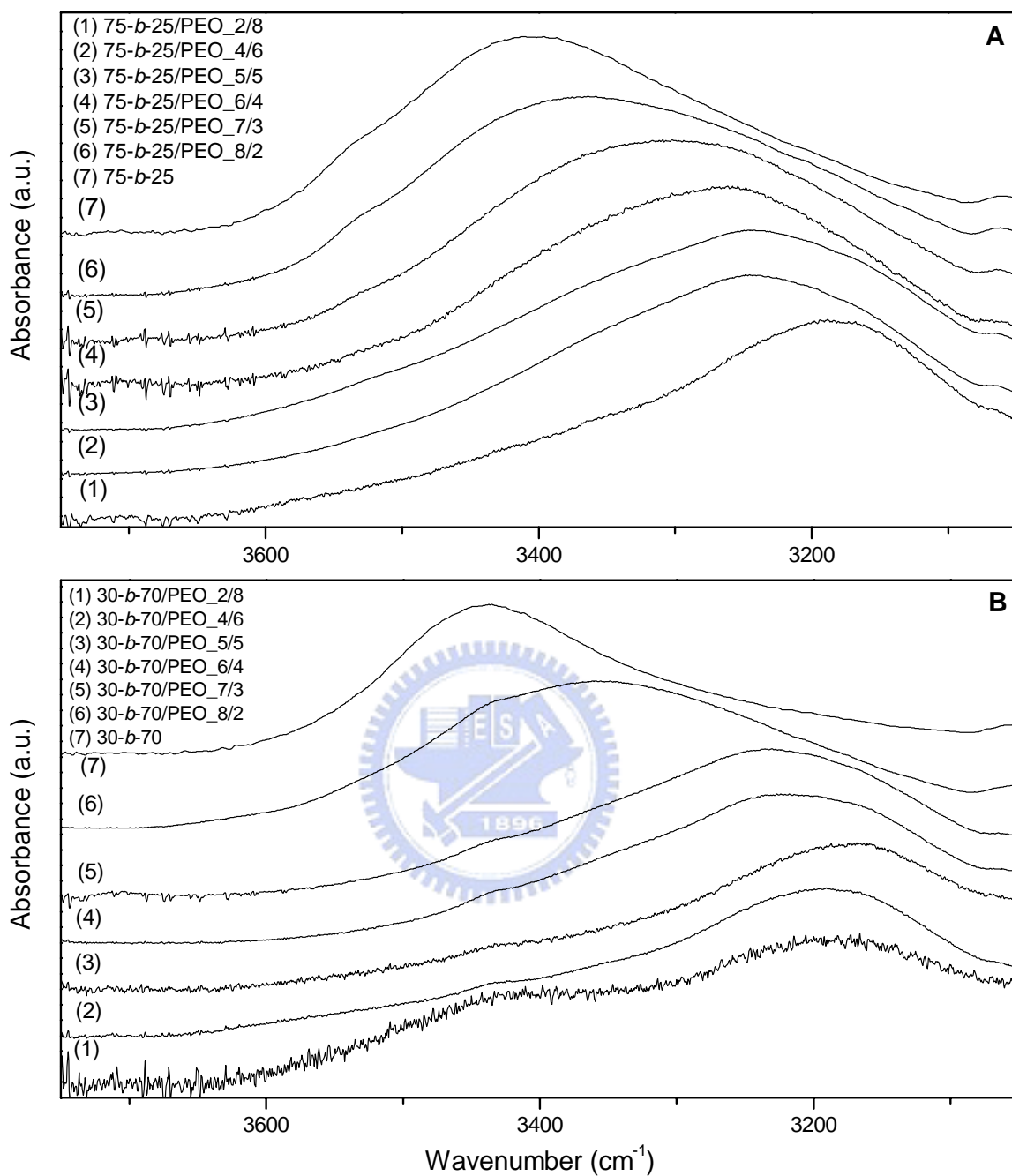
Figure 5-5: FTIR spectra in the 3050 – 3750 cm^{-1} region for (A) 75-*b*-25/PEO and (B) 30-*b*-70/PEO.
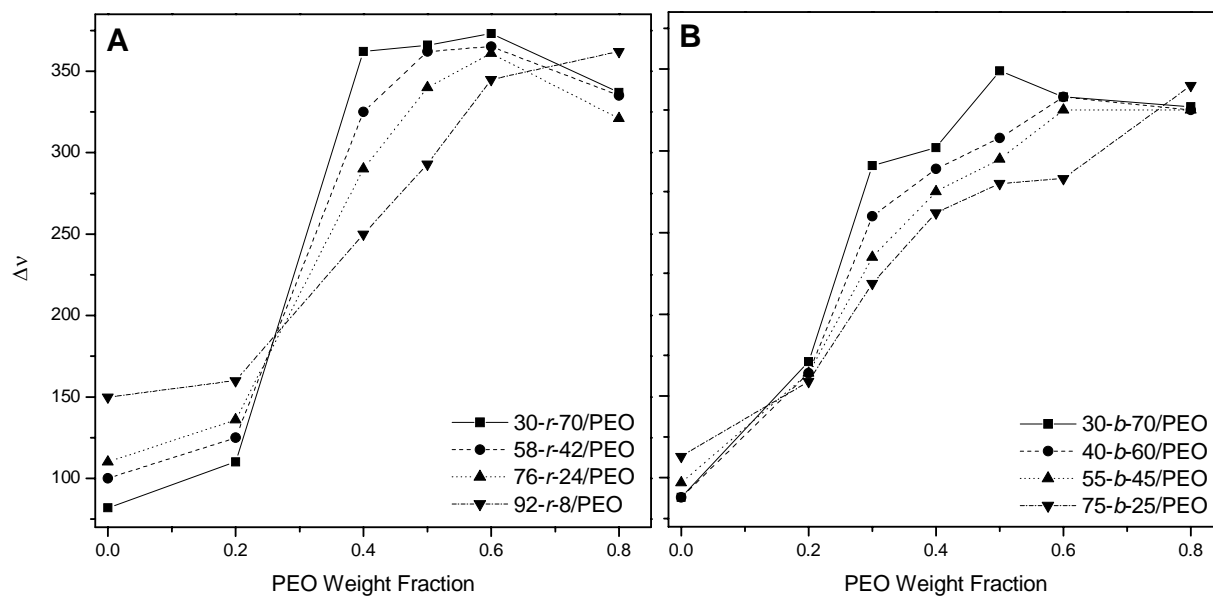
Figure 5-6: Plots of Δν vs weight of PEO for the copolymer/PEO: (A) PVPh-*r*-PMMA/PEO and (B) PVPh-*b*-PMMA/PEO blends.
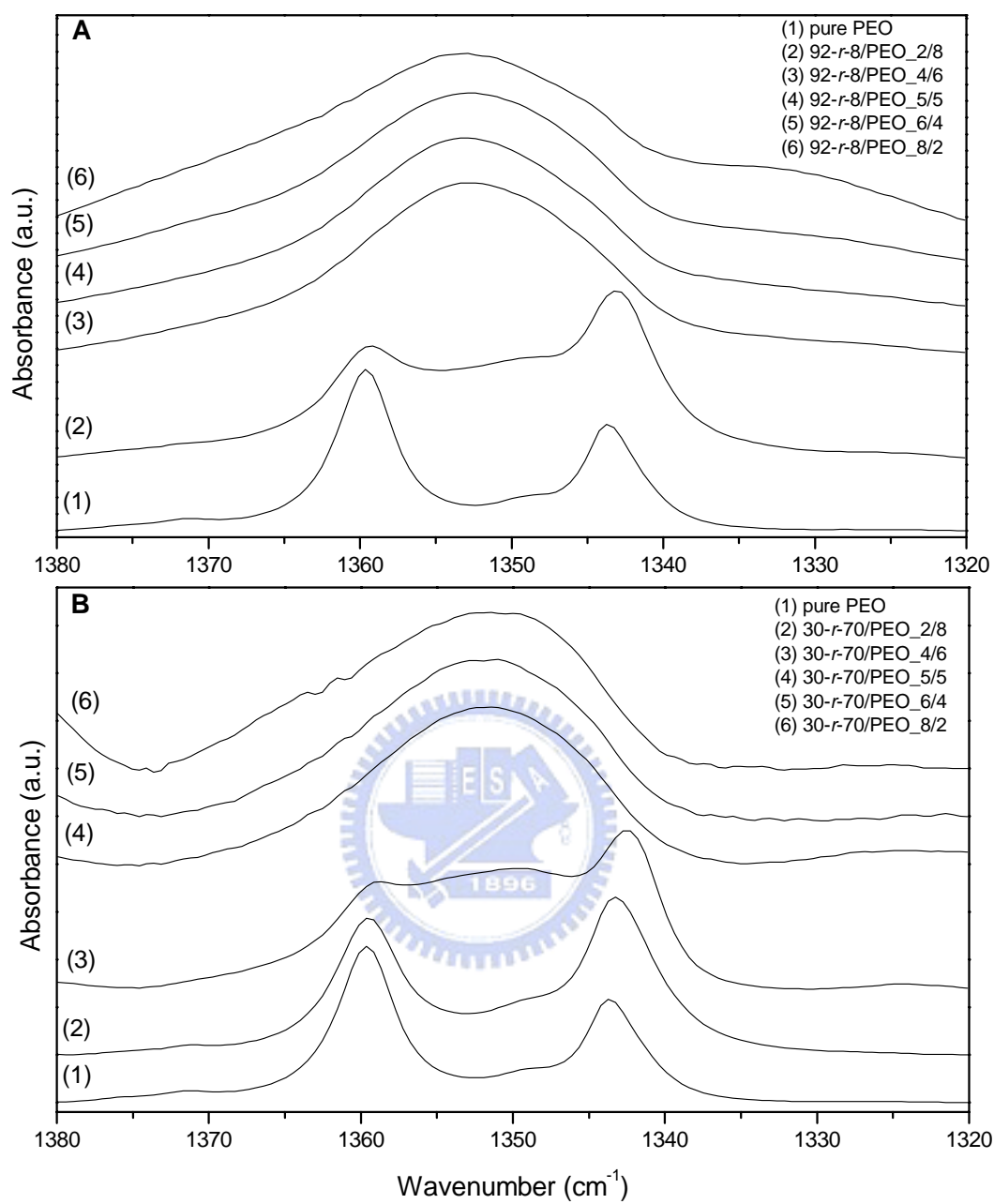
Figure 5-7: FTIR spectra in the 1320 – 1380 cm^{-1} region for (A) 92-*r*-8/PEO and (B) 30-*r*-70/PEO.
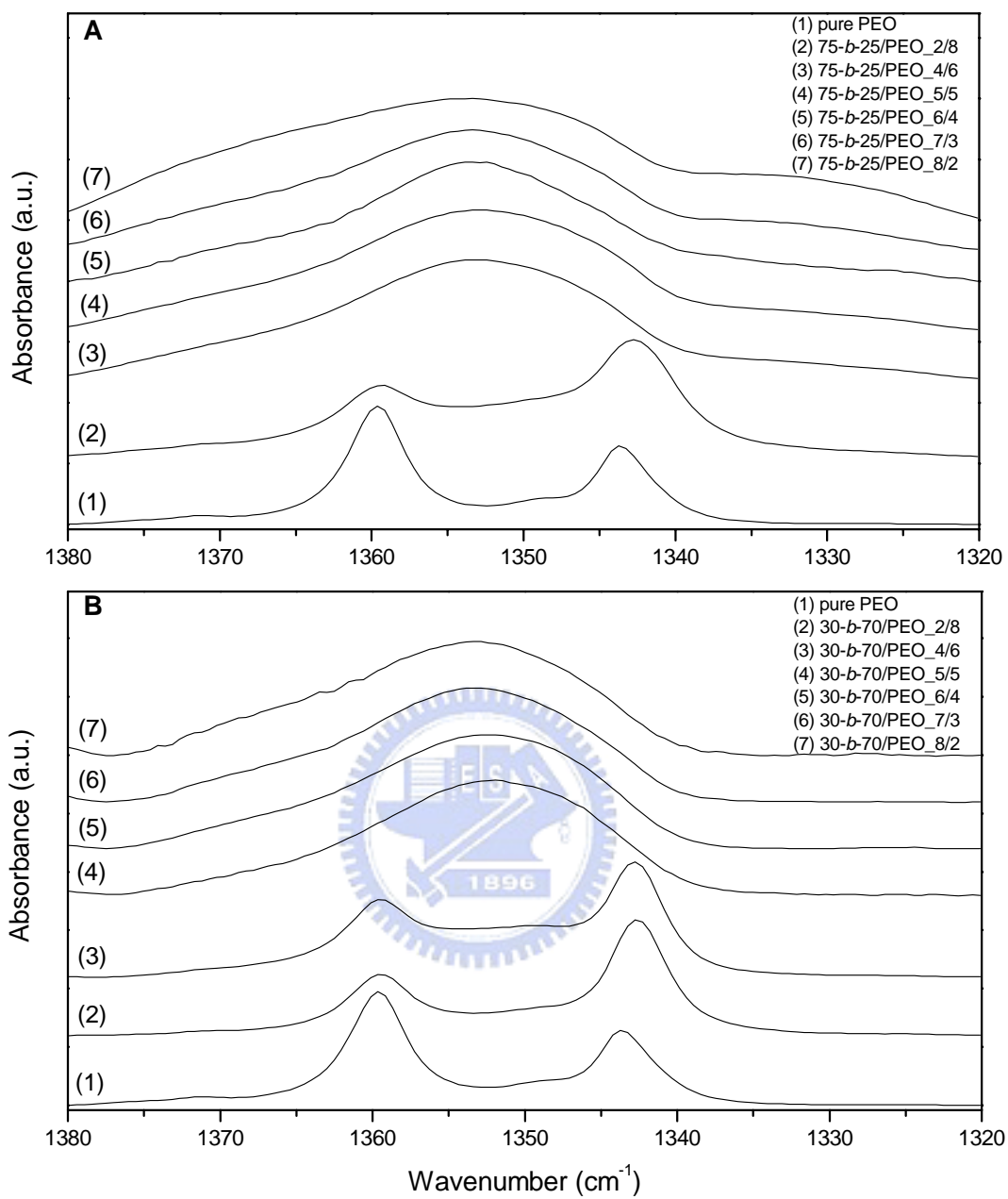
Figure 5-8: FTIR spectra in the 1320 – 1380 cm^{-1} region for (A) 75-*b*-25/PEO and (B) 30-*b*-70/PEO.
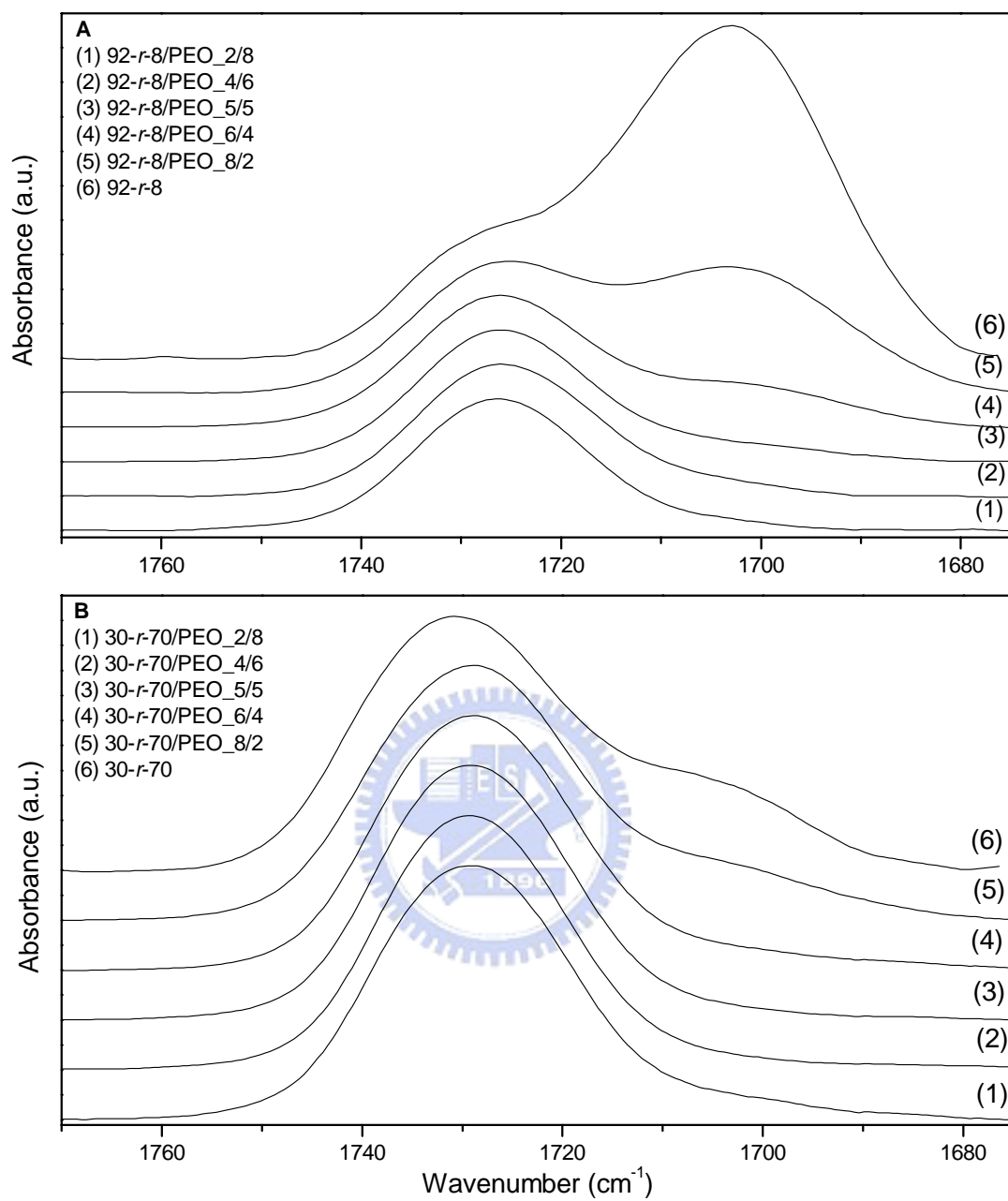
Figure 5-9: FTIR spectra (1670 – 1780 cm^{-1}) of a (A) 92-*r*-8/PEO and (B) 30-*r*-70/PEO.
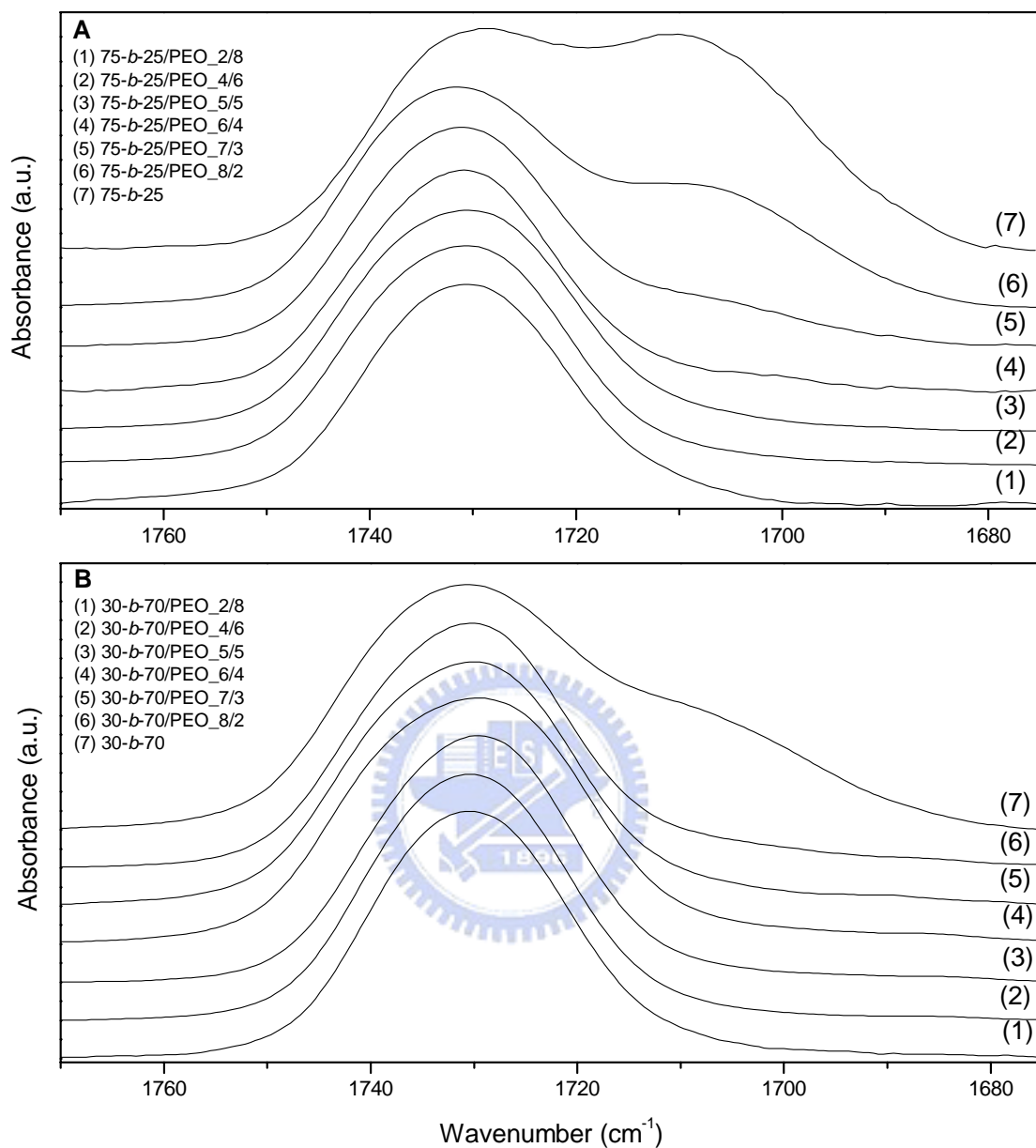
Figure 5-10: FTIR spectra (1670 – 1780 cm⁻¹) of a (A) 75-*b*-25/PEO and (B) 30-*b*-70/PEO.
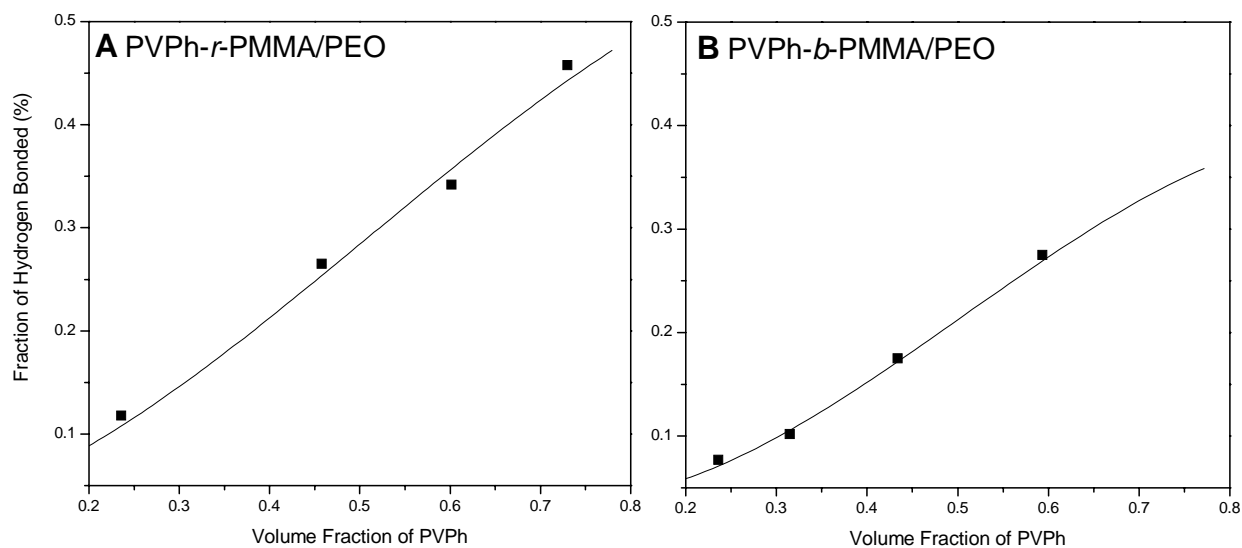
Figure 5-11: Plot of the calculated ($-$) and experimental (■) values of the fraction of hydrogen bonded carbonyl groups in blends of (A) PVPh-*r*-PMMA/PEO and (B) PVPh-*b*-PMMA/PEO blends where the volume fraction of PEO was hold at 0.2.
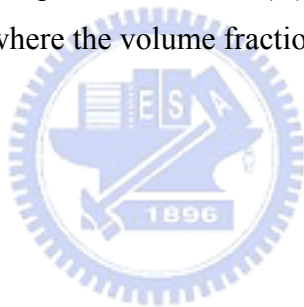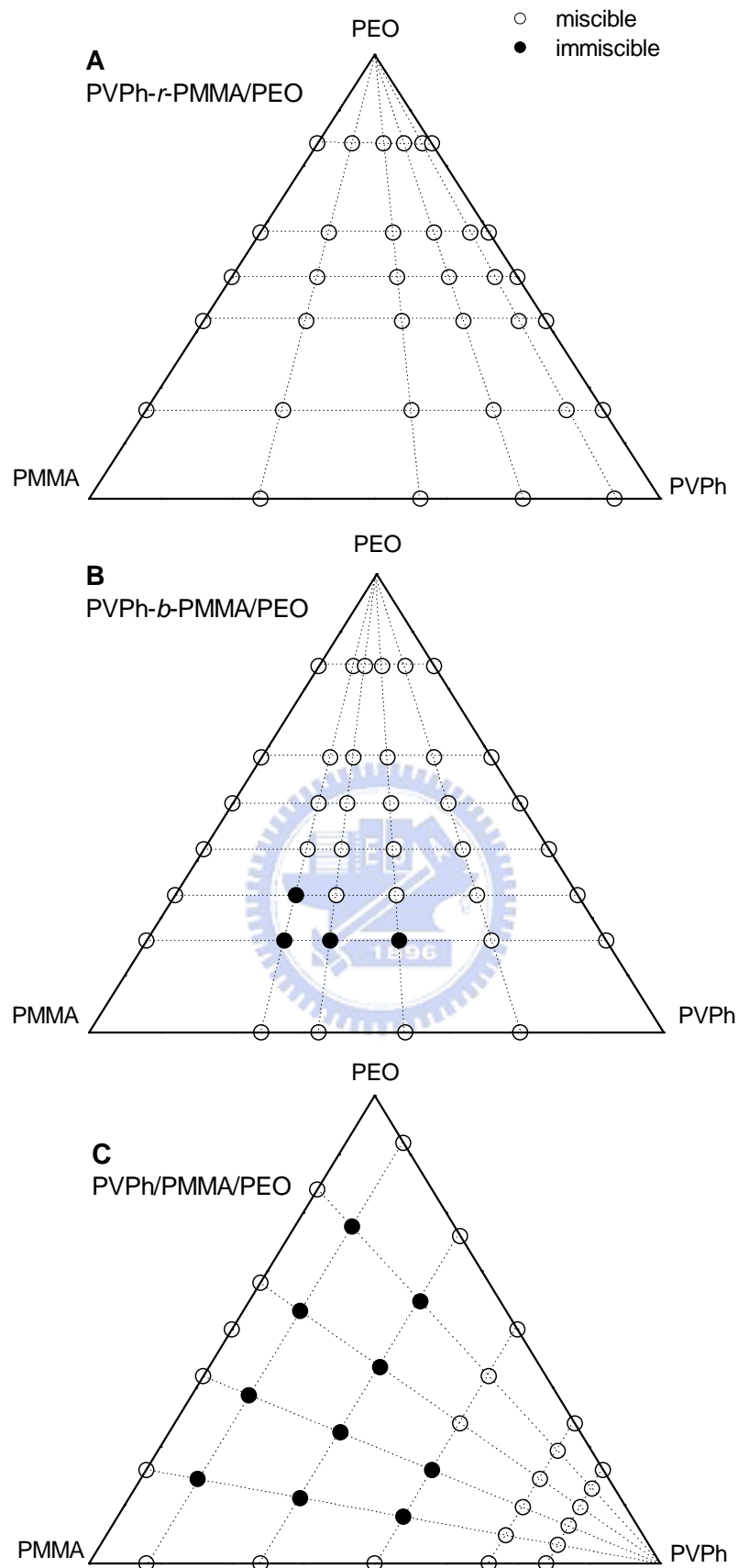
Figure 5-12: Ternary phase diagram of (A) PVPh-*r*-PMMA/PEO and (B)
PVPh-*b*-PMMA/PEO blends. The open circles represent a miscible ternary blend, and
the full circles represent an immiscible ternary blend.

Chapter 6

The Totally Miscible in Ternary Hydrogen Bonded Polymer Blend of Poly(vinyl phenol)/Phenoxy/Phenolic

Abstract

The individual binary polymer blend of phenolic/phenoxy, phenolic/poly(vinyl phenol)(PVPh) and phenoxy/PVPh has specific interaction through inter-molecular hydrogen bonding of hydroxyl-hydroxyl group to form homogeneous miscible phase. In addition, the miscibility and hydrogen bonding behaviors of ternary hydrogen bond blends of phenolic/phenoxy/PVPh were investigated by using differential scanning calorimetry (DSC), Fourier transform infrared spectroscopy and optical microscopy. According to the DSC analysis, every composition of the ternary blend shows single glass transition temperature (T_g), indicating that this ternary hydrogen bonded blend is totally miscible. The inter-association equilibrium constant between each binary blend were calculated from the appropriate model compounds. The inter-association equilibrium constant (K_A) of each individually binary blend is higher than any self-association equilibrium constant (K_B), resulting in the hydroxyl group tend to form inter-association hydrogen bond. Photographs of optical microscopy show this ternary blend possess lower critical solution temperature (LCST) phase diagram. In other words, this ternary hydrogen bonded blend is totally miscible at room temperature.

6-1 Introduction

During the past twenty years, comprehensive experimental studies were executed that the miscibility and phase behavior of binary polymer blends.[1-3] Many well-known binary pairs of polymers have been found to obtain miscible blend. In general, these binary polymer blends have been investigated with specific interaction including intermolecular hydrogen bonding, ionic interaction, charge transfer complex, and the like.[4] On the contrary, ternary polymer blends have received much less attention due to complexity of calculating phase diagram and problems of experimental accuracy. Although an increase on the number of polymer components is a complication, there are several good reasons to study the phase behavior of ternary polymer blends in polymer science resulting from the industrial importance. For example, the Scott[5] and Tompa[6] worked on the ternary polymer blends that polymer B, which is miscible with each of polymer A and C, can compatibilize the immiscible binary pair A and C. Polymer B acts as a "compatibilizer" to reduce the size domain of heterogeneous phase separation structure. Classical examples are the ternary blends of poly(vinylidene fluoride) (PVDF)/poly(methyl methacrylate) (PMMA)/poly(ethyl methacrylate) (PEMA),[7] PVPh/PMMA/PEMA,[8] and SAN/PMMA/PEMA.[9] While PMMA and PEMA are immiscible with each other, the addition of a large amount of PVDF, PVPh and SAN leads to a miscible ternary polymer blend due to significant "$\Delta\chi$"[10] or "ΔK"[11] effect in these ternary blend systems. On the other hand, when all three binary pairs (B-A, B-C, and A-C) are individually miscible, a completely homogeneous or a closed immiscibility loop phase diagram has been observed.[11] The phase separation is caused by the difference in the interaction energy of the binary system, the so-called "$\Delta\chi$" and "ΔK" effects in ternary polymer blends such as phenoxy/PMMA/poly(ethylene oxide) (PEO),[12] PVPh/poly(vinyl acetate) (PVAc)/PEO,[11] poly(styrene-co-acrylic acid)/PMMA/PEO[13] and phenolic/PEO/PCL[14]

blend systems. For our knowledge, only a very few ternary polymer blends have been reported to be homogeneous over the entire compositions. These totally miscible ternary blends include poly(epichlorohydrin) (PECH)/PMMA/PEO,[15] PVDF/PVAc/PMMA,[16] PECH/PVAc/PMMA[17] and poly(3-hydroxybutyrate)/PEO/ PECH[18] because do not lead to a $\Delta\chi$ effect. Here, we need to emphasis that these totally miscible ternary blends do not have hydrogen-bonding interaction between their polymer segments. As a result, they are easy to obtain totally miscible ternary blend due to omitting the ΔK effect in ternary polymer blend. In previous Coleman and Painter study,[11] they considered that it would be difficult to find totally miscible ternary blend over a wide composition range due to significant $\Delta\chi$ and ΔK effect in ternary hydrogen bonded polymer blend. Only in very rare cases such as ternary blend of PVPh/PVAc/poly(methyl acrylate) (PMA)[11] give a completely miscible ternary polymer blend because the $\Delta\chi$ and ΔK interaction are finely balanced. Taking into account the both structures of PVAc and PMA, the repeat units of two polymers are isomorphous. Of course, this ternary polymer blend shows completely homogeneous amorphous phase. However, beside the isomer of two polymers, can we obtain a totally miscible ternary polymer blend involving hydrogen bonding between their polymer segments?

In our previous study,[19] we have found that the hydrogen bonding strength in the poly(ε-caprolactone) blends is the order of phenolic＞PVPh＞phenoxy. The phenolic, PVPh and phenoxy are the well-known hydrogen bonded donor polymers that can interact with polyacrylate, polyester, polyether and polyvinylpyridiene. However, for our knowledge, few studies pay attention on the binary polymer blends of both self-association polymers.[20-22] In our previous studies, we have reported that the phenolic/phenoxy[23,24] and PVPh/phenoxy[25] blends are totally miscible in the amorphous phase due to inter-association hydrogen bonding existing between their

hydroxyl groups of polymer segments. In addition, an unusual totally miscible hydrogen bonded ternary blend of phenolic/phenoxy/PCL was firstly observed in our previous study.[26] We confirm that the complicated intermolecular hydrogen bonding interactions existing in this ternary polymer blend system behaves like a network. Even though the different hydrogen bonding strength in each binary blend, it still exists a completely miscible ternary blend. As a result, if the intermolecular hydrogen bonding exists between each binary component in the ternary blend, it may obtain a completely miscible ternary blend. It's a clue that if the ternary blend components are all hydrogen bonded donor polymer, we would have the totally miscible ternary blend system. Therefore, the ternary hydrogen bonded polymer blends of phenolic/PVPh/phenoxy is reported in this present study. Interestingly, this ternary polymer blend actually gives a completely miscible amorphous phase over the entire compositions range based on DSC analyses. In this paper, we propose another result on completely miscible ternary hydrogen bonded polymer blend except for the isomer of two polymers.
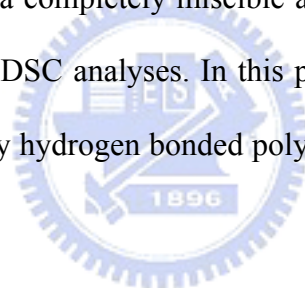
6-2 Experimental

6-2.1 Materials

Polymers used in this study were phenolic, poly(hydroxylether of bisphenol A) (phenolic) and poly(vinylphenol) (PVPh). The phenolic was synthesized with sulfuric acid via a condensation reaction and average molecular weights are $M_n = 500$ g/mole and $M_w = 1200$ g/mole. The poly(vinyl phenol) (PVPh) with a Mw = 9000-10000 g/mole were purchased from Polyscience Inc., USA. The phenoxy was obtained from the Union Carbide Co., with $M_n = 23000$ g/mole and $M_w = 48000$ g/mole. These molecular characteristics of these polymers and their corresponding model compounds were listed in Table 6-1.

6-2.2 Preparation of Blend Samples

The ternary polymer blends of phenolic/phenoxy/PVPh with various compositions were prepared by solution blend. Tetrahydrofuran solution containing 5wt% polymer mixture was stirred for 6-8 h and then allowed to evaporate slowly at room temperature for 1 day. The film of the blend was then dried at 50 °C for 2 days to ensure no any residual solvent.

6-2.3 Differential Scanning Calorimetry (DSC)

The glass transition temperature (T_g) of a polymer blend was determined by using a differential scanning calorimetry (Du-Pont, DSC model 2900). The scan rate was 20 °C/min ranging from 0 to 170 °C with 5-10mg sample on a DSC sample cell, and the specimen was quickly cooled to 0 °C after the first scan. The T_g value was obtained at the midpoint of the transition point of the heat capacity (C_p) change with scan rate of 20 °C /min and temperature range of 0 to 200 °C.

6-2.4 Infrared Spectra

The infrared spectra were recorded by a Nicolet Avatar 320 FT-IR spectrometer. In all cases, at least 32 scans with an accuracy of 1 cm^{-1} were signal-averaged. Infrared spectra of polymer blend films were determined by using the conventional NaCl disk method. The THF solution containing the blend (5% w/v) was cast onto

NaCl disk and dried under condition similar to that used in the bulk preparation. The film used in this study was sufficiently thin to obey the Beer-Lambert law. For the solution samples, an adequate permanently-sealed cell with NaCl windows of 0.2mm path length was used. A single optical path was used for studying the inter-association between 4-ethyl phenol (EPH) and 2,4-xylenol. All model compound solutions in the absorption range obey Beer-Lambert law. Cyclohexane was selected as the solvent because the specific conformation of the cyclohexane is favorable in this study.

6-2.5 Optical Microscopy

Morphological observations of the various blending compositions were carried out with the use of the Olympus BX50 microscope. A small amount of sample was sandwiched between two microscope cover glasses and then heated from room temperature to 280 ^{o}C with heating rate of 10 ^{o}C /min. The hot stage is Mettler Toledo FP90 with temperature accuracy ± 0.1 ^{o}C.

6-3 Results and Discussion

6-3.1 Binary Blend System

Conventionally, the differential scanning calorimetry was used to assess the miscibility of polymer blend by measured the glass transition temperature of the blend composition. Figure 6-1 shows the DSC traces of the series binary polymer blending compositions of the phenolic/PVPh, phenolic/phenoxy and phenoxy/PVPh. All these binary compositions exhibit a single T_g, which strongly suggests that all of the compositions are miscible with homogeneous phase. These T_gs of various compositions of each binary blend are summarized in Figure 6-2, where the negative T_g deviation from additive rule on all compositions is observed, which is similar with the other two self-associating polymer[24-28] blending system. The phenolic contains a high density hydroxyl group that possesses the strong self-association hydrogen bonding which serves as a physical crosslink and results in higher T_g than other polymers with similar molecular weight. The T_g deviation of Figure 6-2(a) can be interpreted as that self-associations of phenolic and PVPh are partially broken off and the hydroxyl groups are diluted by blending each others. In general, the T_g deviation is a result of entropy change corresponding to the change in the number of hydrogen bonding interaction. The phenoxy molecule with the long repeating unit provides relative less potential hydrogen bonding sites to form less interaction with other blending polymers. The reduction of forming inter-association hydrogen bonding is too small to overcome the entropy increase due to remove the self-association hydrogen bonds of each polymer with hydroxyl group. As a result, negative T_g deviations were also obtained in Figure 6-2(b) and Figure 6-2(c) that has been widely discussed in previous studies.[24]

6-3.2 Ternary Blend System

6-3.2.1 Thermal Analyses

Figure 6-3 shows selected DSC thermograms of several phenolic/phenoxy/PVPh ternary blends with various compositions, revealing that every ternary blend has only single glass transition temperature. A single T_g strongly suggests that the ternary polymer blend is fully miscible at total compositions. Based on these evidences, we suggest that any phenolic/phenoxy/PVPh blend composition is miscible at temperatures in the range of 0-170 ^{o}C. The phase diagram of this ternary polymer blend is displayed in Figure 6-4 with T_g of each composition. Therefore, we can confirm that this ternary polymer blend is totally miscible. The well-known Fox equation[29] has been proposed to predict the variation of glass transition temperatures of copolymers and blends as a function of composition,

$$\frac{1}{T_g} = \frac{W_1}{T_{g1}} + \frac{W_2}{T_{g2}} \tag{1}$$

where T_g is the glass transition temperature of this blend, W is the weight fraction and the subscripts indicate the polymers 1 and 2, respectively. This equitation is generally applicable to binary blend systems which are compatible and not too strongly polar. For three miscible components blends, this equitation must be extended to the T_g-composition relationship：$\frac{1}{T_g} = \frac{W_1}{T_{g1}} + \frac{W_2}{T_{g2}} + \frac{W_3}{T_{g3}}$. The calculated T_gs and the T_gs measured from DSC analyses from all compositions are plotted in Figure 6-5. It is obvious found out that these T_gs calculated from the Fox equation don't fit well with T_gs obtained from DSC analyses and many compositions shows significant negative deviation. We supposed that the large deviation between the experimental data and values calculated from Fox equation is resulting from the ternary blend system containing some kinds of strongly intermolecular interactions.

6-3.2.2 FT-IR Analysis

Fourier transform infrared spectroscopy has been used widely in the study of polymer blends. This method is useful to verify the presence of intermolecular interaction between hydrogen bonded donor and various hydrogen bonded accepter groups due to the sensitive of the hydrogen bonding formation. Figure 6-6 shows the scale-expanded infrared spectra of the hydroxyl group stretching absorption of series Phenolic/Phenoxy/PVPh blends with phenolic content fixed at 50wt% in the region of 3700-2700 cm^{-1}. All these bands show two distinct bands, the higher wavenumber centered at 3525 cm^{-1} can be assigned as the free hydroxyl group of phenolic and PVPh and 3570 cm-1 for the free hydroxyl group of phenoxy. In addition, the lower broad band at 3100-3450 cm^{-1} was contributed from the absorption of the hydroxyl groups that formed hydrogen bonded with other hydroxyl groups, so called the multimer hydrogen bonded hydroxyl group absorption. Clearly, the intensity of the free hydroxyl group of phenolic was decreased with the increase of phenoxy and PVPh content in the ternary blend system. Meanwhile, this broad hydrogen bonded hydroxyl band of phenolic shifts into lower frequency with increasing PVPh and phenoxy content. This observed change is come from the switching from the strong intramolecular hydroxyl-hydroxyl bond of phenolic into the intermolecular hydroxyl-hydroxyl bond between phenolic, phenoxy and PVPh segments. However, it is difficult to dwell further on this hydroxyl stretching region and hard to quantify these bands due to each of three polymer component containing hydroxyl group. Therefore, we should simulate this complicated hydrogen bonded ternary polymer blend system by using the individual binary blend of model compound. Figure 6-9 shows the FT-IR spectrum of each model compound, the 0.02M of EPH/cyclohexane (Figure 6-9 (a)) and 2,4-xylenol/cyclohexane (Figure 6-9 (b)) display a strongly absorption band of the "free" hydroxyl stretching (3620 cm^{-1}) and the spectrum of 2-propanol also shows the relatively sharp "free" hydroxyl stretching in 3632 cm^{-1}.

After we mixed the three compounds in cyclohexane (each composition contains constant concentration of 0.02M), a broad band envelope stretching from ca. 3150 − 3550 cm^{-1} became more obvious, illustrated in Figure 6-9 (d). As above results, it indicates that intermolecular hydrogen bond has formed in this mixing solution. Meanwhile, we also can obtain indirect evidence about the intermolecular interaction of the ternary miscible polymer blend.

6-3.2.3 Inter-association Equilibrium Constant (K_A)

According to previous study,[4] the self-association of phenolic, phenoxy and PVPh requires at least two association equilibrium constants, K_2 and K_B, to account for the formation of hydrogen bonded "dimers" and "multimers", respectively. The hydroxyl group exhibits various inter-association equilibrium constants with different type proton acceptor (e.g. hydroxyl, ester, ether and amine group) when mixing with other polymer. These three constants are expressed as self-associated dimer equilibrium constant (K_2), self-associated multimer equilibrium constant (K_B), and the inter-association equilibrium constant (K_A). As can been seen, each component of this ternary hydrogen bonded polymer blend can form self-association by individually hydroxyl group and develop intermolecular hydrogen bond between hydroxyl and hydroxyl groups. These self-association values of phenolic, phenoxy and PVPh are summarized in Table 6-2, which also contains the inter-association equilibrium constants of each binary blend. Therefore, all self- and inter-molecular interaction competitions would be deduced from the relationship of these self- and inter-association equilibrium constants.

A value for the inter-association (K_A), which is described as the ability of the interaction of hydrogen bonding between phenolic and PVPh, was measured in this study based on classical Coggeshall and Saier methodology,[30] using the hydroxyl

stretching region of the infrared spectra of concentrated 2,4-xylenol and 4-ethyl phenol (EPH) mixtures. In order to obtain the free intensity of free hydroxyl group (means unassociated) (f_F^{OH}) stretching of EPH, we chose the cyclohexane as the mixing solution due to the inertness for hydrogen bonded and exhibiting no any fundamental vibrational frequency in the hydroxyl stretching region (3100cm^{-1} – 3700cm^{-1}) of the infrared spectra. As we are dealing the hydroxyl stretching region, the overtone and combination bands of cyclohexane make major contribution that must be subtracted first. At the Figure 6-7 (a) the typical spectrum of 0.02M EPH in a cyclohexane solution is displayed and the pure cyclohexane stretching recorded in the 3100cm^{-1} – 3700cm^{-1} range shows in Figure 6-7 (b). Meanwhile, the spectrum of pure cyclohexane was digitally subtracted as illustrated in Figure 6-7 (c). There is a relative sharp band in 3620cm^{-1} present assigned to the free hydroxyl stretching absorption of EPH.

Now let us turn our attention to the calculation of the inter-association equilibrium constant between the hydroxyl group of Eph and the 2,4-xylenol hydroxyl group. When we introduced the interaction species such as 2,4-xylenol, the hydroxyl-hydroxyl interaction band centered at 3350cm^{-1} was increased and then the free hydroxyl band showed lower and lower intensity as illustrated in Figure 6-8. In Figure 6-8, all series infrared spectra of EPH/2,4-xylenol/cyclohexane mixtures were displayed, the spectrum of various concentration of 2,4-xylenol/cyclohexane was also digitally subtracted. However, the hydroxyl stretching of EPH was overlaid by the hydroxyl stretching of 2,4-xylenol. When the interaction of two hydroxyl group occurred, the background (the subtracted absorption band of various conc. 2,4-xylenol) would be affected. As previous literature,[31] the intensity of free hydroxyl group stretching in 3620 cm^{-1} must be corrected by considering the intensity change of different background. Measurement of f_F^{OH} from the EPH/2,4-xylenol/cyclohexane

181

mixtures allow us to calculate the appropriate inter-association equilibrium constant, K_A, from Eq. (4) derived by Coggeshall & Saier.[30] These values were listed in Table 6-3.

$$K_a = \frac{1 - f_F^{OH}}{f_F^{OH} \left[C_A - \left(1 - f_F^{OH}\right) C_B \right]} \qquad (1)$$

Where C_A and C_B are the concentrations of 2,4-xylenol and EPH, respectively. In previous view,[32] the absolute absorptivity of the free hydroxyl group stretching of FPH was determined by the extrapolation process, $a_F^{OH} = \lim_{c \to 0} A/bc$. The f_F^{OH} of any given concentration of EPH/2,4-xylenol/cyclohexane would be obtained, $f_F^{OH} = A/a_F^{OH}bc$. However, the K_a value is dependent of concentration. A reliable K_a (9.19 in L $\cdot$ mol^{-1}) value would calculate form extrapolation of zero 2,4-xylenol concentration. It is simply to convert K_a value to the dimensionless equilibrium constant K_A by dividing the molar volume of the repeating unit of PVPh (100 mol^3 $\cdot$ mol^{-1}). Thus the inter-association equilibrium constant, K_A, of 91.9 was measured.

In our knowledge, the chain stiffness such as intramolecular screening and functional group accessibility effect[33] plays an important role to determine the conversion between the model compounds and polymer blend. As far as these researches are concerned, no suitable equation to transform from model compounds to polymer blend. Meanwhile, the K_A value calculated from model compounds would not exactly describe the interaction between two polymers containing hydroxyl group. In this study, we attempt to compare the relative magnitude of all inter- and self-association equilibrium constants based on the classical Coggeshall and Saier methodology. Therefore, in this ternary hydrogen bonded blend each K_A constant is significantly higher than any self-association equilibrium constant (K_2 and K_B), which implies the hydroxyl groups of three components favor to form inter-association and then the self-association of individual polymer would be broken off. In general, the

phase diagram of ternary blend is affected by so called "$\Delta\chi$" effect, which is the difference of physical interaction between individual binary blend. When the inter-association of the individual binary blend is difference, named "ΔK" effect, it is tendency to induce phase separation.[11] However, the complicated intermolecular hydrogen bonding interactions existing in this ternary polymer blend system behaves like a network. Even though the different hydrogen bonding strength in each binary blend ("ΔK" effect), it still exists a completely miscible ternary blend. We again confirm here that if the intermolecular hydrogen bonding exists between each binary component in the ternary blend, it may obtain a completely miscible ternary blend such as previous phenolic/phenoxy/PCL.[26]

6-3.2.4 Optical Micrographs Analysis

Figure 6-10 shows optical micrographs of given compositions taken at different temperature. As can be seen in these photographs, there is a homogeneous phase are observed at 100 $^{\circ}$C in the composition of phenolic/phenoxy/PVPh = 30/14/56 (w/w) (Figure 6-10(a)). However, as increase temperature the hydrogen bond would be broken so that the degree of hydrogen bonded hydroxyl group also decreases.[4] A phase-separated structure has been found at 190 $^{\circ}$C showed at Figure 6-10(b). In addition, the same trend which is homogeneous phase at low temperature but heterogeneous phase at higher temperature is also measured in the composition of phenolic/phenoxy/PVPh = 65/17.5/17.5 (w/w) from the Figure 6-10 (c) and (d). From these results, the ternary hydrogen bonded blend follows a lower critical solution temperature (LCST) phase transition.

6-4 Conclusions

The phase behavior and hydrogen bonding of ternary blend of phenolic/phenoxy/PVPh have been investigated by using DSC, FTIR and optical microscopy. All three individual binary blends are miscible and then unusually the ternary hydrogen bonded blend is totally miscible. The magnitude of three kinds of inter-association equilibrium constant (K_A) is higher than any self-association equilibrium constant (K_2 and K_B). At this ternary blend system there is no significant "ΔK" effect and the "$\Delta \chi$" effect doesn't dominate over entire compositions. Meanwhile, the individual three polymers with hydroxyl functional group tend to form more the inter-association hydrogen bond with other two kinds polymer than the self-association of the intramolecular hydrogen bonding of an individual polymer. From the optical microscopy photographs this ternary blend system exhibits lower critical solution temperature (LCST) behavior, indicating that it is homogeneous at room temperature consistent with DSC analysis. These results reveal that this ternary hydrogen bonded blend has an entire totally miscible phase diagram.

Reference

(1) Utracki, L. A. *Polymer Alloys and Blends* Hanser Publishers, Munich, Vienna, New York, 1989.

(2) Bonner, J. G.; Hope, P. S. *Polymer Blends and Alloys*, ed. Folkes, M. J.; Hope, P. S. Blackie, Glasgow, UK, 1993.

(3) Paul, D. R. *Polymers Blends*, Vol. Ⅱ, ed. Paul DR, Newman S, Academic Press, New York, 1978..

(4) Coleman, M. M.; Graf, J. F.; Painter, P. C. *Specific Interactions and the Miscibility of Polymer Blends*, Technomic Publishing Inc, Lancaster, PA, 1991.

(5) Scott, R. L.   *J. Chem. Phys.* **1949**, *17*, 279.

(6) Tompa, H. *Trans Faraday Soc.* **1949**, *45*, 1140.

(7) Kwei, T. K.; Frisch, H. L.; Radigan, W.; Vogel, S. *Macromolecules* **1977**, *10*, 157.

(8) Pomposo, J. A.; Cortazar, M.; Calahorra,E. *Macromolecules* **1994**, *27*, 252.

(9) Fowler, M. E.; Barlow, J. W.; Paul, D. R. *Polymer* **1987**, *28*, 1177.

(10) Patterson, D. *Polym. Eng. Sci.* **1982**, *22*, 64.

(11) Zhang, H.; Bhagwagar, D. E.; Graf, J. F.; Painter, P. C.; Coleman, M. M. *Polymer* **1994**, *35*, 5379.

(12) Hong, B. K.; Kim, J. Y.; Jo, W. H.; Lee, S. C. *Polymer* **1997**, *38*, 4373.

(13) Jo, W. H.; Kwon, Y. K.; Kwon, I. H. *Macromolecules* **1991**, *24*, 4708.

(14) Kuo, S. W.; Lin, C. L.; Chang, F. C. *Macromolecules* **2002**, *35*, 278.

(15) Min, K. E.; Chiou, J. S.; Barlow, J. W.; Paul, D. R. *Polymer* **1987**, *28*, 172.

(16) Guo, Q. P. *Eur. Polym. J.* **1996**, *32*, 1409.

(17) Q. P. Guo, *Eur. Polym. J.* **1990**, *26*, 1329.

(18) Goh, S. H.; Ni, X. *Polymer* **1999**, *40*, 5733.

(19) Kuo, S. W.; Chan, S. C.; Chang, F. C. *Macromolecules* **2003**, *36*, 6653.

(20) Park, Y.; Veytsman, B.; Coleman, M. M.; Painter, P. C. *Macromolecules* **2005**, *38*, 3703.

(21) Hartikainen, J.; Lehtonen, O.; Harmia, T.; Lindner, M.; Valkama, S.; Ruokolainen, J.; Friedrich, K. *Chem. Mater.* **2004**, *16*, 3032.

(22) Wang, F. Y.; Ma, C. C. M.; Hung, A. Y. C.; Wu, H. D. *Chem. Mater.* **2001**, *202*, 2328.

(23) Wu, H. D.; Ma, C. C. M.; Chang, F. C. *Macromol. Chem. Phys.* **2000**, *201*, 1121.

(24) Wu, H. D.; Chu, P. P.; Ma, C. C. M.; Chang, F. C. *Macromolecules* **1999**, *32*, 3097.

(25) Kuo, S. W.; Wu, H. D.; Lin, C. L.; Chang, F. C. *J. Polym. Res.* **2002**, *10*, 87.

(26) Kuo, S. W.; Chan, S. C.; Wu, H. D.; Chang, F. C. *Macromolecules* **2005**, *38*, 4729.

(27) Wu, H. D.; Ma, C. C. M.; Chu, P. P. *Polymer* **1997**, *38*, 5419.

(28) Li, X. D.; Goh, S. H. *J. Polym. Sci., Polym. Phys. Ed.* **2003**, *41*, 789.

(29) Fox, T. G. *J. Appl. Bull. Am. Phys. Soc.* **1956**, *1*, 123.

(30) Coggeshall, N.; Saier, E. *J. Am. Chem. Soc.* **1951**, *73*, 5414.

(31) Wu, H. D.; Chu, P. P.; Ma, C. C. M. *Polymer* **1998**, *39*, 703.

(32) Hu, Y.; Painter, P. C.; Coleman, M. M. *Macromol. Chem. Phys.* **2000**, *201*, 470.

(33) Painter, P. C.; Coleman, M. M. *Polymer Blends* vol. 1, Paul DR (ed) John Wiley & Sons, New York, 2000.

Table 6-1. Summary molecular structure, characteristic, T_g, and model compound of polymers used in this study.
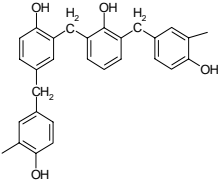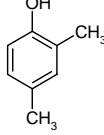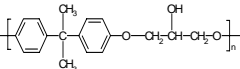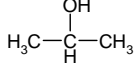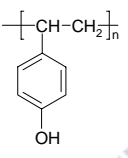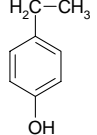
Material	Molecular structure	Molecular weight	T_g (°C)	Model compound
Novolak type phenolic resin		Mn=500 Mw=1,200	65	2,4-xylenol
Phenoxy		Mn=23,000 Mw=48,000	98	2-propanol
Poly(vinylphenol)		Mw= 9,000-10,000	150	4-ethyl phenol

Table 6-2. The various association equilibrium constants and thermodynamic parameters were used in this research.

material	molar volume (cm³/mol)	solubility parameter (cal/mL)^0.5	self-association equilibrium constant		inter-association equilibrium constant
			K_2	K_B	K_A
Phenolic	84[a]	12.1[a]	23.3[a]	52.3[a]	
Phenoxy	216[a]	10.2[a]	14.4[a]	25.6[a]	
PVPh	100[b]	10.6[b]	21[b]	66.8[b]	
Phenolic-Phenoxy					114[a]
Phenoxy-PVPh					101.7[c]
Phenolic-PVPh					91.9[d]

[a] Ref.[24]   [b] Ref.[4]   [c] Ref.[25]   [d] Measured in this study.

Table 6-3: The fraction of free hydroxyl groups of 4-ethyl phenol

Concentration of 2,4-xylenol (M)	Corrected intensity of IR spectra	f_F^{OH}	Inter-association equilibrium constant (K_a) (mol/L)
0.02	0.1154	0.8435	10.3765
0.04	0.1088	0.7953	7.1673
0.08	0.0984	0.7193	5.2462
0.10	0.0979	0.7156	4.2130
0.20	0.1068	0.7807	1.4359
0.25	0.1213	0.8867	0.5158
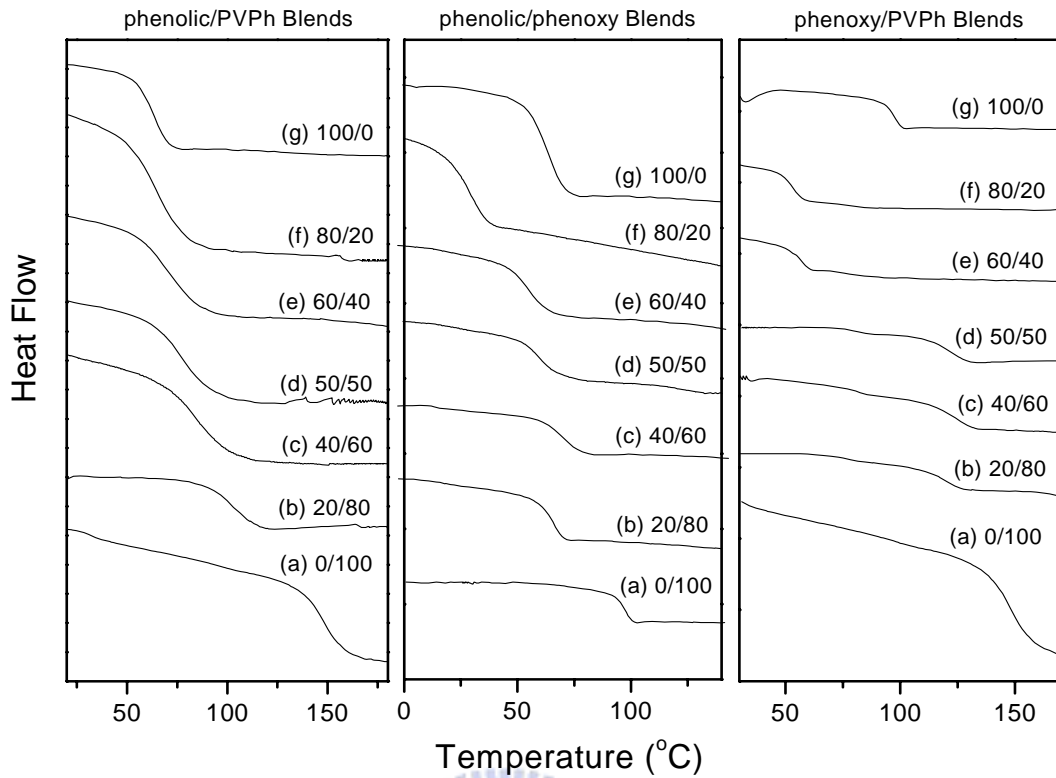
Figure 6-1: DSC traces of the individual binary blends (wt/wt %) having varying compositions: (a) phenolic/PVPh, (b) phenolic/phenoxy, (c) phenoxy/PVPh.
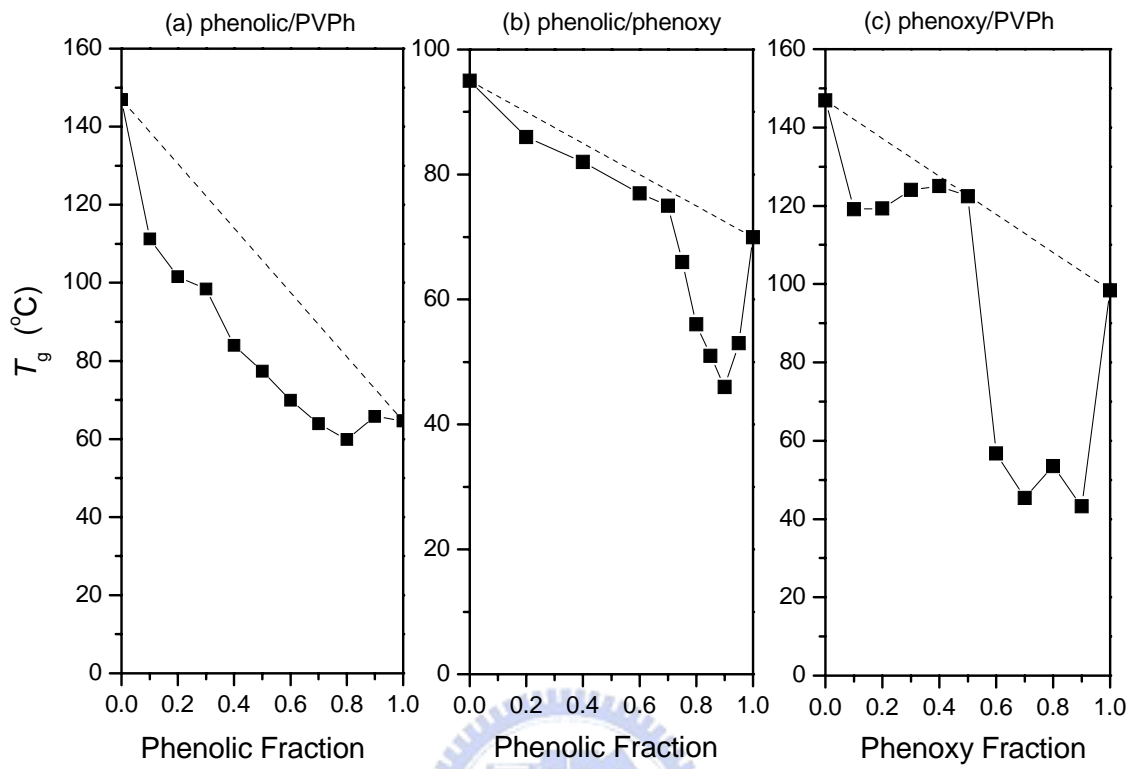
Figure 6-2: Plots of T_g versus the composition of the individual binary blend: (a) phenolic/PVPh, (b) phenolic/phenoxy, (c) phenoxy/PVPh.
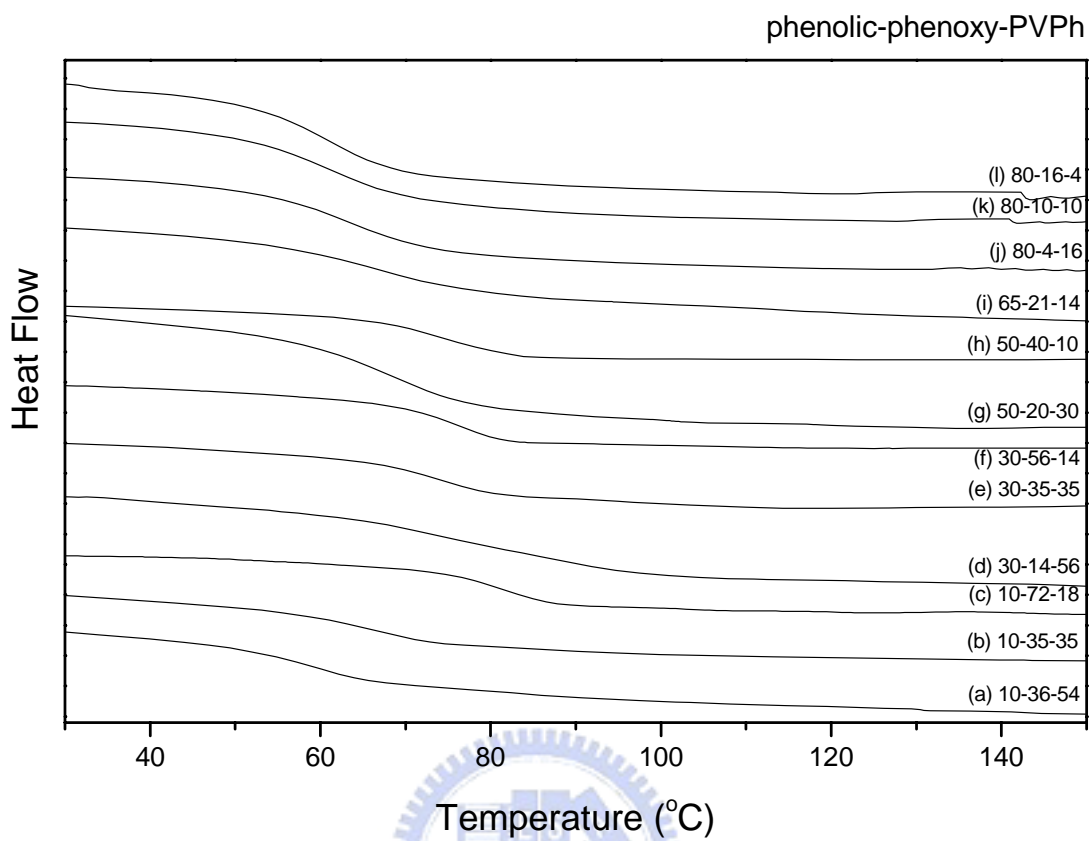
Figure 6-3: DSC thermograms of phenolic/phenoxy/PVPh blends of different compositions. (a) 10/36/54 (wt/wt/wt %); (b) 10/35/35; (c) 10/72/18: (d) 30/14/56; (e) 30/35/35; (f) 30/56/14; (g) 50/20/30 (h) 50/40/10; (i) 65/21/14; (j) 80/4/16; (k) 80/10/10; (l) 80/16/4.
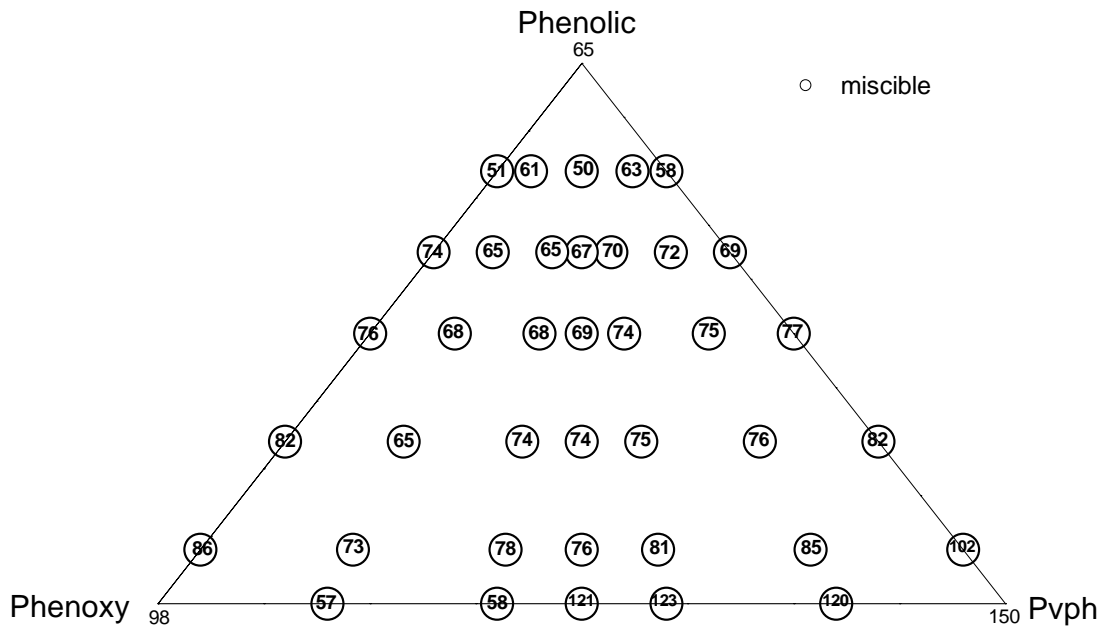
Figure 6-4: Ternary phase diagram of the phenolic/phenoxy/PVPh system with individual values of T_g indicated for the composition shown in each cycle.
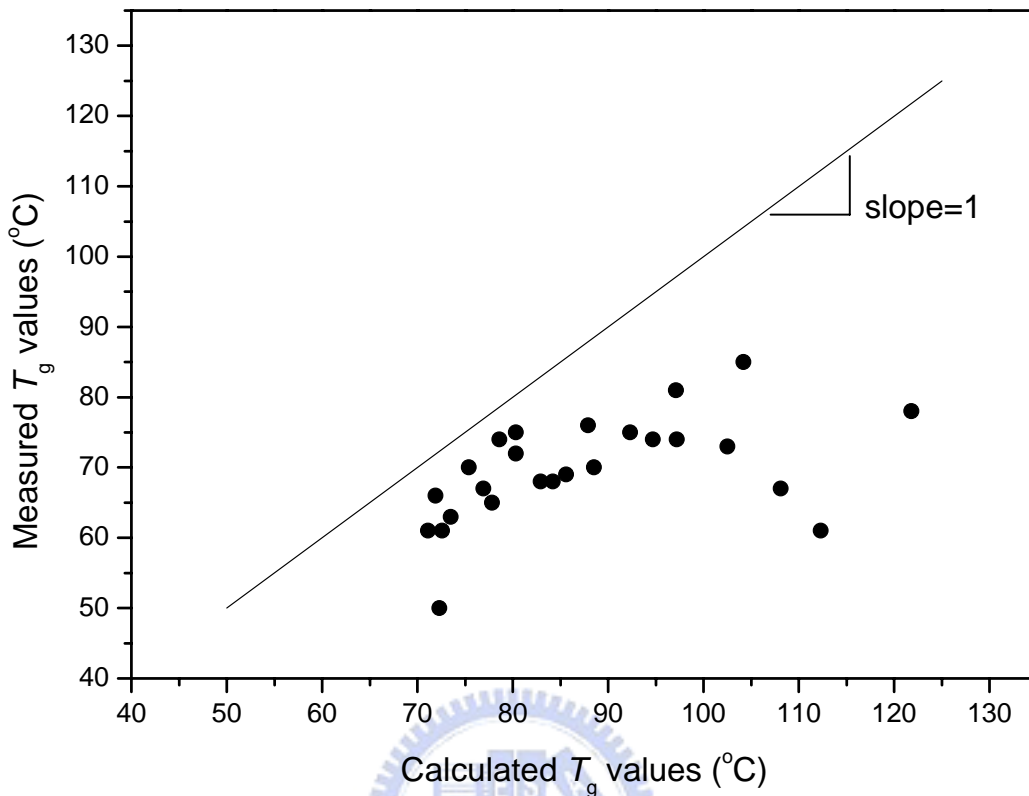
Figure 6-5: Scatter plots of the values of T_g based on experimental data (●) and the
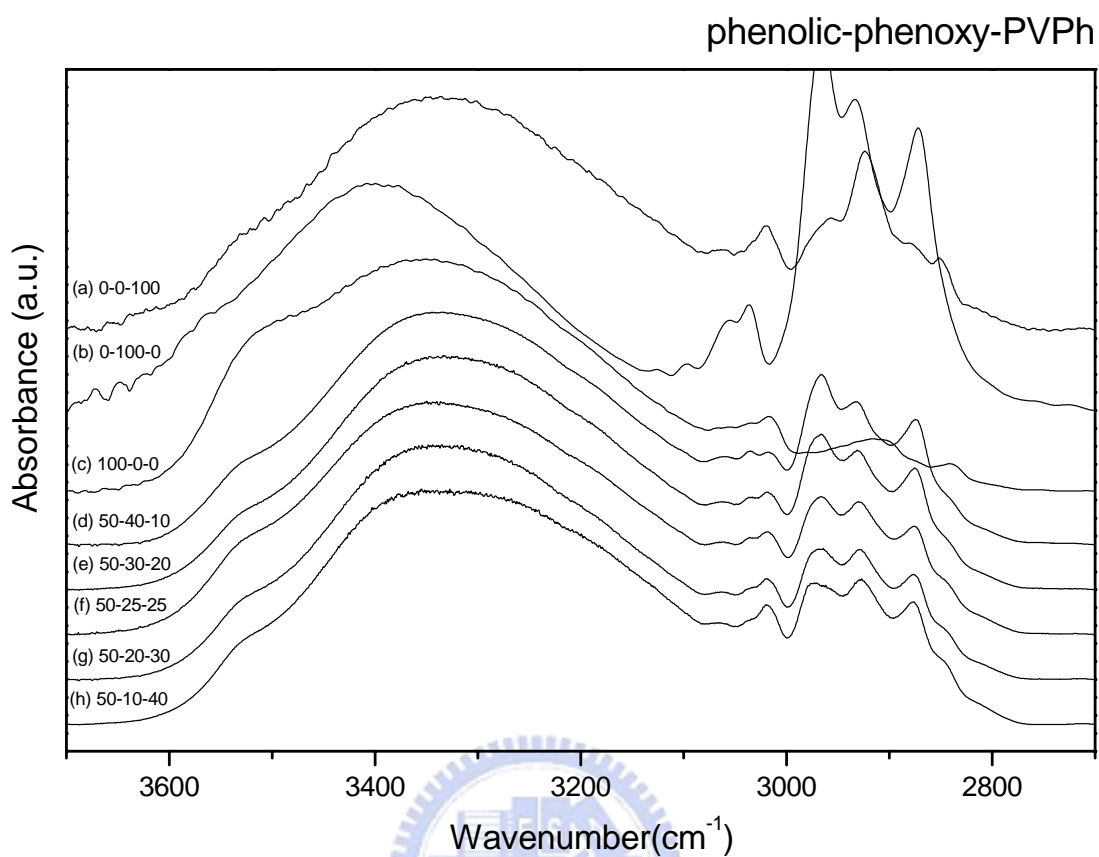
solid line calculated using the Fox equation.

Figure 6-6: Infrared spectra recorded in the region 2700-3700 cm^{-1} for a series of phenolic/phenoxy/PVPh compositions: (a) 0/0/100 (wt/wt/wt %); (b) 0/100/0; (c) 100/0/0; (d) 50/40/10; (e) 50/30/20; (f) 50/25/25; (g) 50/20/40; (h) 50/10/40.
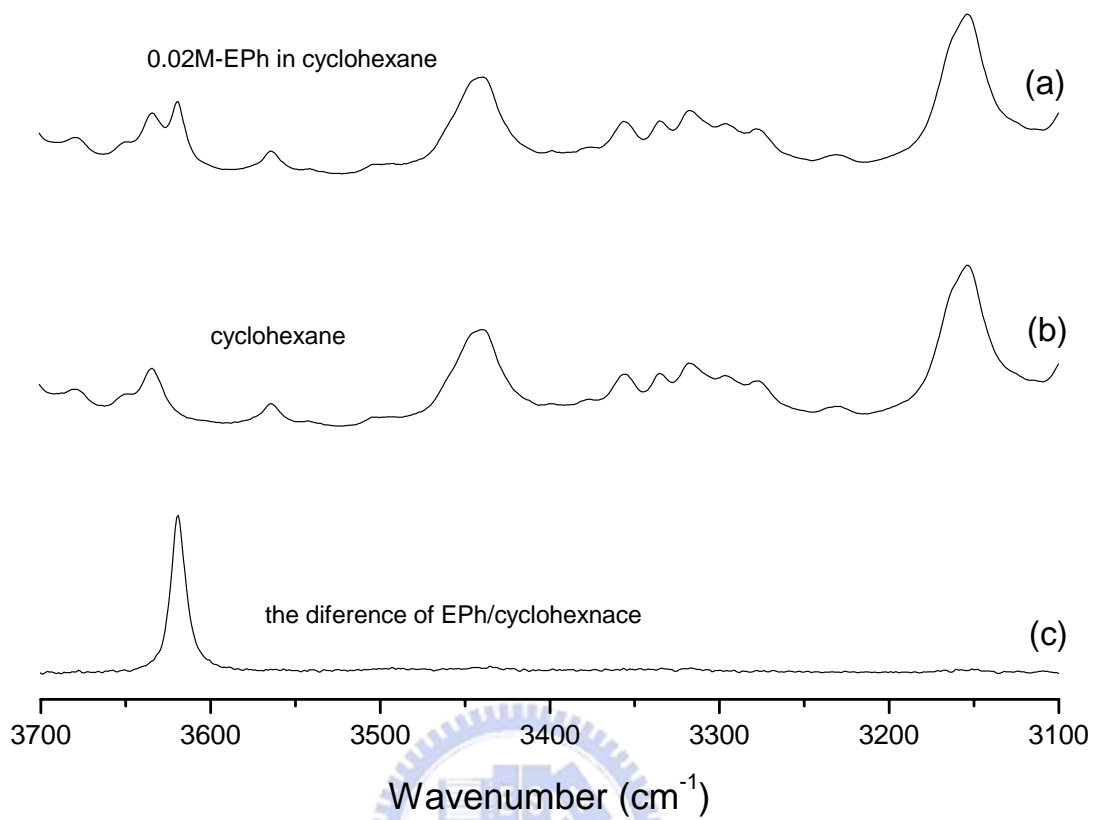
0.02M-EPh in cyclohexane

(a)

cyclohexane

(b)

the diference of EPh/cyclohexnace

(c)

3700 3600 3500 3400 3300 3200 3100

Wavenumber (cm^{-1})

Figure 6-7: Infrared spectra recorded at room temperature in the region from 3100-3700 cm^{-1}.

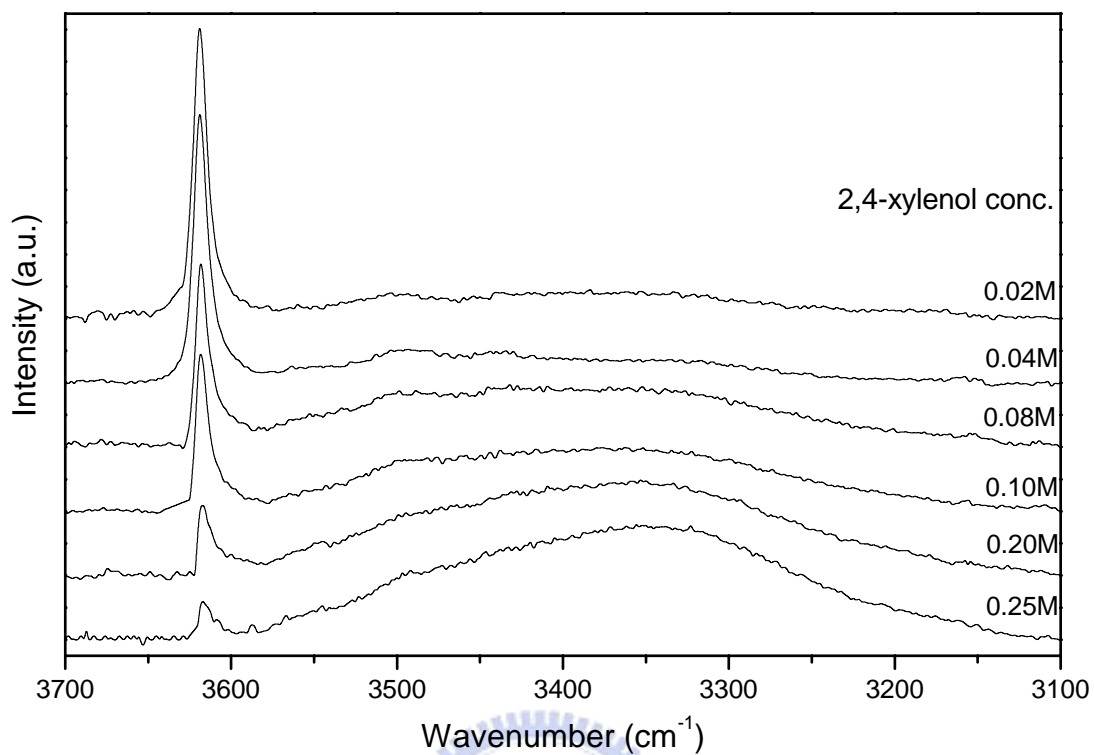EPH was fixed in 0.02M with various 2,4-xylenol

Figure 6-8: The absorption band of the free hydroxyl group of 4-ethylphenol (0.02 mol/L) in EPH/2,4-xylenol/cyclohexane solutions, ranging from 3100-3700 cm^{-1}.
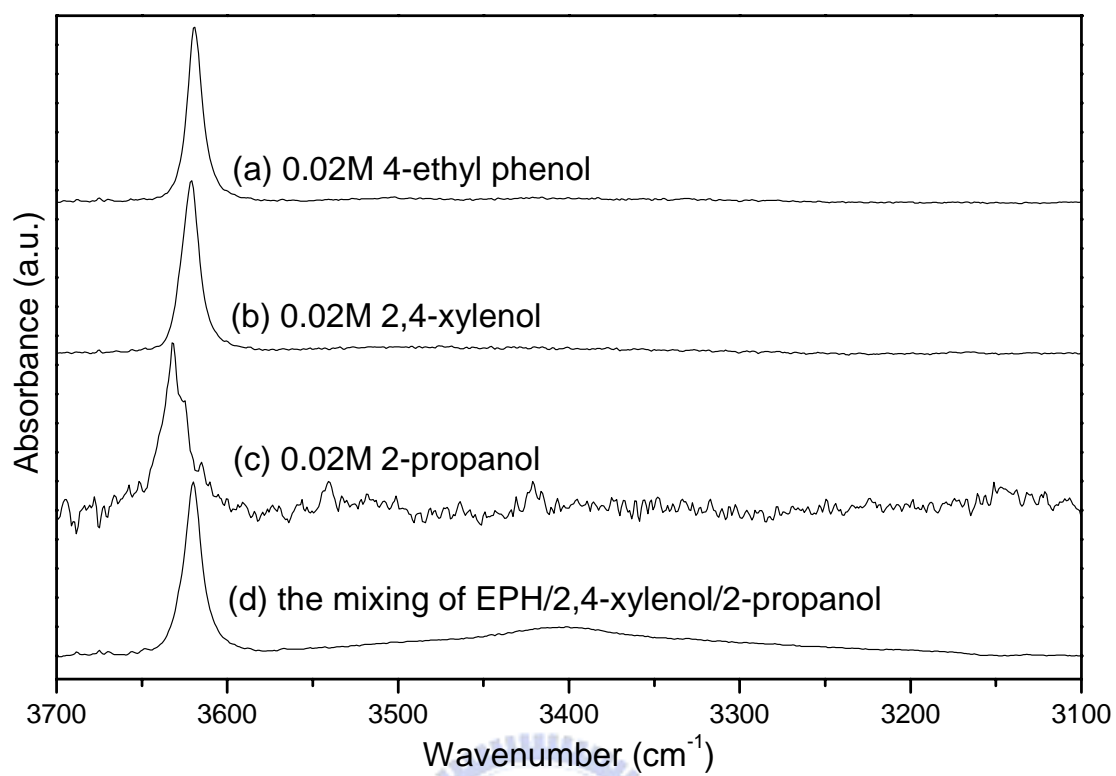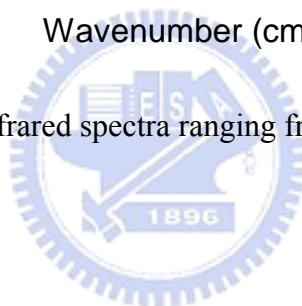
(a) 0.02M 4-ethyl phenol

(b) 0.02M 2,4-xylenol

(c) 0.02M 2-propanol

(d) the mixing of EPH/2,4-xylenol/2-propanol

Figure 6-9: Scale-expanded infrared spectra ranging from 3100-3700 cm^{-1}.

(a) 30-14-56 at 100 °C

(b) 30-14-56 at 190 °C

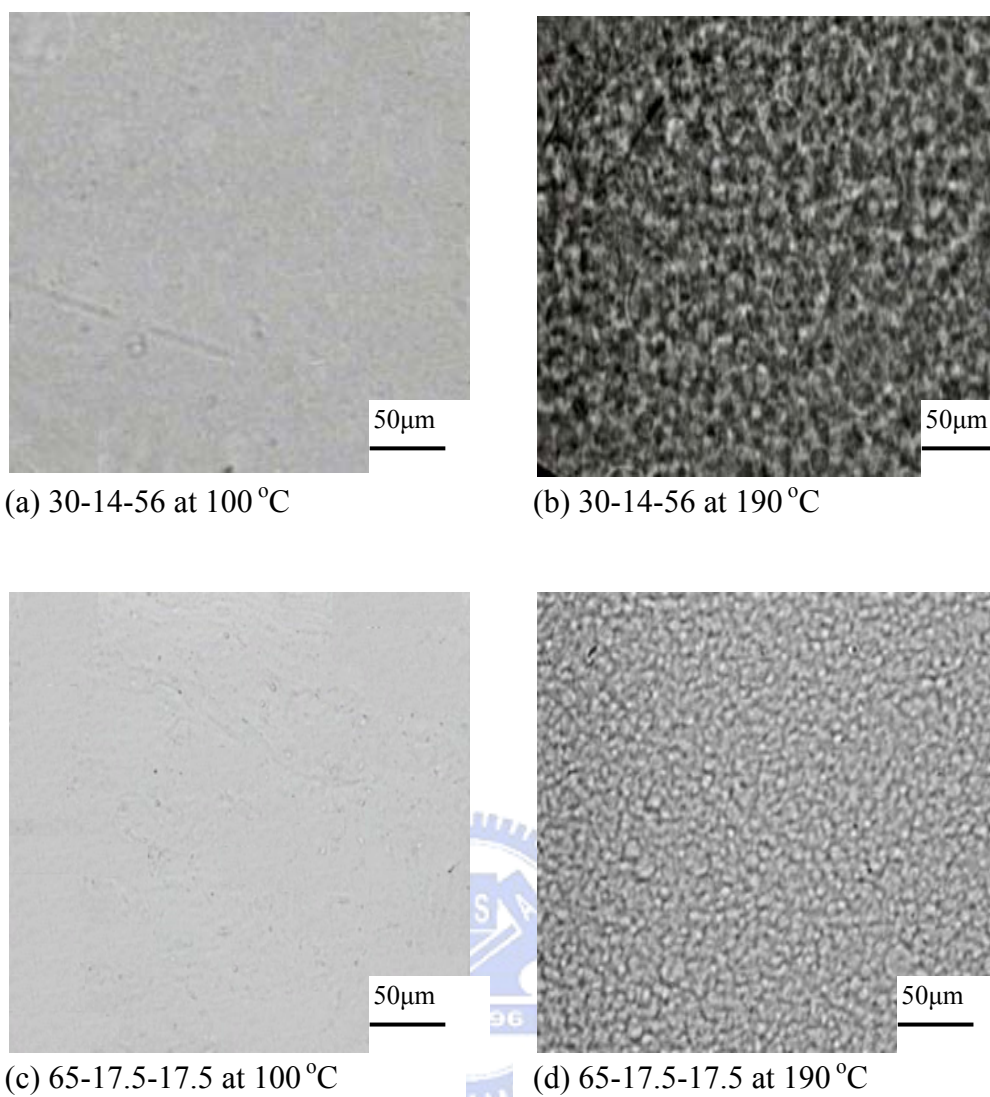(c) 65-17.5-17.5 at 100 °C

(d) 65-17.5-17.5 at 190 °C

Figure 6-10: Optical micrographs of phenolic/phenoxy/PVPh blends of various compositions and at different temperatures. (a) 30/14/56, 100 °C; (b) 30/14/56, 190 °C; (c) 65/17.5/17.5, 100 °C; (d) 65/17.5/17.5, 190 °C.

Chapter 7

Conclusions

We have synthesized the rod–coil diblock copolymers using the versatile ATRP method. The methyl ketone-terminated PMMA has a higher value of T_g than does the virgin PMMA because of its syndiotactic-like structure. The decomposition temperature (T_d) of the rod–coil diblock copolymer is higher than that of the PMMA homopolymer because the presence of the PPQ block retards the early decomposition of PMMA chains. Regular, porous honeycomb-structured films were prepared from the dichloromethane solution of the diblock copolymer in an air-flow hood. A higher polymer concentration results in larger pores, because the aggregation of polymer is fast. If the concentration of the polymer solution is too low, water droplet coalescence tends to enlarge the pore size and size distribution, and forms polygon structures. Higher relative molecular masse (Mr) tends to create larger pores. The wall thickness between the pores increases linearly with the increase of the relative molecular mass (M_r).

In the studies of hydrogen bonded polymer blend, the block copolymer PVPh-*b*-PMMA and random copolymer PVPh-*r*-PMMA were designed and synthesized by anionic and free radical copolymerization of 4-*tert*-butoxystyrene and methyl methacrylate and the *tert*-butoxy protective group was selectively removed through hydrolysis reaction. The fractions of hydrogen bonded carbonyl groups and glass transition temperatures of two copolymers are higher than those of the PVPh/PMMA blend system at similar PVPh content. This observation can be attributed to the difference in degrees of rotational freedom between polymer blend and copolymer. Meanwhile, the polymer chain architecture of a homopolymer is significantly different to that of copolymers due to intramolecular screening and

functional group accessibility caused by the covalent bond connectivity. In addition, the inter-association equilibrium constant of PVPh-r-PMMA copolymer obtained from curve fitting method of f_b and based on PCAM is larger than that of PVPh-b-PMMA copolymer. The block copolymer has the highest T_g value because it has the lowest polydispersity index.

For copolymer/homopolymer system, PVPh-co-PMMA/PEO blends are investigated. PVPh-r-PMMA/PEO blends are completely miscible in an amorphous phase over the entire composition range. On the contrary, the PVPh-b-PMMA and PEO are formed a closed-looped of phase separated region in the phase diagram due to the $\Delta\chi$ effect and ΔK effect in ternary polymer blend. According to the values of frequency difference ($\Delta\nu$) in all copolymer/PEO blends, it implies that the interassociation between PVPh and PEO is considerably stronger than either the self-association of hydroxyl groups in PVPh or the interactions between hydroxyl groups in PVPh and carbonyl groups in PMMA. Based on the Painter-Coleman association model (PCAM), we obtained a value for $K_C = 300$ in PVPh-b-PMMA/PEO blend system at room temperature. The results give a fine agreement between the experimental and theoretical fraction of hydrogen bonded carbonyl groups for the two sets of copolymer/PEO blends corresponding to fixed volume fractions of PEO ($\Phi_C = 0.2$).

The ternary polymer blend system with three self-association hydrogen bonding polymer are totally miscible. Because there is no significant "ΔK" effect and the "$\Delta\chi$" effect doesn't dominate over entire compositions.

List of Publications

(1) Shiao-Wei Kuo, **Chen-Lung Lin** and Feng-Chih Chang, "*Phase Behavior and Hydrogen Bonging in ternary Polymer Blends of Phenolic Resin/Poly(ethylene oxide)/Poly(-caprolactone)*", *Macromolecules* **2002**, *35*, 278.

(2) Shiao-Wei Kuo, **Chen-Lung Lin** and Feng-Chih Chang, "*The Study of Hydrogen Bonding and Miscibility in Poly(vinylpyridines) with Phenolic Resin*" *Polymer* **2002**, *43*, 3943.

(3) Shiao-Wei Kuo, **Chen-Lung Lin**, Hew-Der Wu and Feng-Chih Chang, "*Thermal property and hydrogen bonding in blends of poly(vinylphenol) and poly(hydroxylether of bisphenol A)*" *Journal of Polymer Research*, **2003**, *2*, 87.

(4) **Chen-Lung Lin**, Shiao-Wei Kuo and Feng-Chih Chang, "*The Totally Miscible in Ternary Hydrogen Bonded Polymer Blend of Poly(vinyl phenol)/Phenoxy/Phenolic*" *Journal of Polymer Research*, **2005**, submitted.

(5) **Chen-Lung Lin**, Pao-Hsiang Tung and Feng-Chih Chang, "*Synthesis of Rod-Coil Diblock Copolymers by ATRP and their Honeycomb Morphologies formed by the "Breath Figures" Method*" *Polymer* **2005**, in press.

(6) **Chen-Lung Lin**, Wan-Chun Chen, Chun-Syong Liao, Yi-Che Su, Chih-Feng Huang, Shiao-Wei Kuo and Feng-Chih Chang "*Sequence Distribution and Polydispersity Index Affect the Hydrogen Bonding Strength of Poly (vinylphenol-co-methyl methacrylate) Copolymers*" *Macromolecules* **2005**, *38*, 6435.

(7) **Chen-Lung Lin**, Wan-Chun Chen, Shiao-Wei Kuo and Feng-Chih Chang "*Sequence Distribution Affect the Phase Behavior and Hydrogen Bonding Strength in Blends of Poly(vinylphenol-co-methyl methacrylate) with Poly(ethylene oxide)*" *Macromolecules* **2005**, submitted.

(8) Wen-Yi Chen, Yen-Zen Wang, Chao-Chen Yang, **Chen-Lung Lin** and Feng-Chih Chang "*Novel Nanocomposite of Low D_k Introduced Fluorine-Containing POSS Structure Based on Epoxy Resin*" *Materials Chemistry and Physics* **2005**, submitted.

Introduction to Author

English name: Chen-Lung Lin

Chinese name: 林振隆

Birthday: 1979, 10, 07

Address: 台中縣龍井鄉新庄村學園路 19 號

Education:

1997.09~2001.06   **B. S.,** Department of Applied Chemistry, National Chiao Tung

University, Hsin Chu, Taiwan

2001.09~2002.07   **M. S.,** Institute of Applied Chemistry, National Chiao Tung

University, Hsin Chu, Taiwan

2002.08~2005.09   **Ph. D.,** Institute of Applied Chemistry, National Chiao Tung

University, Hsin Chu, Taiwan